MEASURING TERRESTRIAL NET PRIMARY PRODUCTIVITY IN ARCTIC ECOSYSTEMS WITH AVHRR SATELLITE IMAGERY

By

Daniel T. O'Brien

A Thesis Submitted to the Faculty of Graduate Studies,
University of Manitoba.

In Partial Fulfilment of the Requirements for the Degree
Master of Science
Department of Botany

THE UNIVERSITY OF MANITOBA

FACULTY OF GRADUATE STUDIES

*****

COPYRIGHT PERMISSION PAGE

MEASURING TERRESTRIAL NET PRIMARY PRODUCTIVITY IN ARCTIC ECOSYSTEMS WITH AVHRR SATELLITE IMAGERY

BY

Daniel T. O'Brien

A Thesis/Practicum submitted to the Faculty of Graduate Studies of The University of Manitoba in partial fulfillment of the requirements of the degree of

Master of Science

ACKNOWLEDGEMENTS

I would like to express sincere gratitude to my advisor Norm Kenkel for guiding me through this research, and for always having time for discussions and feedback on my thesis. Thanks also to my committee members, Drs. McLachlan, Barber and McCanny for valuable advice. Special thanks to Stephen McCanny, Micheline Manseau, Tom Naughten, and Joanne Tuckwell at Parks Canada for making this project possible, and for providing technical support and advice. Thanks also to Brad Sparling, Ryan Brook, and Dr. Larry Stene for unyielding assistance in the field.

This project would not been possible without the generous financial support of Parks Canada, NSERC, The University of Manitoba Faculty of Science and Faculty of Graduate Studies, and the Northern Studies Training Program. Thanks to the friendly and helpful staff at the Aurora Research Institute in Inuvik, NWT, for providing lodging and logistical support during the field trip. Equipment and logistical support were also generously provided by The Polar Continental Shelf Project.

ABSTRACT

Accurate estimates of terrestrial net primary productivity (NPP) are critical for monitoring the effects of climate change, managing wildlife, and for sustainable resource management in Canada's northern National Parks. The remoteness, inaccessibility, and large spatial extent of the Canadian arctic makes remote sensing a necessary tool for estimating NPP at the landscape scale. Parks Canada currently receives GEOCOMP-n AVHRR cloud-free composite images for all of Canada every 10-days and is currently developing methods to utilize this imagery for ecosystem monitoring in Canada's National Parks. The primary objectives of this thesis are:

1. To develop methodology for estimating arctic NPP using the 1x1 km resolution AVHRR satellite imagery produced by the GEOCOMP-n image processing system.

2. To assess the influence of variable topography and sub-pixel water bodies on AVHRR reflectance measurements.

3. To evaluate the correspondence between the GECOMP-n AVHRR image products and ground data.

A method is presented for computing terrestrial NPP of arctic vegetation using the satellite image products produced by the GEOCOMP-n image processing system. The NPP model is parameterized using a combination of ground data collected in TNNP during the summer of 2000, as well as data available from previous research. The model results are evaluated with an expected productivity map produced using a vegetation classification and expected annual NPP values compiled from the literature. Proportion of water cover and vegetation cover and topographic complexity within each pixel are measured and the influence of these variables on the difference between modelled and expected values are evaluated. Finally, ground spectral reflectance measurements are scaled-up to AVHRR resolution to evaluate the correspondence between the GEOCOMP-n image products and actual ground measurements.

Annual NPP computed using the modified soil adjusted vegetation index (MSAVI), showed the best correspondence with the expected annual NPP map, with 84.43% of the pixels within 30% of the difference. Within Tuktut Nogait National Park, the average annual NPP for 2000 was 149.4 (±68.4) g/m^2yr. Highest productivity occurred along the east side of the Hornaday River Valley. Lowest productivity occurred in the central region of the Park along the Melville Hills, and in the northeast region of the Park near the coast. Onset of the growing season occurred between June 1 and June 11. NPP was highest between July 1 and July 11, with mean NPP at 22.61(±11.1) g/m^2*10-days. The growing season ended between September 11 and September 21.

Topography and water cover had significant effects on the regression between modelled NPP and expected NPP. With increasing water cover within the AVHRR

pixels, modeled NPP values tended to be greater than expected. In areas with complex topography (i.e., high slope variance within the AVHRR pixels), the model may underestimate NPP. In areas with steep terrain (high mean slope within the AVHRR pixels), the model NPP estimates are higher than expected. Although significant, the effect of these variables on the overall regression were relatively small.

Rescaled ground reflectance measurements trended well with AVHRR measurements. Although, ground measurements of NDVI were consistently higher than atmospherically corrected AVHRR NDVI. This difference is likely attributable to directional reflectance effects as a result of large sun angles. Applying a bi-directional reflectance correction (BRDF) should improve correspondence between AVHRR NDVI and NDVI computed from field measurements of surface reflectance. However, current BRDF corrected imagery should not be used until improvements have been made to the GEOCOMP-n bi-directional reflectance correction procedures.

Model estimates of NPP provide an excellent relative measure of NPP in Tuktut Nogait National Park. The model is easily implemented and uses the GEOCOMP-n AHVRR data exclusively. The AVHRR NPP maps will be useful for ecosystem monitoring, providing the ability to identify temporal and spatial trends and fluctuations in NPP at a regional scale. These data will be particularly useful for identifying areas of interest that warrant further examination, either with high resolution imagery, or ground surveys.

TABLE OF CONTENTS

LIST OF FIGURES

LIST OF TABLES

1. INTRODUCTION

Maintaining the ecological integrity of Canada's National Parks is a fundamental objective of park managers (Dearden and Rollins 1993). The key to this objective is a consistent and reliable source of understandable information about ecosystem processes. This information base should provide extensive coverage of the park and surrounding region, and be available at a number of time scales.

In Canada's northern parks, an understanding of arctic vegetation structure, composition and productivity is critical to maintaining ecological processes and ensuring ecosystem biodiversity and sustainability. Estimates of net primary productivity (NPP) in the arctic are important, since whole-biome estimates of CO_2 flux are required to accurately model global circulation and carbon budgets. Furthermore, precise measurements of NPP are crucial for monitoring the effects of climate change on arctic ecosystems. Global warming will increase permafrost thawing, potentially transforming the arctic into a CO_2 source as previously inaccessible carbon is released as a result of increased microbial activity (Piochl and Cramer 1995). The monitoring of arctic vegetation productivity also has great cultural and ecological significance: many indigenous peoples rely on sustenance hunting, and reliable NPP estimation will improve our ability to monitor and sustainably manage the wildlife habitat of caribou, migratory birds, and musk oxen (e.g. Hansen 1991; Colpaert et al. 1995). A quantitative arctic NPP model that utilizes remotely sensed data can provide the empirical data necessary to meet these important objectives.

The information available from such a model will provide a powerful tool for wildlife managers, since the timing of green-up and duration of the growing season has large implications on caribou fecundity. Over time, the satellite monitoring program will make possible a continuous data set spanning many years. This will allow for the detection of long term changes in vegetation structure, providing the necessary empirical data to monitor and verify the potential effects of climate change on arctic ecosystems.

The following chapter provides a description of the study area located in Tuktut Nogait National Park. This section provides information about the floristic structure of the vegetation communities within the Park, a summary of vegetation data collected in the field, as well as details on the climate, physical geography, and fauna existent in the Park.

The third chapter describes a method for modelling terrestrial net primary productivity in Tuktut Nogait National Park using the GEOCOMP-n AHVRR satellite data. The model is parameterized using a combination of field measurements obtained within the study area and published data sets from similar areas. The model estimates are validated using a map of expected annual NPP derived from a Landsat vegetation classification and expected annual net primary productivity (ANPP) values obtained from literature sources.

The fourth chapter discusses validation of the atmospherically corrected AVHRR NDVI using scaled-up field measurements of surface reflectance. The effects of landscape complexity on scaling fine resolution measurements of NDVI to AVHRR resolution are examined by comparing Landsat NDVI pixels aggregated to 1x1 km, with

spatially corresponding AVHRR NDVI pixels in both homogeneous and heterogeneous areas.

The final chapter discusses the factors influencing NPP in Tuktut Nogait National Park, and suggestions for improvements to the satellite monitoring of northern ecosystems.

2. DESCRIPTION OF STUDY AREA

2.1. INTRODUCTION

Tuktut Nogait National Park is located within the southern arctic ecozone and is representative of the Tundra Hills Natural Region. The Park covers 16,340 km^2 and the vegetation is characteristic of the low arctic ecoregion. The Park was established in 1996 after Canadian Parks Service recognized the exceptional biological and physical attributes of the area. The current boundary encompasses the calving grounds of the Bluenose caribou herd, a large nesting area for birds of prey, as well as an area of diverse vegetation in the lower Hornaday and Brock rivers (Figure 2.1). There are plans to extend the current boundary south and east into Nunavut, with the intention of encompassing Bluenose Lake.

Climate

The climate of Tuktut Nogait National Park is summarized in Zoltai et al (1992). The Park lies within the Low Arctic Ecoclimatic region and has a mean annual temperature of –11.4°C. Summers are short and cool with a mean daily temperature for July of 7.4°C. Winters are long and cold with a mean daily temperature for January of –27.6 °C. Annual precipitation is low: mean annual precipitation is 181.5mm, with 96.6mm falling as rain and 85.0cm as snow. Snow cover persists for up to 250 days per year.

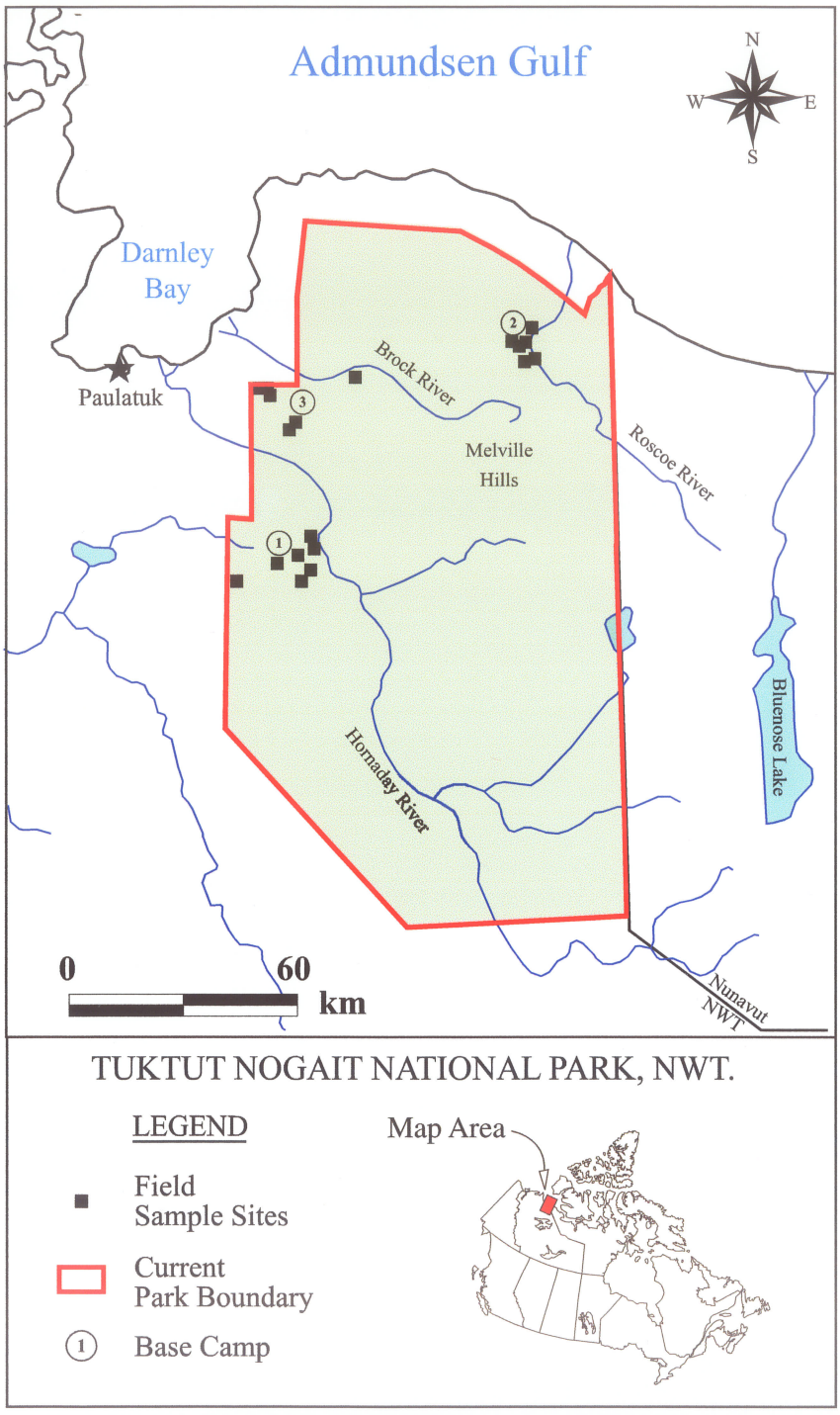

Figure 2.1. Map of study area within Tuktut Nogait National Park, NWT. Most sample sites were located within hiking distance (~10km) of three base camps: (1) Cache Lake, 68° 53'N, 122° 49'W; (2) Roscoe River, 69° 22'N, 121° 24'W; (3) Seven Islands Lake, 69° 16'N, 122° 58'W.

Geology

The geology of the area is documented in Zoltai et al. (1992). Most of the Park is underlain by Upper Proterozoic sedimentary rocks, composed entirely of marine strata. The oldest strata are composed of shales, argillite and siltstone which outcrop along the coast of Darnley Bay. These strata are overlain by Precambrian layers of dolomite, sandstone, and quartzite which outcrop along the Admundsen Gulf Shoreline and in the Melville Hills as far south as the Little Hornaday River. Palaeozoic sedimentary rocks overlie these strata and consist of sandstone, shale, siltstone, mudstone and dolomite. These rocks outcrop along the mid portion of the Hornaday River. Upper Cambrian and Lower Ordovician layers are next and consist mostly of dolomite. Lower Cretaceous bedrock is exposed near the mouth of the Hornaday, and consists of soft shale, mudstone and beds of sandstone. The most recent strata consist of Quaternary glacial deposits. Glacial moraines are common on the north slopes of the Melville hills with thick deposits of glaciofluvial sand and gravel in glacial meltwater channels. Moraines are absent from the central part of the Melville Hills.

Soils within the Park are cryosolic with permafrost occurring within one meter. Most soils are turbic cryosols, which are characterized by frost heaves and polygon formations. Static cryosols are found mainly on glaciofluvial parent materials. Accumulations of peat occur in wetter areas.

Hydrology

The 350 km long Hornaday River and its tributaries is the main river system in the Park. The Hornaday River originates to the southwest at Bluenose Lake and drains north

into Darnley Bay near Paulatuk (Figure 2.1). Lesser river systems include: the Brock river, which originates in the Melville Hills and flows into Darnley Bay; and the Roscoe River, which flows north into the Admundsen Gulf (Figure 2.1). Lakes are scarce in the central hills, but there are numerous small lakes elsewhere in the Park.

Fauna

A large variety of habitats in Tuktut Nogait National Park support a high faunal biodiversity: 22 species of mammals, 81 species of birds and 21 species of fishes are known to occur in or near the Park (Zoltai et al. 1992). Common mammals include: Arctic ground squirrel, collared lemming, tundra vole and arctic fox. Less common mammals include: arctic hare, brown lemming wolf, red fox, barren ground grizzly bear, ermine, wolverine and muskox (Zoltai et al. 1992). Polar bears also occur in coastal areas (Zoltai et al. 1992).

The Melville Hills and other areas to the west are the traditional calving grounds for the Bluenose caribou herd. The windswept hills make ideal calving habitat as they are dry and relatively free of insects. One survey estimated the size of the herd to be 95,000, with a range extending 29 000 km^2 between the Mackenzie and Coppermine rivers, and north of Great Bear Lake to the Arctic Ocean (Hawley et al. 1979).

The major rivers in the Park carve steep canyons with cliffs as high as 100m. These cliffs, in addition to large rock outcrops, provide ideal nesting habitat for birds of prey. There is a large Peregrine Falcon population in the canyons of the Hornaday River; Gyrfalcons are also present, but are less common (Zoltai et al. 1992). Golden Eagles and Rough Legged Hawks are also common in this area (Zoltai et al. 1992).

Flora

The exceptionally high floristic diversity in Tuktut Nogait National Park is thought to be the result of extensive glacial refugia in the central regions during the Wisconsinan and Pleistocene periods (Zoltai et al. 1992). Regional flora include 103 species of bryophytes, 158 species of lichens, 236 species of vascular plants (Zoltai et al. 1992).

Most of the vegetation within the park is characteristic of the Low-Arctic Ecoclimatic region, with some areas more characteristic of the Mid-Arctic Ecoclimatic region, and five main vegetation communities exist within the Park (Zoltai et al. 1992). A barren **Herb-nudum** community exists on excessively drained sandy and gravely soils. In scattered patches *Potentilla spp., Astragalus alpinus, Hedysarum alpinum,* and *Dryas integrifolia* are found. **Dwarf Shrub-Herb-Sedge** is found on calcareous soils and is dominated by *Dryas integrifolia* and *Kobresia myosuroides* with *Salix arctica* in wetter areas. *Hedysarum alpinum, Oxytropis maydelliana* and *Astragalus alpina* are often present. **Cottongrass-Willow** is present on quartzite bedrock. In wetter areas the non-tussock-forming cottongrass *Eriophorum scheuchzeri* occurs with *Sphagnum spp.*. In better drained areas tussock forming *Eriophorum vaginatum* and *Salix arctica* are dominant. **High Shrub** is found in closed stands on south facing slopes and alluvial sites. *Salix spp,* with herbs and grasses form the ground vegetation. *Equisetum pratense* is also present on alluvial sites. **Sedge Meadow** is common in wet sites. Dominant species include: *Carex aquatilus, C. saxatilis, C. membranaceae.* Other common species include: *Saxifraga hirculus, Polygonum viviparum,* and *Pedicularis sudetica.*

2.2. METHODS

A total of 18 1x1 km sample sites were located in areas with homogeneous vegetation, few lakes, and relatively simple topography (Figure 2.1). Most sites were located within hiking distance (~10 km) of 3 base camps located at Cache Lake (68° 53'N, 122° 49'W), Roscoe River (69° 22'N, 121° 24'W), and Seven Islands Lake (69° 16'N, 122°58'W) (Figure 2.1). Several sites were accessed by helicopter (n=3). Within each 1x1 km sample site, 9 30x30 m plots were located in a 3x3 grid. Within each 30x30 m plot, 5 1x1 m quadrats were located in a cross pattern. Within each quadrat, percent ground cover of water, rock, bare ground, moss, lichen, dwarf shrub, and graminoid/ herbaceous vegetation was visually determined. A detailed description of the sampling design is provided in the following section.

Vegetation classes defined for the present study emphasized the structural properties of the vegetation, rather than species composition. These classes were intended to characterize and categorize the range in vegetation productivity within the Park, while enabling the classes to be separated spectrally in a Landsat vegetation classification. Furthermore, it was necessary to define classes that could be matched to those defined elsewhere in the literature. This was necessary in order to assign an expected annual productivity value to each of the classes. The dominant vegetation class within each site was determined from the mode of the vegetation class assigned to each 30x30 m plot within each site.

2.3. RESULTS AND DISCUSSION

Table 2.1 provides a floristic and physiographic description for each of the vegetation classes identified in Tuktut Nogait National Park. Figure 2.2 summarizes the vegetation and ground cover typical of these classes. This summary is based on mean cover data determined within each of the 30x30 m plots. The dominant vegetation class within each 1x1 km site is determined from the mode of the vegetation classes assigned to each 30x30 m plot within each site (Table 2.2). Mean percent cover of each ground cover type, as well as mean dry green biomass and mean NDVI were determined from the field measurements (Table 2.2). The photographs in Figure 2.3 provide a visual description for each of the defined vegetation types.

Table 2.1. Physiographic and floristic descriptions of the vegetation classes identified in Tuktut Nogait National Park, NWT.

Class	Vegetation Cover	Substrate	Wetness	Dominant Vegetation Type	Dominant Species
Barren Ground	< 10 %	Mineral; clay/ sand/ gravel/ rock	Dry.	Small tufts of prostrate herbs; crustose lichens	*Dryas integrifolia, Cetraria spp., Saxifraga spp.,*
Sparsely Vegetated	10 - 50%	Sandy clay loam/ pebbles/ rocks/ boulders/ bedrock outcrops.	Variable: xeric to wet.	Small patches of dwarf shrubs; small sedges.	*Dryas integrifolia, Kobresia mysuroides, Cassiope tetragona, Silene acaulis, Cetraria spp.*
Dwarf Shrub Tundra.	100%	Organic sandy loam.	Dry to mesic.	High dwarf shrub cover. Some sedge	*Lupinus arcticus, Cassiopea tetragona, Silene acaulis, Betula glandulosa, Eriophorum angustifolia, Carex spp., Arctostaphylus sp., Rhododendron laponicum., Salix spp., Dryas spp., Euliginosum sp.*
Mesic Meadow	100%	Organic sandy loam.	Mesic.	High graminoid cover with some dwarf shrubs.	*Eriophorum angustifolia, Carex sp., Equisetum arvense, Hedysarum mackenzii, Tofieldia pusilla, Dryas integrifolia, Arctostaphylos sp.*
Tussock Tundra	100%	Organic Peat	Mesic to Wet.	Cotton grass tussocks with dwarf shrubs and sphagnum growing between tussocks	*Eriophorum vaginatum, Ledum decumbens Sphagnum teres, S. russowii, Salix arctica, Vaccinium vitis-idea, Arctostaphylus sp.*
Wet Sedge Meadow	100%	Organic clay loam.	Wet. Some standing water.	Graminoid dominant.	*Carex aquatilus, Eriophorum angustifolia, Salix spp., Carex membranacea, Saxifraga hirculus, Polygonum viviparum.*

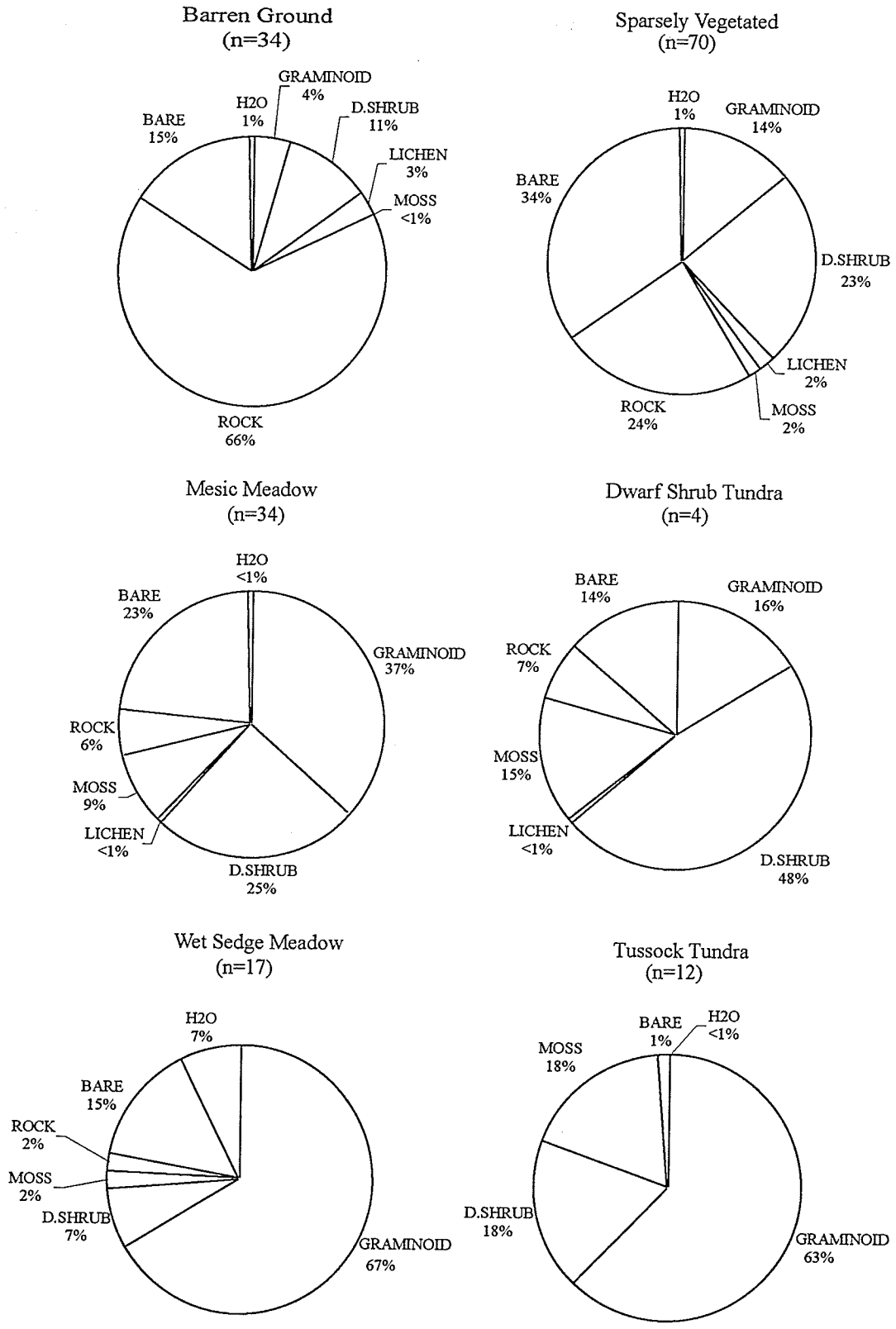

Figure 2.2. Average percent ground cover for each vegetation class. Mean values determined for cover within each 30x30 m field plot. D.Shrub = Dwarf Shrub.

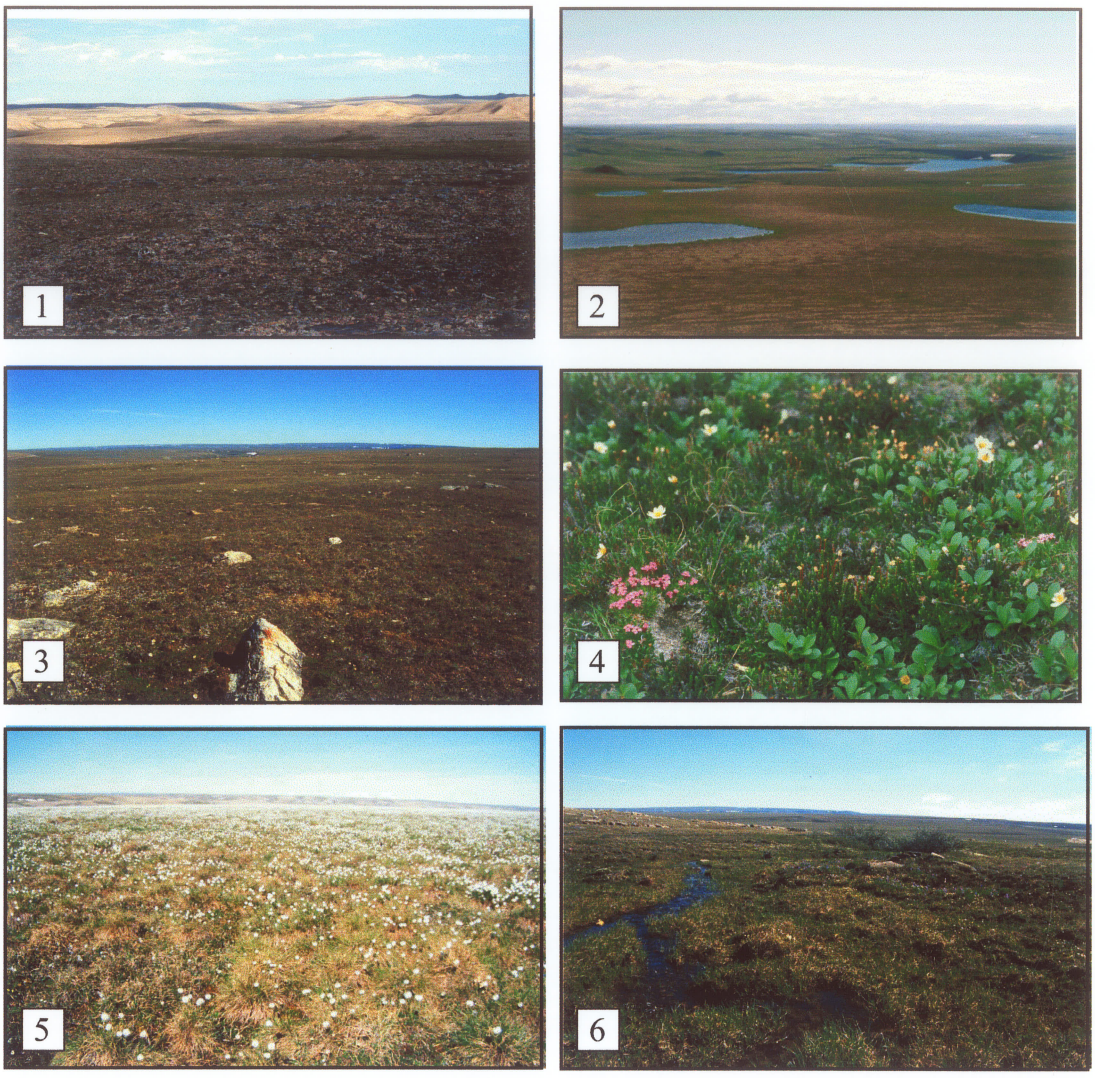

Figure 2.3. Photographs of the vegetation classes defined for Tuktut Nogait National Park. 1) Barren Ground: Small isolated plants, <10% cover; 2) Sparsely Vegetated Ground: Dwarf shrubs and prostrate herbs, 10-50% cover; 3) Mesic Meadow: Hummocky sedge/moss tundra, 100% cover; 4) Dwarf Shrub Tundra: Ericaceous shrubs, dwarf willows, lupins and moss; 5) Tussock Tundra: Cottongrass tussocks, dwarf shrubs, sphagnum moss; 6) Wet Sedge Meadow: Sedges, moss, water at the surface.

Table 2.2. Summary of field data for each 1x1 km sample site . The dominant vegetation class is determined from the mode of the vegetation classes assigned to each 1x1m quadrat. Values for ground cover, biomass and NDVI are computed from the mean value of the 45 1x1 m quadrats within each 1x1 km sample site.

		Percent Cover									
1x1 km Sample Site	**Dominant Vegetation Class**	**Total Vegetation Cover (%)**	**Graminoid (%)**	**Dwarf Shrub (%)**	**Lichen (%)**	**Moss (%)**	**Rock and Gravel (%)**	**Bare Soil (%)**	**Water (%)**	**Dry Green Biomass (g/m^2)**	**NDVI**
1	Sparsely Vegetated	43.78	16.89	21.89	3.33	1.67	22.78	33.27	0.00	18.35	0.30
2	Sparsely Vegetated	45.76	17.93	24.67	2.22	0.93	14.22	38.87	1.33	20.76	0.41
3	Wet Sedge Meadow	82.56	73.78	8.22	0.00	0.56	0.44	7.56	9.22	28.50	0.49
4	Sparsely Vegetated	59.04	29.62	28.91	0.36	0.16	8.00	30.44	2.44	13.00	0.37
5	Tussock Tundra	98.44	59.22	18.11	0.00	21.11	0.00	1.56	0.00	55.90	0.60
6	Mesic Meadow	63.33	47.89	13.78	0.00	1.67	7.69	24.87	3.22	20.23	0.42
7	Sparsely Vegetated	31.38	10.87	19.11	0.40	1.00	25.22	44.13	0.00	9.85	0.24
11	Mesic Meadow	62.33	21.22	36.33	0.00	4.78	10.22	27.89	0.00	68.30	0.55
12	Mesic Meadow	83.33	40.78	25.00	0.44	17.11	1.89	14.78	0.00	63.33	0.58
13	Mesic Meadow	53.56	23.00	25.33	1.89	3.33	18.44	28.56	0.00	n/a	0.43
14	Barren Ground	15.91	3.11	9.93	2.76	0.11	76.89	7.24	0.00	12.13	0.13
15	Barren Ground	19.36	4.44	10.91	3.78	0.22	59.42	21.18	0.00	30.49	0.15
16	Barren Ground	21.53	7.04	11.73	2.09	0.67	60.58	17.84	0.11	23.00	0.18
17	Barren Ground	27.76	9.80	15.69	2.04	0.22	54.58	14.56	3.22	15.97	0.20
19	Sparsely Vegetated	35.27	14.40	15.04	1.62	4.20	51.60	12.93	0.33	62.15	0.25
20	Sparsely Vegetated	38.13	12.29	21.00	1.16	3.69	18.78	43.09	0.00	35.70	0.35
21	Sparsely Vegetated	52.09	15.78	30.38	0.67	5.27	8.22	38.51	0.00	51.50	0.42
22	Tussock Tundra	77.84	36.67	28.22	1.82	11.13	7.67	14.84	0.11	n/a	0.59

The Tussock Tundra class can be considered equivalent to the Cottongrass-Willow community described by Zoltai et al. (1992). Tussock tundra is commonly described in the literature as being dominated by *Eriophorum vaginatum,* which co-occurs with *Betula nana, Vaccinium spp., Ledum decumbens* and *Sphagnum spp.* (Bliss et al. 1973; Shaver and Chapin 1986; Shaver and Chapin 1991; Chapin et al. 1996; Shaver et al. 1997). Cover in the tussock tundra plots was predominantly graminoid (i.e. Cottongrass), with high dwarf shrub and moss cover, with low bare ground and water cover (Figure 2.2).

The Wet Sedge Meadow class can be considered equivalent to the Sedge Meadow community defined by Zoltai et al. (1992). Wet Sedge Meadow is also commonly described in the literature, with *Carex aquatilus* consistently identified as the dominant species (Muc 1973; Haag 1974; Miller et al. 1980; Shaver and Chapin 1991; Gilmanov and Oechel 1995; Shaver and Chapin 1991). In the wet sedge meadow plots, graminoid cover dominated, with some dwarf shrub cover, some moss cover, and relatively high bareground and water cover (Figure 2.2).

The Dwarf Shrub Tundra vegetation class covers a range of shrub communities with similar structural properties, and overlaps with the Dwarf Shrub-Herb-Sedge and High Shrub classes defined by Zoltai et al. (1992). Various Low Arctic shrub communities are defined in the literature including: heath tundra and hillslope shrub-lupin (Shaver and Chapin 1991; Shaver et al. 1997); birch-willow-heath (Miller et al. 1980); and low shrub (Bliss and Matveyeva 1992). Common to all these communities is the presence of short statured deciduous and evergreen shrubs, lupins, herbs and mosses. This vegetation type occurs in small patches, and was dominant in only a small number

of field plots (n=4). These plots were dominated by dwarf shrub cover, with high graminoid/ herb and moss cover and some rock and bareground cover (Figure 2.2).

The Mesic Meadow vegetation class represents a transition between the wetter Sedge Meadow and the Herb-Nudum communities described by Zoltai et al. (1992). This class corresponds to a variety of low arctic vegetation communities identified in the literature, including: hummocky sedge-moss meadow (Bliss et al. 1973); frost boil sedge moss meadow (Muc 1973); and mesic, moist and herb-moss meadows (Gilmanov and Oechel 1995). Plant species in the Mesic Meadow field plots coincided with the community descriptions described in the literature, and consisted of a mix of graminoids and dwarf shrubs with some mosses, with higher bareground and rock cover than the Dwarf Shrub Tundra and Wet Sedge Meadow classes (Figure 2.2).

The Sparsely Vegetated and Barren classes are similar to the Herb-Nudum and Dwarf-Shrub-Herb-Sedge communities described by Zoltai et al. (1992). However, the Sparsely Vegetated and Barren classes represent the low end of the productivity spectrum covered by these communities. Communities described in the literature that are similar to the Sparsely Vegetated class, include: cushion plant (Bliss et al. 1984); and cryptogamic crust and polar desert (Bliss and Gold 1999). The Barren class is similar to the polar desert and polar barrens described by Bliss et al. (1973), Bliss et al. (1984), and Bliss and Matveyeva (1992). In plots designated Sparsely Vegetated, bareground and rock cover was high with considerable graminoid and dwarf shrub cover and little lichen and moss cover (Figure 2.2). Comparatively, the Barren plots had higher rock cover, and very little graminoid and dwarf shrub cover and lichen cover was relatively high (Figure 2.2).

3. MEASURING TERRESTRIAL NET PRIMARY PRODUCTIVITY IN ARCTIC ECOSYSTEMS USING AVHRR SATELLITE IMAGERY

3.1. ABSTRACT

A method is presented for computing terrestrial net primary productivity (NPP) for low-arctic vegetation using the AVHRR satellite image products produced by the GEOCOMP-n image processing system. The NPP model is parameterized using a combination of field data collected in Tuktut Nogait National Park, NWT during the summer of 2000, as well as data available from previous research. The model results are evaluated using a map of expected annual net productivity produced from a Landsat TM vegetation classification and expected annual NPP values compiled from the literature. Proportion of water cover and vegetation cover and topographic complexity within each pixel are measured, and the influence of these variables on the difference between modelled and expected values are evaluated.

Annual NPP computed using the modified soil adjusted vegetation index (MSAVI) showed the best correspondence with the expected annual NPP map, with 84 % of the modelled annual NPP values within 30% of the expected annual NPP values. Within Tuktut Nogait National Park, the average annual NPP for 2000 was 149.4 (±68.4) g/m^2yr. Highest productivity occurred along the east side of the Hornaday River Valley. Lowest productivity occurred in the central region of the Park along the Melville Hills, and in the northeast region of the Park near the coast. Onset of the growing season occurred between June 1 and June 11. NPP was highest between July 1 and July 11, with mean NPP at 22.61(±11.1) g/m^2*10-days. The growing season ended between September 11 and September 21.

Topography and water cover had significant effects on the regression between modelled NPP and expected NPP. With increasing water cover within the AVHRR pixels, modeled NPP values tended to be greater than expected. In areas with complex topography (i.e., high slope variance within the AVHRR pixels), the model may underestimate NPP. In areas with steep terrain (high mean slope within the AVHRR pixels), the model NPP estimates are higher than expected. Although significant, the effect of these variables on the overall regression was relatively small.

3.2. INTRODUCTION

The remoteness, inaccessibility, and large spatial extent of the Canadian arctic makes remote sensing a necessary tool for monitoring arctic ecosystems at the landscape scale. High resolution satellite imagery (e.g. Landsat TM and SPOT HRV) has been used to study arctic vegetation phenology (Shippert et al. 1995; Walker et al. 1995), but such data sources are expensive and not regularly available. An alternative source of data is from the advanced very high resolution radiometer (AVHRR) carried aboard National Oceanic and Atmospheric Administration (NOAA) satellites. Although AVHRR data are of lower spatial resolution (1x1 km), images are inexpensive and cloud-free composites are available over 10-day intervals. With a 10-day measurement frequency it is possible to detect both annual and inter-annual trends in arctic vegetation phenology (Hansen 1991; Markon et al. 1995; Walker 1999). As part of the Northern National Parks Ecological Monitoring Program (McCanny 1998), Parks Canada is currently receiving GEOCOMP-n AVHRR satellite image coverage for 11 northern national parks in Canada. The main challenge of this research is to develop the methodology to utilize these data in order to effectively measure arctic vegetation productivity.

Background

Coarse-scale estimates of annual terrestrial NPP are available by interpolating average annual NPP values across the total area defined for each vegetation class in a tessellated vegetation map (Gilmanov and Oechel 1995). However, this method assumes homogeneity within each vegetation class polygon, and it is impossible to infer any spatial or temporal variation within the defined landscape class.

Climate or statistical NPP models link vegetation productivity to meteorological parameters and/or evapotranspiration using regression analysis (Leith 1975; Melillo et al. 1993). This approach assumes that climate regulates nutrient availability and other factors influencing NPP. Because these models are based solely on climate simulation, they are useful for producing NPP estimates over very long time periods; however, climate models assume that natural ecosystems tend toward fixed combinations of species with functional properties that vary consistently with climate and resources (Field et al. 1995). Thus, they provide no insight into non-equilibrium phenomena.

Process or mechanistic NPP models utilize knowledge and measurements of the biophysical properties directly influencing vegetation productivity (i.e. decomposition rates, nutrient availability, photosynthesis, respiration, and transpiration) (Miller et al. 1976; Field et al. 1995; Liu et al. 1997; Vourlitis et al. 2000). Estimates of NPP using a process model should be more reliable than other methods because they are based on a detailed understanding of the ecosystem. For example, the boreal ecosystem productivity simulator (BEPS), developed at the Canadian Centre for Remote Sensing (CCRS), operates at large scales (10^6 to $10^7 km^2$) at a 1 km resolution (Liu et al. 1997). BEPS models the soil-plant-atmosphere processes influencing vegetation productivity, utilizing remote sensing, GIS, and meteorological techniques to derive the input variables. It requires daily meteorological inputs, and calculates NPP on a daily and annual basis. However, this approach is limited by the availability and quality of data required to measure these parameters. In areas lacking ground measurements these processes must either be simulated or interpolated from available data. Furthermore, BEPS uses algorithms calibrated for conifer and deciduous forest stands, which, for lack of

validation data, are unreliable in arctic tundra (Liu et al. 1997). Thus, in arctic regions generalized constants and interpolated data must be used to derive NPP estimates, resulting in a dramatic loss of spatial detail and accuracy.

Attempts have been made to estimate NPP directly from spectral vegetation indices computed from remotely sensed satellite imagery at both local (Stow et al. 1998) and global scales (Goward et al. 1985; Box et al. 1989). Because vegetation is absorptive of visible light (380-710nm), and reflective of NIR light (710-1000nm), a ratio of NIR to Red light reflectance is directly related to photosynthetic biomass:

$$SR = NIR / Red \qquad [1]$$

where SR is the simple ratio (Jordan 1969; Carneggie et al. 1975). However, direct relationships between the simple ratio and vegetation biomass are highly variable across space and time (Colwell 1971; Rouse et al. 1973; Smith and Oliver 1974). To correct for the angular effects of bi-directional spectral reflectance under varying sun-sensor angles, the ratio is normalized by dividing the difference of NIR and Red reflectance by the sum:

$$NDVI = (NIR-Red) / (NIR+Red) \qquad [2]$$

where NDVI is the normalized difference vegetation index (Rouse et al. 1973). The NDVI is based on proportions of the original values, and as intended the error component due to spatial and temporal variation is much reduced compared to using the simple ratio (Tucker 1979). At a local scale (i.e. 1-10m), there is a strong positive correlation between NDVI and photosynthetic biomass for temperate grasslands and crops (Rouse et al. 1973; Tucker 1979; Holben et al 1980; Townsend and Tucker 1984), as well as subarctic

vegetation (Hansen 1991). When integrated over the growing season, NDVI measured from 1x1 km resolution AVHRR imagery produced relative estimates of annual NPP that correspond well with annual NPP values reported in the literature (Goward et al. 1985; Box et al. 1989; Los et al. 1994).

Estimating NPP at large scales using a direct relationship with NDVI is problematic because relationships between NPP and NDVI are highly variable for different vegetation types. In shrublands and forests, the relationship between NIR reflectance and vegetation biomass is highly variable, producing NDVI values considerably lower than for other community types (Peterson et al. 1987; Ranson and Williams 1992; Chen 1996; Walker and Kenkel 2000). The influence of physiographic features inherent to areas of complex terrain, high latitudes and extreme deserts results in extreme NDVI values that are not representative of the underlying vegetation (Box et al. 1989; Paruelo et al. 1997). In arctic environments, unique vegetation spectral surfaces (e.g. lichens), low vegetation cover, highly variable ground moisture, the presence of numerous water bodies, variable topography, and low sun angle can influence NDVI values in unpredictable ways (Hope et al. 1995; Markon et al. 1995; Shippert et al. 1995; Rees et al. 1998). Furthermore, using NDVI measured from 1x1 km resolution AVHRR imagery presents a challenge in separating information about the vegetation from the background noise. Typically, landscape features in arctic ecosystems have a spatial resolution of less than 1 km, with the dimensions no larger than 700 m^2 (Stow et al. 1998). The background reflectance from unvegetated surfaces, numerous water bodies, and variable topography all contribute to the reflectance signal received by the satellite, making it difficult to resolve the vegetated component of the pixel. Although NDVI has

been related to annual productivity and vegetation biomass, it is difficult to measure inter-annual patterns of NPP using NDVI. NDVI is a cumulative measure of aboveground vegetation biomass from the beginning of the growing season, whereas NPP is a measure of accumulated above- and belowground biomass within a specific time period.

NPP Model Description

A NPP model that relies exclusively on remotely sensed data is ideally suited for measuring arctic vegetation productivity (e.g. Prince and Goward 1995; Goetz et al. 1999). Such a model enables estimation of primary productivity in remote areas where detailed ground data are unavailable. Typically, landscape-scale productivity models that utilize remotely sensed data compute NPP (i.e., the accumulation of phytomass per unit area over time) as a linear function of the amount of photosynthetically active radiation absorbed by vegetation:

$$NPP = \varepsilon \, APAR_{can} - R_a \qquad [3]$$

where ε is the energy to dry matter conversion coefficient (g/MJ); $APAR_{can}$ is the amount of photosynthetically active radiation (PAR) absorbed by the vegetation canopy over a given time period (MJ/m^2); and R_a is autotrophic plant respiration (Prince 1991; Law and Waring 1994; Ruimy et al. 1994; Prince and Goward 1995; Paruelo et al. 1997; Goetz et al. 1999).

Photosynthetically Active Radiation Absorbed by the Canopy: $APAR_{can}$

$APAR_{can}$ is determined by measuring incident photosynthetically active radiation ($PAR\downarrow$), and estimating the fraction that is absorbed by the canopy (FPAR):

$$APAR_{can} = PAR\downarrow * FPAR \qquad [4]$$

The PAR incident to the canopy ($PAR\downarrow$) can be determined by estimating the reduction in the total incident solar radiation at the top of the atmosphere (a constant) by atmospheric attenuation and cloud and aerosol scattering. However, this method requires knowledge about cloud reflectance and atmospheric conditions, which must be estimated from satellite measurements of UV reflectance (Eck and Dye 1991) or from artificial data generated using a weather simulator (Paruelo et al. 1997). Alternately, total surface PAR absorption ($APAR_{sfc}$) can be computed from the difference of upwelling and downwelling PAR measured at the top of the atmosphere, and an atmospheric correction for ozone absorption, aerosol scattering and aerosol absorption (Li and Moreau 1996; Figure 3.1). $PAR\downarrow$ is then computed by dividing $APAR_{sfc}$ by 1- (surface PAR albedo). This method provides more accurate estimates of $APAR_{sfc}$ for all sky conditions, as it does not require knowledge of cloud reflectance, or assumptions about the fraction of the total solar radiation reaching the surface as PAR (Li and Moreau 1996; Cihlar et al. 1997b; Gower et al 1999). GEOCOMP-n computes daily mean $APAR_{sfc}$ using this method. Thus, $APAR_{can}$ is calculated as:

$$APAR_{can} = APAR_{sfc} / (1 - A_{par}) * FPAR \qquad [5]$$

where A_{par} is surface PAR albedo (a unitless proportion) (Moreau and Li 1996). A_{par} is measured by integrating clear-sky measures of visible surface reflectance (i.e. AVHRR

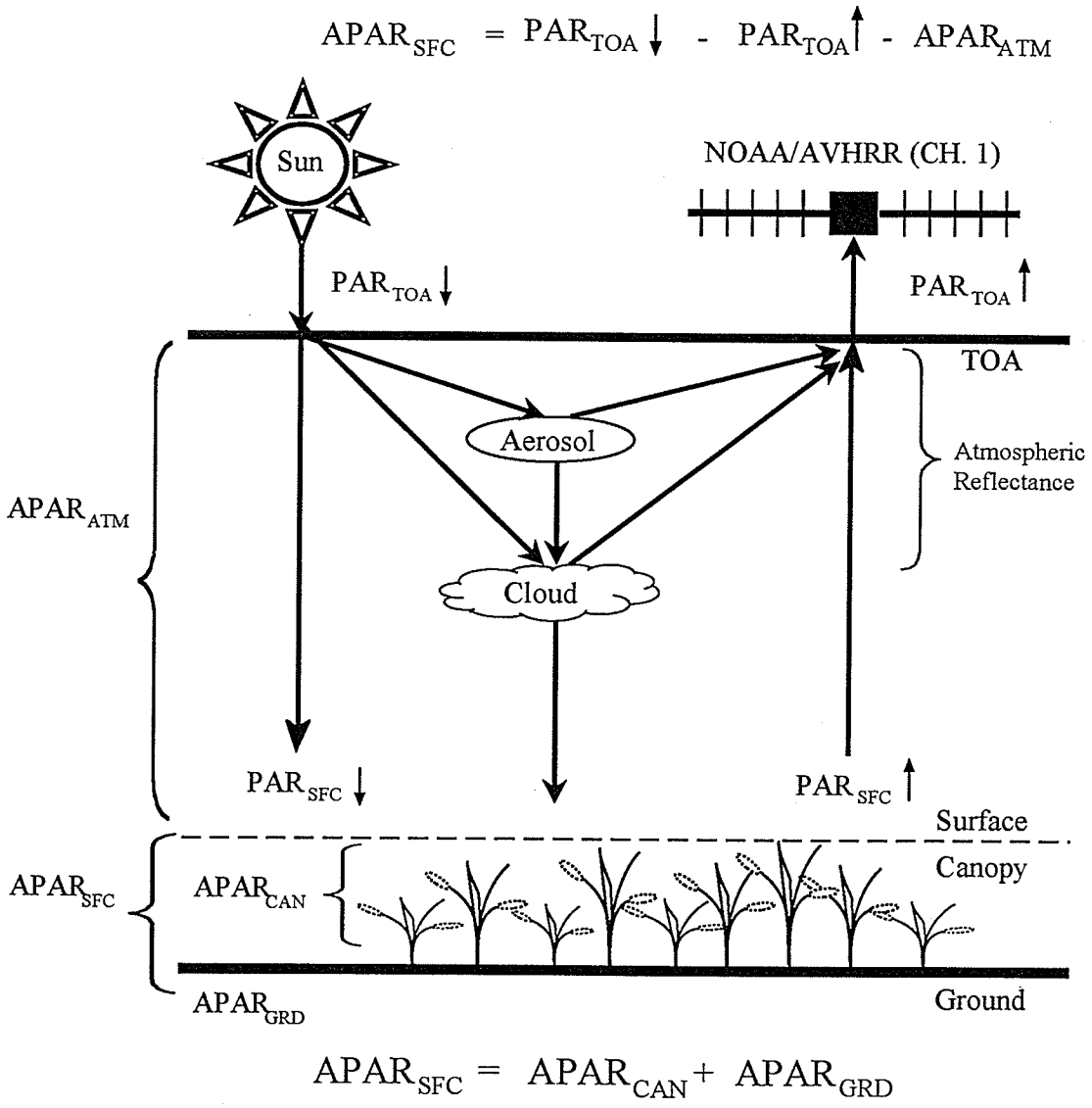

Figure 3.1. Diagram illustrating the method and parameters used by GEOCOMP-n to compute $APAR_{sfc}$ from AVHRR band 1 reflectance. The amount of photosynthetically active radiation absorbed by the surface ($APAR_{sfc}$) is equal to the difference of the downwelling PAR (PAR↓) and upwelling PAR (PAR↑) at the top of the atmosphere and then further reduced by the amount of PAR absorbed by the atmosphere ($APAR_{atm}$). $APAR_{sfc}$ is the sum of the PAR absorbed by the photosynthetic component of the surface ($APAR_{can}$) and the PAR absorbed by the soil and non-photosynthetic components of the surface ($APAR_{grd}$). Diagram adapted from Li and Moreau (1996).

channel 1) over the PAR spectrum, and correcting for atmospheric and bidirectional reflectance effects (Cihlar et al. 1997a).

The inclusion of A_{par} in equation [5] is necessary to convert $APAR_{sfc}$ to PAR↓. If $APAR_{sfc}$ is the difference between downwelling PAR (PAR↓) and upwelling PAR (PAR↑) measured above the canopy:

$$APAR_{sfc} = PAR\downarrow - PAR\uparrow \qquad [6]$$

and the canopy albedo is equivalent to the proportion of upwelling PAR to downwelling PAR:

$$A_{par} = PAR\uparrow / PAR\downarrow \text{ or } PAR\uparrow = A_{par} * PAR\downarrow \qquad [7]$$

then, substituting equation [7] for PAR↑ in equation [6] gives:

$$APAR_{sfc} = PAR\downarrow * (1 - A_{par}) \text{ or } PAR\downarrow = APAR_{sfc} / (1 - A_{par}) \qquad [8]$$

Fraction of PAR Absorbed by the Canopy: $FPAR_{can}$

$FPAR_{can}$ is estimated from an empirical relationship with a spectral vegetation index, such as the normalized difference vegetation index (NDVI) (Asrar et al. 1984; Goward and Huemmrich 1992; Begue and Myneni 1996; Braswell et al. 1996; Moreau and Li 1996). There is experimental evidence, and theoretical substantiation, that FPAR is a monotonic but slightly non-linear function of NDVI (Goward and Huemmrich 1992). However, the relationship is typically defined as linear to preserve scale invariance (Begue and Myneni 1996). FPAR-NDVI relations have been defined from empirical measurements of FPAR from PAR sensors positioned above and below a canopy (Asrar

et al. 1984; Hatfield et al. 1984; Peterson and Running 1989; Peterson et al. 1990; Chen 1996). The variation in FPAR calculated with these models is large, as each relation is specific to a particular vegetation type and sensor configuration (Table 3.1 a).

Global productivity modelers often require a relationship between NDVI and FPAR that is applicable across many vegetation types. This relationship is often developed from a linear interpolation between maximum and minimum NDVI values measured directly from satellite data (Ruimy et al. 1994; Sellers et al. 1994). The Max/Min method assumes that the FPAR–NDVI relationship is linear, that maximum measured NDVI values correspond to a FPAR value nearly equal to 1, and that minimum NDVI values corresponds to a FPAR value equal to 0. The range in these relations is very large and can be attributed to variability in image processing, as well as differences in the choice of location and time for the Max/ Min NDVI measurements (Table 3.1 b).

More commonly, models of radiative transfer are used to simulate the interaction between incident light and a vegetated surface in order to derive the relationship between FPAR and NDVI. Generally, radiative transfer models assume a fully vegetated, homogenous surface and are parameterized to a specific vegetation type (Baret et al 1989; Leon 1991; Goward and Huemmrich 1992; Goward et al. 1994; Moreau and Li 1996). Considerable variation also exists between relations derived from these models. Furthermore, such models tend to oversimplify canopy structure, making them inapplicable to heterogeneous vegetation canopies (Table 3.1 **c**).

To account for canopy heterogeneity, three-dimensional radiative transfer models have been designed that simulate an incomplete canopy as well as incorporating

Table 3.1 Summary of relationships defined for FPAR and vegetation indices compiled from the literature. NDVI = Normalized Vegetation Index; SR = Simple Ratio; SAVI = Soil adjusted Vegetation Index; MSAVI = Modified Soil Adjusted Vegetation Index.

	Algorithm	R^2	Method	Vegetation Type	Reference
a)	FPAR = 1.25 * NDVI - 0.11	-	PAR Measurements	Spring wheat. Growing Phase	Asrar et al. 1984
	FPAR = 1.2 * NDVI - 0.18	0.974	PAR Measurements	Spring wheat. Growing Phase	Hatfield et al. 1984
	FPAR = 1.28 * NDVI - 0.14	-	PAR Measurements	Corn, soybeans. Growing Pase	Daugherty 1988
	FPAR = 1.408 * NDVI - 0.396	0.92	PAR Measurements	Alfalfa	Pinter 1993.
	FPAR = 0.6 - (2.2 * NDVI) + (2.9 * $NDVI^2$)	-	PAR Measurements	Corn. Growing Phase	Gallo et al. 1985
	FPAR = 1.23 * NDVI - 0.06	-	PAR Measurements	Winter Wheat. Growing Phase	Baret and Olioso, 1989
	FPAR = 1.0 * NDVI - 0.20	-	PAR Measurements	Conifers	Peterson and Running 1989
	FPAR = 1.27 * NDVI - 0.31	0.73	PAR Measurements	-	Hall et al. 1992
	FPAR = 2.21 * NDVI - 0.681	0.665	PAR Measurements	-	Hall et al. 1992
b)	FPAR = 1.25 * NDVI - 0.025	-	MAX / MIN	Rainforest/ Desert	Ruimy et al. 1994
	FPAR = 0.279 * SR - 0.294	-	MAX / MIN	Alaska in winter/ theoretical max	Helman and Keeling 1989
	FPAR = 1.468 * NDVI - 0.381	-	MAX / MIN	Rainforest/ Desert	Loudjani 1993
	FPAR = 0.171 * SR - 0.186	-	MAX / MIN	Tall Vegetation/ Desert	Sellers et al. 1994
	FPAR = 0.248 * SR - 0.268	-	MAX / MIN	Short Vegetation/ Desert	Sellers et al. 1994
	FPAR = 1.27 * NDVI - 0.190	-	MAX / MIN	Niger: before/ After Rainy season	Ouaidrari 1994
c)	FPAR = 1.33 * NDVI - 0.31	-	1D Radiative Transfer Model	-	Baret and Olioso 1989
	FPAR = 1.24 * NDVI - 0.23	-	1D Radiative Transfer Model	-	Baret et al. 1989
	FPAR = 1.28 * NDVI - 0.15	-	1D Radiative Transfer Model	-	Leon 1991
	FPAR = 1.08 NDVI - 0.08	0.99	1D Radiative Transfer Model	-	Goward and Heummerich 1992
	FPAR = 1.164 * NDVI - 0.143	0.92	1D Radiative Transfer Model	-	Myneni and Williams 1994
	FPAR = 1.21 * NDVI - 0.04	0.99	1D Radiative Transfer Model	-	Goward et al. 1994
	FPAR = 1.67 * NDVI - 0.08	-	1D Radiative Transfer Model	-	Prince and Goward 1995
	FPAR = 0.8462 * NDVI - 0.08014	0.92	3D Radiative Transfer Model	Sparse vegetation	Myneni et al. 1992
	FPAR = 1.164 * NDVI - 0.143	0.92	1D Radiative Transfer Model	-	Myneni and Williams 1994
	FPAR = 0.105 - (0.323 * NDVI) + (1.468 * $NDVI^2$)	0.85	1D Radiative Transfer Model	-	Moreau and Li 1996
	FPAR = 3.257 * SAVI - 0.070	0.86	1D Radiative Transfer Model	-	Moreau and Li 1996
	FPAR = 1.189 * NDVI - 0.025	0.909	3D Radiative Transfer Model	Savannah Vegetation	Begue and Myneni 1996
	FPAR = 1.723 * MSAVI - 0.137	0.968	3D Radiative Transfer Model	Savannah Vegetation	Begue and Myneni 1996
	FPAR = 2.213 * (ΔMSAVI) **	0.931	3D Radiative Transfer Model	Savannah Vegetation	Begue and Myneni 1996
	FPAR = 1.710 * (ΔNDVI) **	0.931	3D Radiative Transfer Model	Savannah Vegetation	Begue and Myneni 1996

** Δ indicates the difference between pre-onset and post -onset vegetation index values.

vegetation clumping parameters and soil background reflectance (Myneni et al. 1992). Begue and Myneni (1996) derived relationships between FPAR and two vegetation indices, NDVI and the modified soil adjusted vegetation index (MSAVI) (Qi et al. 1994). Best estimates of FPAR were derived from a relation with MSAVI measured from AVHRR data (Begue and Myneni 1996). Subtracting pre-onset of the growing season MSAVI values from MSAVI acquired during the growing season further minimized background effects (Begue and Myneni 1996). However, these algorithms were calibrated for Savannah vegetation, which differs spectrally and structurally from arctic vegetation. Applying an FPAR algorithm calibrated for temperate vegetation to arctic vegetation could produce erroneous results. For example, in sparsely vegetated landscapes where vegetation index values are extremely low, FPAR will be overestimated as a result of the slight non-linearity of the relationship between vegetation indices and FPAR. It is therefore necessary to derive an FPAR relationship specific to arctic vegetation from empirical ground data, rather than adopting a relationship derived for temperate vegetation.

Energy conversion coefficient: ε

The energy conversion coefficient (ε) is the amount of carbon fixed (g/m^2) per unit of PAR absorbed by the canopy (MJ/m^2). It is estimated from the slope of the relation between empirically derived GPP measurements and $APAR_{can}$ (Law and Waring 1994; Ruimy et al. 1994; Paruelo et al. 1997). When first defined, ε was determined as the slope of the relationship between NPP and $APAR_{can}$ (Monteith 1972; Asrar et al. 1985). A

number of agricultural NPP experiments that have measured ε in this way produced estimates ranging between 0.2 and 4.8 g/MJ (Prince 1991). This variability has been attributed to large differences in rates of growth and maintenance respiration among species, and the influence of environmental stressors on photosynthetic efficiency such as low or high temperature, high vapour pressure deficit, and drought (Prince 1991; Runyon et al. 1994; Law and Waring 1994; Hunt 1994). Defining the energy conversion coefficient in terms of gross primary productivity (GPP) enables variability in respiration to be considered separately (Jarvis and Leverenz 1983; Prince 1991; Goetz et al. 1999). NPP can then be obtained by subtracting respired carbon from the GPP.

The energy conversion coefficient has been defined as the theoretical maximum of GPP per MJ of absorbed PAR (ε_{max}) using the quantum yield for C3 photosynthesis under ideal environmental conditions (Jarvis and Leverenz 1983; Goward et al. 1994; Prince and Goward 1995). Productivity models that utilize ε_{max} must also include parameters to quantify the reduction in ε_{max} attributable to environmental stressors. It is possible to estimate these environmental variables from AVHRR imagery utilizing NDVI and surface temperature data (Goward et al. 1994; Prince and Goward 1995; Prihodko and Goward 1997); however, these methods are problematic when applied to arctic ecosystems because of the high number of small sub-pixel water bodies inherent to these landscapes (personal observation). The inclusion of environmental parameters can be circumvented by deriving the energy conversion coefficient from the slope of average measures of GPP and $APAR_{can}$ acquired throughout the growing season. Thus, the annual fluctuations in environmental conditions are incorporated into the averages.

Autotrophic Respiration: R_a

Autotrophic respiration (R_a) is the proportion of total ecosystem respiration attributable to plants. Estimating R_a requires knowledge of both above and below-ground biomass. R_a is temperature-dependent and respiration coefficients for many arctic plants are available from the literature (e.g. Billings et al. 1978). Utilizing these coefficients requires data for ambient temperature. Although weather stations exist in many arctic parks, the data represent single points in space separated by large distances. Obtaining spatially continuous measurements of environmental conditions would require interpolating single point values over extremely large distances. As a result, accurate and spatially continuous measurements of most climatic variables are unavailable for most areas of the Arctic. As with the energy conversion coefficient, a respiration parameter derived from annually integrated measurements will incorporate variability attributable to annual fluctuations in temperature and other factors. Respiration can then be directly related to a vegetation index that quantifies vegetation biomass.

Objectives

The primary objective of this paper is to define and calibrate a model to estimate terrestrial NPP in arctic ecosystems from GEOCOMP-n AVHRR data. This objective will be accomplished by:

- defining an empirical relationship between FPAR and a spectral vegetation index; either NDVI or MSAVI,
- determining an Energy Conversion Coefficient (ε) for Low Arctic vegetation,
- determining an empirical relation between a spectral vegetation index (i.e. NDVI) and Autotrophic Respiration (R_a),

- producing a map of expected annual NPP that will be used to validate the results of AVHRR NPP model.

Other objectives include:

- evaluating the influence of sub-pixel water bodies and variable topography on the difference between modelled and expected NPP,
- determining what vegetation types influence discrepancies between modelled and expected ANPP.

3.3. METHODOLOGY

Collection of Field Data

Ground data were collected between July 8th to August 10th, 2000 in three areas within Tuktut Nogait National Park (See Chapter 2: Study Area). A total of 18 (1x1 km) sites were selected to represent the range of vegetation types within the Park. Within each site, 9 (30x30 m) plots were located in a 3x3 grid, located 250 m in from the edge of the site boundary. Within each plot, 5 (1x1 m) sample quadrats were located in a cross pattern (Figure 3.2). Vegetation communities sampled included: tussock tundra, wet sedge tundra, dwarf shrub tundra, sparsely vegetated tundra, and barren ground (See Chapter 2: Study Area).

For each quadrat (n=865), incident and reflected radiance were measured in 5 spectral regions (450-520 nm, 520-600 nm, 630-690 nm, 760-900 nm and 1550-1750 nm) using a Cropscan MSR5 radiometer (Cropscan Inc., www2.isl.net/cropscan). The radiometer was attached to a boom and held 2 meters above the surface, enabling a 1 meter field of view, and the mean of five scans was recorded. The up and down-looking sensor pairs were calibrated, and all radiance measurements were corrected for sensor-temperature effects and variable sun-angle using a post-processing program supplied by the manufacturer. Percent surface reflectance of each sample was calculated from the down- and up-looking radiance measurements. With both up and down-looking sensors it is possible to accurately measure surface reflectance under variable cloud conditions and various sun-angles.

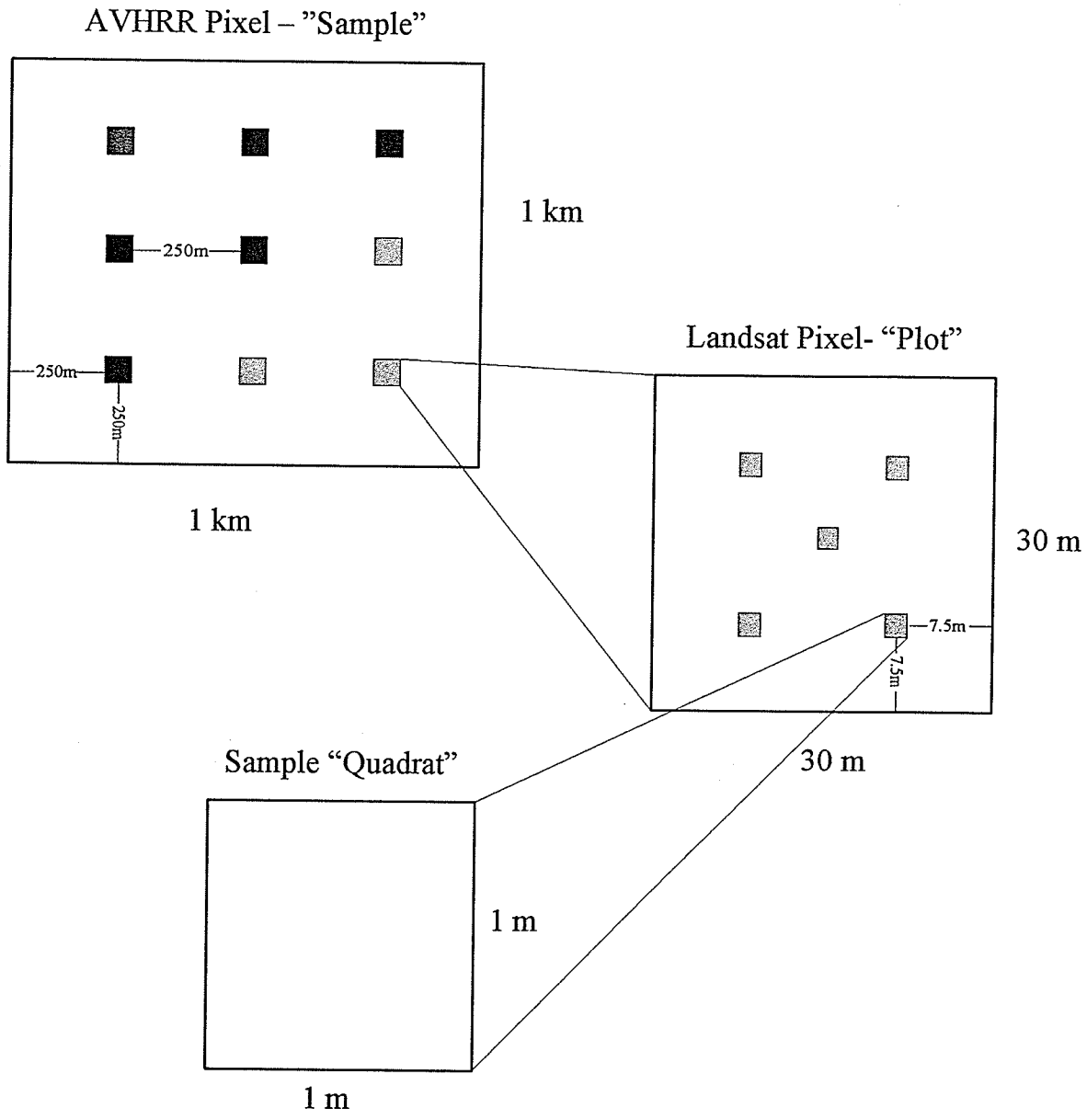

Figure 3.2. Schematic of ground sampling design. A 1x1km sample was located in the field. Within this sample, nine, 30x30m plots were located in a grid pattern 250m meters from the perimeter of the 'sample' area, and 250m apart. Within each 'plot', five 1x1m sample quadrats were located in a cross pattern, 7.5m from the perimeter of the 'plot'.

Visual estimates of ground cover were recorded, as well as topography and soil characteristics. An overhead digital image referenced with a GPS coordinate was also collected to verify the vegetation cover estimates and community type assignments.

Calculation of Vegetation Indices

Two vegetation indices were used in this study: NDVI and MSAVI. The formula for NDVI is:

$$NDVI = (NIR - VIS) / NIR + VIS) \quad [8]$$

Radiometer channels 3 (630-690 nm) and 4 (760-900 nm) were selected to represent to the Visible (VIS) and Near-infrared (NIR) portions of the spectrum, respectively. AVHRR channels 1 (VIS) and 2 (NIR) were used to compute AVHRR NDVI. The MSAVI minimizes the influence of background reflectance by incorporating a soil adjustment factor (L) (Qi et al. 1994). MSAVI is computed as:

$$MSAVI = [(NIR - VIS) / (NIR + VIS + L)] * (1 + L) \quad [9]$$

The soil adjustment parameter, L, is derived from the product of the NDVI and the Weighted Difference Vegetation Index (WDVI), such that:

$$WDVI = NIR - \gamma * VIS \quad [10]$$

$$L = 1 - 2 * \gamma * NDVI * WDVI \quad [11]$$

where γ is the slope of the linear relationship for the regression between visible (VIS) and near infrared (NIR) reflectance values of bare ground (i.e. where vegetation cover <

10%). Bare ground pixels were determined using a threshold NDVI value of 0.03 (i.e. Bare ground = 0 < NDVI < 0.03).

Calibration of NPP Model

FPAR – Vegetation Index Relationship

Physical measurements of FPAR require up- and down-looking PAR sensors positioned both above and below the canopy (Chen 1996). For arctic vegetation, which is essentially 2-dimensional, it is obviously impossible to obtain below canopy PAR measurements. Therefore, an indirect approach was used to determine the relationship between FPAR and a spectral vegetation index.

Total surface FPAR ($FPAR_{sfc}$) is equal to 1 – (PAR reflectance) measured above the canopy:

$$FPAR_{sfc} = 1 - A_{par} \qquad [12]$$

where A_{par} is the surface PAR albedo. If the proportion of PAR absorbed by the ground and non-photosynthetic components of the vegetation is known (i.e. $FPAR_{grd}$), then the proportion of PAR absorbed by the photosynthetic components of the vegetation (i.e. $FPAR_{can}$) can be determined as:

$$FPAR_{can} = (FPAR_{sfc} - FPAR_{grd}) \,/\, FPAR_{sfc} \qquad [13]$$

Where vegetation cover is low (i.e. <30% cover), $FPAR_{grd}$ is constant. Sparsely vegetated canopies consist mainly of low-growing prostrate shrubs and sedges and the ratio of non-photosynthetic biomass to live biomass is low compared to other vegetation types (Bliss et al. 1973). Thus, $FPAR_{grd}$ can be assumed to be constant and equal to $FPAR_{sfc}$ measured

at 0% cover (Figure 3.3). However, $FPAR_{grd}$ will decrease as vegetation cover increases, as more PAR is absorbed by the photosynthetic components of the vegetation, and less by the soil and structural components of the vegetation (Figure 3.3). With increasing cover, $FPAR_{grd}$ gradually decreases, while $FPAR_{sfc}$ approaches an asymptotic constant; $FPAR_{can}$ will increase in direct relation to vegetation cover, as the photosynthetic components of the canopy intercept more light (Figure 3.3). For vegetation cover greater than 100%, $FPAR_{grd}$ approaches 0, while $FPAR_{can}$ will approach $FPAR_{sfc}$.

FPAR is directly related to leaf area (i.e. LAI) (Asrar et al. 1984, Hatfield et al. 1984), and for arctic vegetation, where there is no real third dimension and leaf overlap is minimal, cover is approximately equivalent to leaf area. Thus, for arctic vegetation, FPAR is also directly related to vegetation cover. Furthermore, if vegetation cover is directly related to a spectral vegetation index (i.e NDVI or MSAVI), then it is possible to substitute the vegetation index for vegetation cover and define a direct relation between FPAR and the vegetation index.

A linear relationship was defined between two vegetation indices (NDVI and MSAVI) and vegetation cover. Samples with greater than 100% vegetation cover were excluded from the regression (n=106) because at 100% vegetation cover, a third dimensional component exists in the vegetation (i.e. LAI > 1) and cover can no longer be considered equivalent to FPAR.

A linear relation between $FPAR_{sfc}$ and vegetation cover indicates that $FPAR_{grd}$ is constant (Figure 3.3); therefore, it was necessary to determine the maximum vegetation

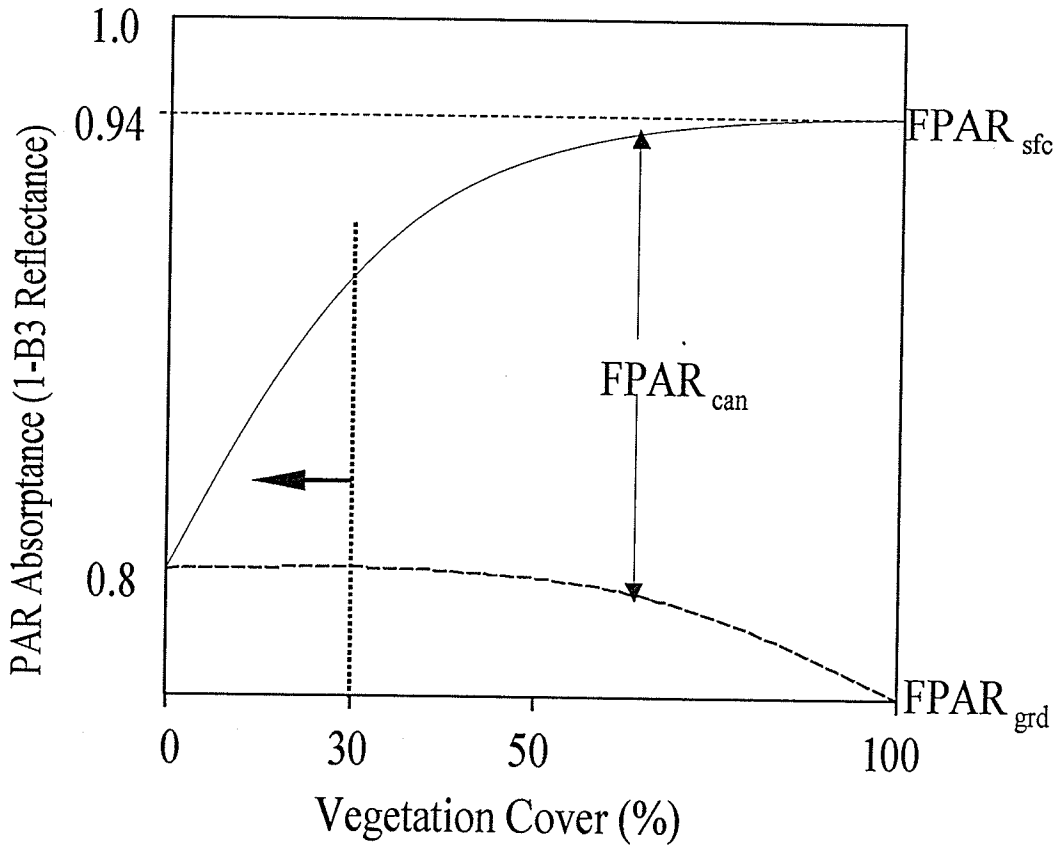

Figure 3.3. Diagram illustrating how the fraction of PAR absorbed by the canopy ($FPAR_{can}$) is determined from measurements of the fraction of PAR absorbed by the entire surface ($FPAR_{sfc}$). At less than 30% vegetation cover, $FPAR_{grd}$ is constant and equal to $FPAR_{sfc}$ at 0% vegetation cover. Thus, $FPAR_{can} = (FPAR_{sfc} - FPAR_{grd})/FPAR_{sfc}$).

cover at which the relationship between $FPAR_{sfc}$ and Vegetation Cover was linear. Only those samples below this threshold were used to determine the $FPAR_{can}$-Vegetation Cover relationship. The linearity of the relationship was evaluated by testing the significance of the regression between the residuals and the predicted value for samples below a specified vegetation cover. A significant residual regression indicated non-linearity. A number of samples were considered outliers because they contained either high amounts of standing water, rock cover or had a slope greater than 40%. These were removed from the analysis.

$FPAR_{sfc}$ was determined from 1 - (radiometer band 3 reflectance) for samples with vegetation cover below the linearity threshold. $FPAR_{can}$ was determined using equation [13], where $FPAR_{grd}$ was set equal to the value of the y-intercept of the regression line determined between $FPAR_{sfc}$ and vegetation cover for samples with vegetation cover less than the linearity threshold. The equation for the linear regression between $FPAR_{can}$ and vegetation cover was then determined. Vegetation cover values were then converted to NDVI and MSAVI using an equation defined for the linear regression between vegetation cover and each spectral vegetation index. The equation for the linear regression between the vegetation index values and $FPAR_{can}$ was then determined. The result was an equation for the linear relationship between the vegetation indices and $FPAR_{can}$.

Energy Conversion Coefficient

An energy conversion coefficient specific to Low-Arctic vegetation was derived from the results of a study measuring CO_2 exchange, incident PAR and NDVI in wet meadow and dry upland ecosystems near Bethel, Alaska (61 N, 162.5°W) (Whiting et al.

1992). Whiting et al. (1992) defined a relation between NDVI and Net Ecosystem CO_2 exchange (NEE) normalized by the incident PAR flux:

$$NDVI = 7.6 * (NEE / PAR) + 0.41; (n = 35; R^2 = 72\%) \quad [14]$$

NEE is equal to the sum of GPP and total ecosystem respiration (ER). In this study NEE was determined by first measuring GPP using a closed CO_2 chamber embedded in the ground then adding ER, which was measured by covering the chamber with a dark shroud. PAR and NDVI were measured concurrently with the CO_2 exchange measurements.

Because the energy conversion coefficient is defined as the slope of the relationship between GPP and $APAR_{can}$, it was necessary to modify the above equation. NDVI was converted to FPAR using the FPAR-NDVI relation defined previously. Incident PAR photon flux was converted to incident PAR radiation flux (i.e. from Einsteins (E) to Megajoules (MJ)) using a conversion factor derived from an integration of the total energy of photon flux over the PAR region of the spectrum (400 – 725nm). Wavelength weights were defined from radiation flux measurements for different wavelengths within the PAR region of the spectrum (Mayo et al. 1977)

The energy, in Joules, for one photon of PAR was calculated by summing the weighted energies calculated for a single photon of light at each wavelength:

$$\text{PAR energy per photon} = {}^{I=\lambda}\Sigma_{400\text{-}725} (K_i * (h * C * \lambda_i^{-1})) \quad [15]$$

where h is Planck's constant (6.626×10^{-34} J * S); K is the i^{th} wavelength weight; C is the speed of light; and λ is the i^{th} wavelength.

$APAR_{can}$ was then determined from the product of FPAR and PAR (MJ) (see Equation [4]). NEE (gCO_2) was converted to grams of dry matter (gDM) by multiplying NEE by 0.681. This value is based on the proportion CH_2O produced from CO_2 in photosynthesis:

$$1\ CO_2 + H_2O + PAR = 0.681\ CH_2O + O_2 \qquad [16]$$

NEE was converted to GPP by adding the Ecosystem Respiration (ER), where ER was determined from an empirical relation with NDVI (See next section). Finally, the energy conversion coefficient for GPP was determined from the slope of the resulting linear equation between GPP and $APAR_{can}$.

Autotrophic Respiration

Autotrophic respiration (R_a) is the proportion of ecosystem respiration (ER) attributable to the vegetation (ER = R_a (plant respiration) + R_h (soil respiration)). The R_a:ER ratio was defined in an extensive summary of International Biome Project (IBP) data collected at Truelove Lowland, Devon Island (Bliss 1977). Of total ER, 91% was attributable to R_a (Bliss 1977). Compared to temperate ecosystems, the proportion of heterotrophic respiration (R_h) is remarkably low. However, considering the limited microbial activity in cold, wet, and acidic tundra soils, this value is reasonable.

A relationship between NDVI and ER was defined from data presented in McMichael et al. (1999). These data consisted of concurrent NDVI, PAR and CO_2 exchange measurements for ecosystem respiration (i.e. a CO_2 chamber covered with a dark shroud). Measurements were made in tussock tundra and wet sedge tundra ecosystems in Prudhoe Bay, Alaska (70°21'N, 148°58'W) (McMichael et al 1999).

Computing Annual Net Primary Productivity with GEOCOMP-n AVHRR Data

Net primary productivity was computed for each 10-day composite period during the growing season using equations [3] and [5]. NPP was determined using the GEOCOMP-n AVHRR image products exclusively. MSAVI was computed from atmospherically corrected band 1 and band 2 reflectance. FPAR was computed for both the atmospherically corrected NDVI and MSAVI. AVHRR band 1 corrected for atmospheric and bi-directional reflectance effects, was used as a surrogate for A_{par}, which is currently unavailable from GEOCOMP-n. For comparison, NPP was computed with FPAR derived from NDVI and with FPAR derived from MSAVI. Annual NPP was computed from the sum of the 10-day NPP estimates.

Expected Annual Net Primary Productivity

To provide reasonable validation for the model, a 1x1 km resolution expected annual NPP map was created using a data set and methodology entirely independent of the model described above. Expected annual NPP (ANPP) was determined by combining a Landsat TM vegetation classification and expected ANPP values for each vegetation class compiled from literature sources.

Landsat TM Vegetation Classification

A preliminary vegetation map was provided by the NWT Centre for Remote Sensing. This classification was created by combining results of an unsupervised classification of a cloud-free Landsat 5 TM scene (acquired June 29, 1992) with ground data collected within the Park.

The classification and the original Landsat imagery was projected as UTM, whereas the AVHRR imagery was projected as Lambert Conformal Conic (LCC). It was therefore necessary to reproject the Landsat image to LCC using a third degree polynomial with 25 ground control points using nearest neighbour resampling.

The preliminary classification contained 24 ground cover types, many of which were deemed redundant for this analysis. There were also a high number of unclassified pixels within the image, especially in areas of high topographic complexity. The spectral separability of the preliminary classes was evaluated using the Jeffries-Matusita and Transformed Divergence separability measures and the original Landsat image bands (Richards 1994). Georeferenced overhead images for each sample quadrat were linked to a vector point layer and used to visually assess the preliminary classes. Then, using a combination of the class separability results and visual verification with the overhead images, each of the preliminary classes was combined into one of the following 11 classes: Barren, Sparsely Vegetated, Mesic Meadow, Dwarf Shrub Tundra, Tussock Tundra, Wet Sedge Meadow, Water, Ice/Snow, Mud, Sand, Bedrock.

Single unclassified pixels were assigned the mode of the surrounding 8 pixels using a 9x9 pixel modal filter. A mask was then created of the remaining unclassified pixels, and these pixels were assigned to one of the new classes using a supervised maximum likelihood classification. Training sites were developed by creating masks of the 11 new classes.

An error analysis was performed on the resultant vegetation classification by comparing the classified Landsat pixels with the spatially collocated 30x30 m field plots

(n=172). The mode of the vegetation classes assigned to the 5 (1x1m) quadrats within each 30x30m plot was determined and compared to the corresponding Landsat vegetation classification pixel using a confusion matrix.

The classification was then separated into a series of mask images for each vegetation class, with mask pixels representing only those pixels assigned to that class. The proportion of each vegetation class within a 1x1 km area was determined by computing the proportion of mask pixels within a 40x40 pixel window. The result was a series of vegetation class proportion images with pixel dimensions equal and matched to the AVHRR imagery.

Expected annual net primary productivity (ANPP) values for each of the six vegetated classes were compiled from various literature sources (Bliss et al. 1973; Haag 1974; Muc 1977; Miller et al. 1980; Bliss et al. 1984; Shaver and Chapin 1986; Shaver and Chapin 1991; Bliss and Matveyeva 1992; Gilmanov and Oechel 1995; Bliss and Gold 1999). Only ANPP values were included for which both above and below-ground annual NPP were measured. The literature ANPP values were assigned to one of the 6 vegetation classes based floristic descriptions and geographic proximity. A mean value of ANPP for each class was then determined. The 1x1 km proportion layer was then multiplied by the expected ANPP value for that class. The resulting weighted ANPP layers were then summed to produce the expected ANPP map at 1x1 km resolution.

Water and Topographic Effects

A water mask was created from an unsupervised k-means classification of a Landsat 7 ETM image acquired for the study area on July 13th, 2000. The proportion of

water cover within each 1x1 km AVHRR pixel was determined using the same technique as described for the vegetation proportions.

A 100x100 m resolution digital elevation model (DEM) was created from the digital 1:250 000 national topographic survey hypsography vectors using a contour line interpolation. The result was smoothed with a 9x9 mean filter to remove the residual effects of the interpolation. A slope map was then created from the DEM as well as a series of variables to characterize the topographic complexity of the landscape. Topographic complexity within each 1x1 km AVHRR pixel was characterized using mean slope, slope variance, elevation variance. These variables were computed using a series of algorithms designed to pass a 10x10 pixel window across the DEM at 10 pixel intervals.

Model Evaluation

To illustrate the correspondence between modelled and expected NPP, the percent normalized difference was computed as [(Modelled ANPP – Expected ANPP / Modelled ANPP + Expected ANPP) * 100]. The normalized difference provides a relative difference between modelled and expected ANPP such that the magnitude of the differences are equal in both high and low productivity areas. Multiple regression analysis was used to determine the influence of water cover and topography on the difference between modelled and expected ANPP. Similarly, multiple regression analysis was used to evaluate the effects of different ground cover types on the difference between modelled ANPP and Expected ANPP.

3.4. RESULTS

NPP Model Calibration

Predicting Vegetation Cover with NDVI and MSAVI

There is a strong positive relationship between vegetation cover and both NDVI and MSAVI, with 72.5% of the variation in NDVI explained by vegetation cover, and 70.3% of the variation in MSAVI explained by vegetation cover (Figure 3.4 **a,b**).

Surface PAR absorption and Vegetation Cover

A semi-logarithmic relationship exists between total surface PAR absorption ($FPAR_{sfc}$) (i.e. 1-B3 reflectance) and vegetation cover (Figure 3.5). $FPAR_{sfc}$ increases with vegetation cover to ~50% cover, at which point $FPAR_{sfc}$ approaches the asymptote at ~ 0.94. This sill is equivalent to a surface PAR albedo of approximately 6% for ground with >100% vegetation cover. Surface PAR albedo values for well developed canopies of 5-7% have been reported elsewhere (Moreau and Li 1996).

Derivation of the FPAR-Vegetation Index Relationship

The steps used to derive the relationship between NDVI and $FPAR_{can}$ are summarized in Figure 3.6. At 30% vegetation cover, the regression of the residuals and the predicted values for the relationship between surface PAR absorptance and vegetation cover is not significant, indicating a linear relation between $FPAR_{sfc}$ and vegetation cover (P=0.504 at 30% Cover). Thus, only samples with less than 30% vegetation cover were used to derive the FPAR-Vegetation Index relationship.

A significant positive relationship exists between $FPAR_{sfc}$ and vegetation cover for areas with less than 30% cover (R^2=45.9%, $p<0.001$, Figure 3.6). For low vegetation

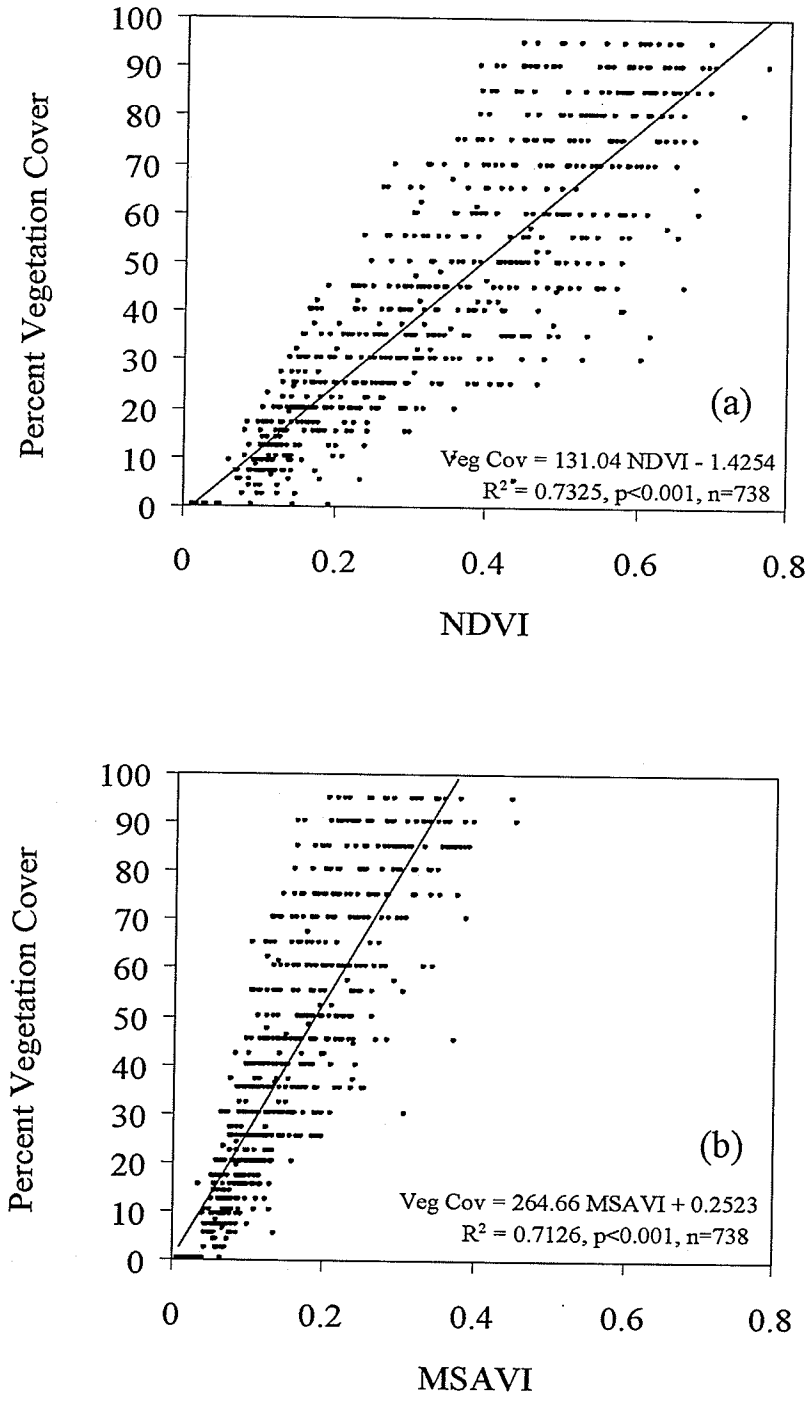

Figure 3.4 Scatterplots of a) NDVI and Vegetation cover, and b) MSAVI and Vegetation Cover measured from field sample quadrats. The linear regression is significant in both cases.

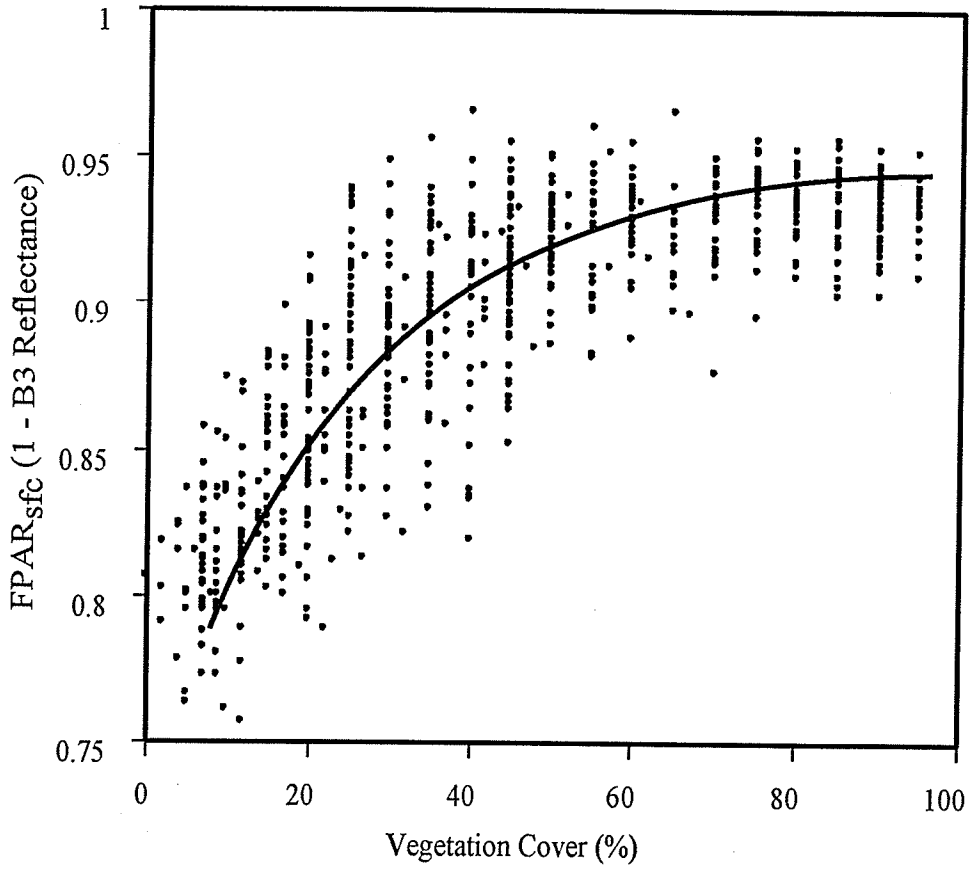

Figure 3.5. Relationship between total surface PAR absorption ($FPAR_{sfc}$) measured as (1-radiometer B3 reflectance), and percent vegetation cover measured from 1x1m quadrats. Only samples with less than 100% cover were used (n= 720). A significant logarithmic function best-fits the relationship ($FPAR_{sfc} = 0.71 + (0.05 \ln (\%VC)$; $p<0.0001$, $R^2=71.3\%$).

(1) $FPAR_{sfc} = (VC * 0.344) + 0.786$
($R^2 = 51\%$, $P<0.01$, n=291)

$$FPAR_{can} = \frac{FPAR_{sfc} - FPAR_{grd}}{FPAR_{sfc}}$$

(2) $FPAR_{can} = (VC * 0.378) + 0.004$
($R^2 = 52\%$, $P<0.01$, n=291)

$NDVI = (VC * 0.572) + 0.0881$

(3) $FPAR_{can} = (NDVI * 0.64) + 0.056$
($R^2 = 52\%$, $P<0.01$, n=291)

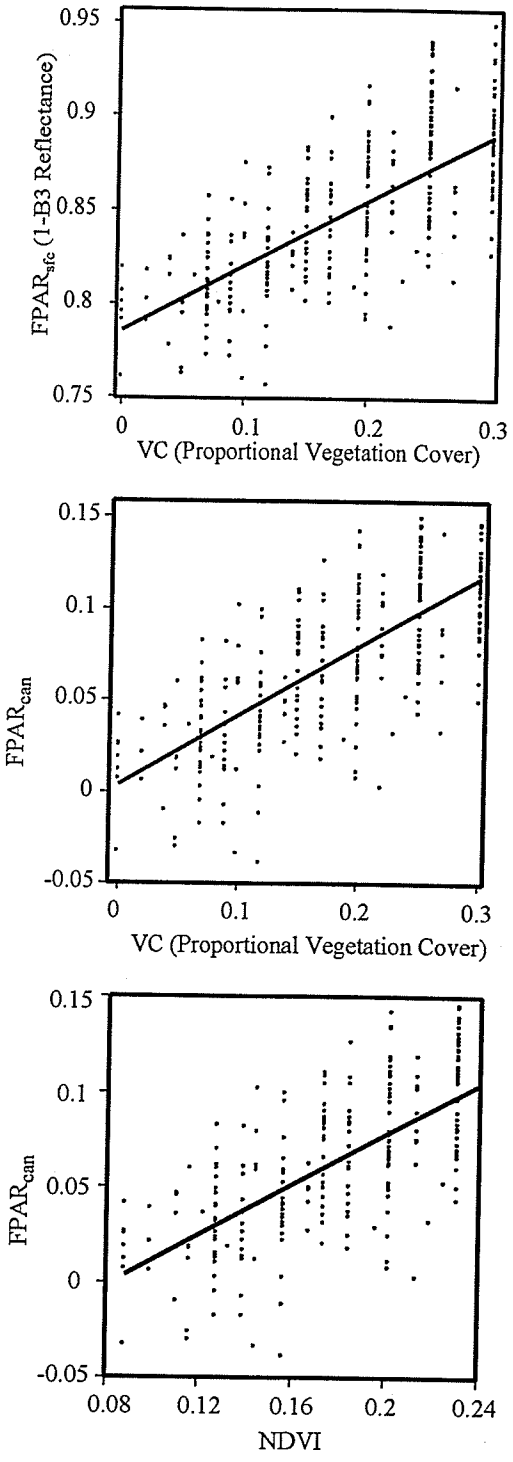

Figure 3.6. Derivation of the relationship between $FPAR_{can}$ and NDVI. (1) A linear relationship was defined between Total Surface PAR Absorption ($FPAR_{sfc}$) and proportional vegetation cover (VC) for quadrat samples with VC < 30% (2) $FPAR_{sfc}$ was converted to $FPAR_{can}$, assuming background PAR absorptance ($FPAR_{grd}$) was equal to $FPAR_{sfc}$ at VC = 0%. A linear relationship was then defined between $FPAR_{can}$ and VC. (3) VC was then converted to NDVI using the relationship between NDVI and VC defined in Fig. 3.5. A linear relationship was then defined between $FPAR_{can}$ and NDVI. The relationship between $FPAR_{can}$ and MSAVI was defined using the same method.

cover samples, $FPAR_{grd}$ is assumed equivalent to the y-intercept which is equal to 0.79 (Figure 3.6). This value corresponds to a surface PAR albedo for bare soil of 0.21. $FPAR_{can}$ was then determined from $FPAR_{sfc}$ and $FPAR_{grd}$ using equation [13], and vegetation cover was substituted with NDVI and MSAVI using the relationship defined previously between vegetation cover and these vegetation indices (Figure 3.6). From the substituted values, the following relationships were defined between $FPAR_{can}$ and NDVI and MSAVI:

$$FPAR_{can} = NDVI * 0.638 + 0.056 \quad [17]$$

$$FPAR_{can} = MSAVI * 1.34 + 0.059 \quad [18]$$

Energy Conversion Coefficient

A conversion factor for PAR photon flux to PAR radiation flux of 0.21386 MJ/E was determined (Table 3.2).

Table 3.2. PAR wavelength weights determined by integrating the total energy of photon flux over the PAR region of the spectrum. Radiation in wavelengths spanning the PAR spectrum was measured at noon for six dates between 21-6-71 and 12-8-71 in Barrow, Alaska.

	Wavelength (nm)			
	Blue			**Red**
	400	**500**	**650**	**725**
Mean Radiation (W/m^2) for 6 dates throughout the growing season	23.667	40.333	42.900	36.492
Mean wavelength weightings	0.165	0.281	0.300	0.254
Weighted Energy for one photon (Joules)	8.21122E-20	1.1163E-19	9.18252E-20	6.95638E-20
Total PAR energy (Joules) for one photon:			**3.55131E-19 Joules**	
Total PAR energy (Joules) for one Einstein:			**213860.0063 Joules**	
Total PAR energy (Mega Joules) for one Einstein:			**0.21386 MJ/E**	

Substituting FPAR for NDVI, converting PAR photon flux to PAR radiation flux, and converting NEE to GPP, in the NEE equation presented in Whiting et al. (1992), the equation for the linear relation between GPP and $APAR_{can}$ was determined to be:

$$GPP = 2.8033 * (FPAR * PAR\downarrow) - 10.022 \quad [17]$$

The slope of this relation is equal to the energy to GPP conversion coefficient (ε_{GPP} = 2.8033). The intercept was assumed equal to zero because when $APAR_{can}$=0, GPP = 0.

Autotrophic Respiration

A second degree polynomial relationship was fit to the ecosystem respiration and NDVI data in McMichael et al (1999) ($R^2 = 0.968$, $p<0.001$, Figure 3.7):

$$ER = 6.1972 * NDVI^2 + 1.4138 * NDVI - 0.1485 \quad [18]$$

Although a significant linear relation could be fit to the data, this relationship results in negative ER values for low NDVI values. Using a polynomial relationship maintains positive ER values at low NDVI.

A proportional value of 0.91 was used to convert total ER attributable to autotrophic respiration (Bliss 1977).

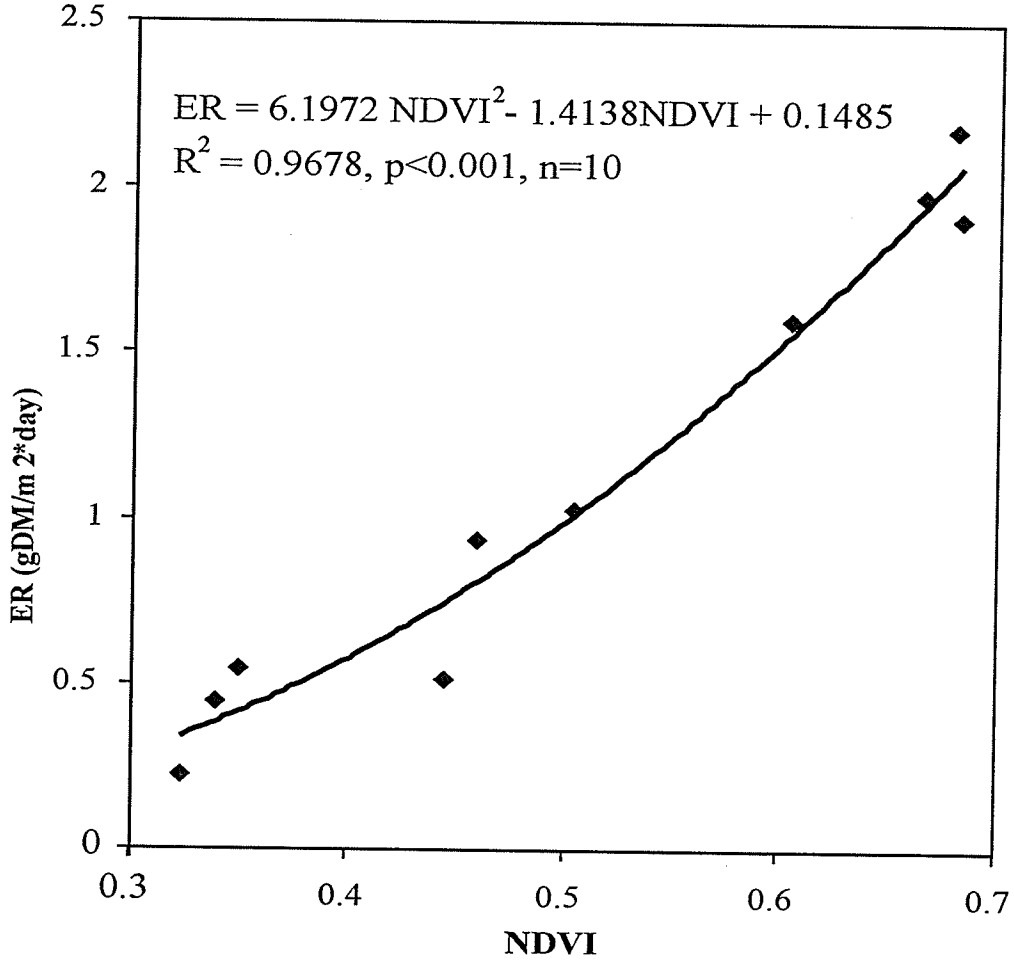

Figure 3.7. A second degree polynomial is fit to the relationship between ER and mean NDVI values obtained from a data set for ecosystem respiration (ER) and NDVI measured concurrently in tundra vegatation (from McMichael et al. 1999).

Table 3.3 summarizes the model parameters derived from the preceding analyses.

Table 3.3. Summary of NPP model parameters

Parameter	Units	Relation / Value
FPAR	unitless	FPAR = (NDVI * 0.637) + 0.056
FPAR	unitless	FPAR = (MSAVI * 1.34) + 0.059
ε_{GPP}	g DM / MJ	2.8033
CO_2 to. Dry Matter	g CO_2 / g DM	0.681
Einsteins (E) to Megajoules (MJ)	MJ / E	0.233647
ER	gC/ m^2 * 10days	ER = 10* (6.1972 * $NDVI^2$) - (1.4138*NDVI) + 0.1485
R_a : ER	unitless	0.91

Expected annual productivity

Landsat Vegetation Classification

The Landsat vegetation classification is presented in **Figure 3.8**. When compared to the field plots, the overall classification accuracy was determined to be 62.2 % (Table 3.4). Classification accuracy was considerably higher in the sparsely vegetated, dwarf shrub tundra, tussock tundra and barren classes. Although the classification accuracy of water was very high, this class was not included in the error assessment. Classification accuracy was lowest in the mesic meadow class, with a classification accuracy of 38.8% (Table 3.4). Of the 49 mesic meadow ground samples, 27 were classified as sparsely vegetated pixels in the vegetation map, suggesting overlap between these classes in areas with either higher productivity sparse vegetation, or lower productivity mesic meadow.

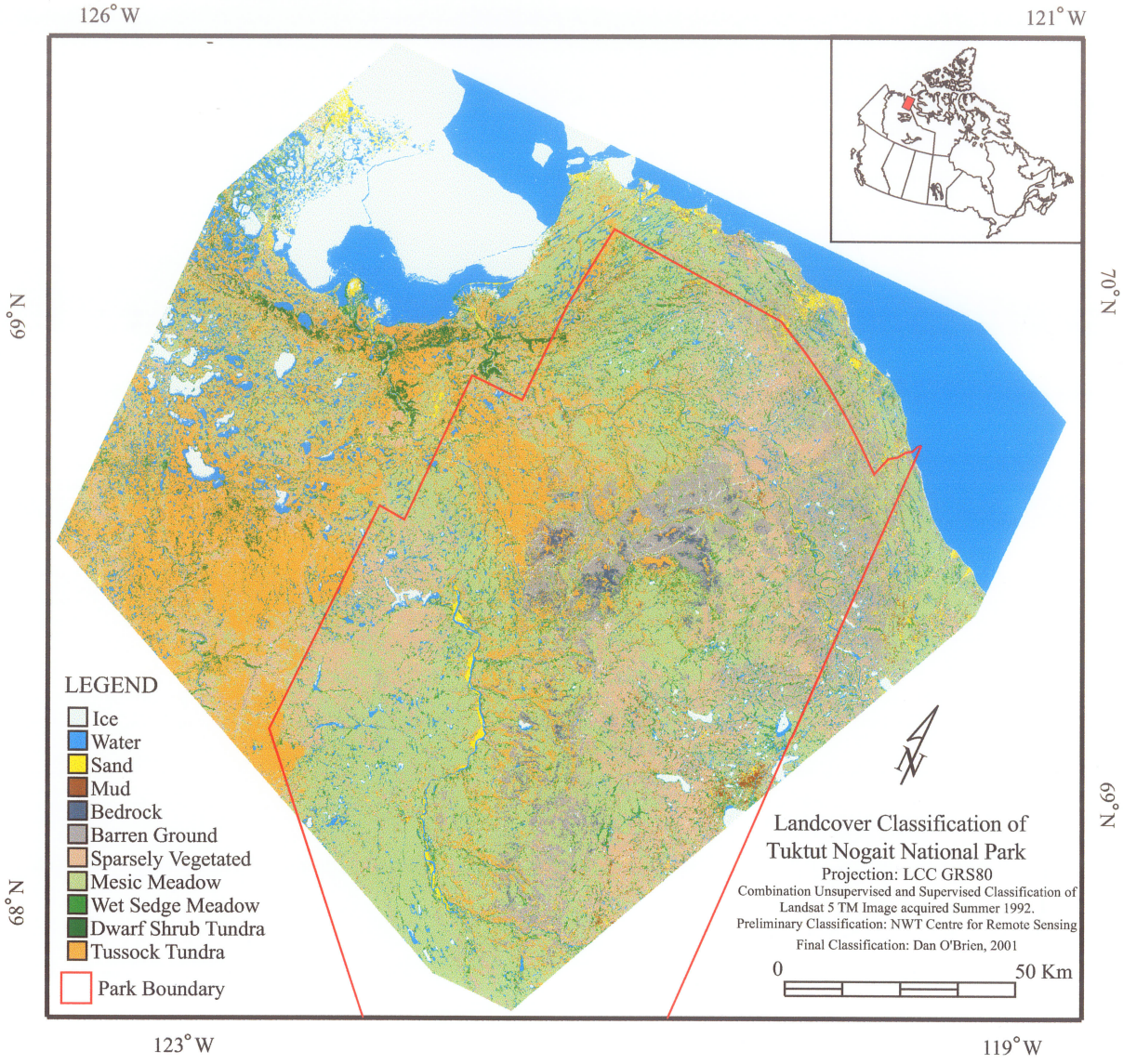

Figure 3.8. Landcover classification of Tuktut Nogait National Park, NWT. Landcover classes were assigned to an unsupervised classification of a Landsat 5 TM image acquired in early summer of 1992. Unclassified pixels were assigned to existing classes with a supervised maximum liklihood classification, using training statistics defined from the existing classes. Overall classification accuracy was 62.2% when compared to ground truth data collected in the summer of 2000.

Table 3.4. Confusion matrix of Landsat TM classification validation using ground data. Ground classifications are based on the mode of the class assignment for the 5 (1x1m) quadrats located within each 30x30m plot. Numbers on the diagonal represent counts of correctly classified pixels. Numbers off the diagonal represent misclassified pixel counts. In total, 62.2% of the Landsat vegetation classification were correctly classified. WSM = Wet sedge meadow; MM= Mesic Meadow, DST= Dwarf shrub tundra; TT= Tussock tundra; SPV= Sparsely vegetated ground; BRN=Barren ground.

		Vegetation Map								
		WSM	MM	DST	TT	SPV	BRN	ROCK	SNOW	Total (n=172)
Ground Data	WSM	**15**	3	0	0	8	0	0	0	26
	MM	0	**19**	0	2	27	1	0	0	49
	DST	0	0	**4**	0	0	0	0	0	4
	TT	0	2	0	**10**	0	0	0	0	12
	SPV	1	9	0	0	**32**	7	0	0	49
	BRN	0	1	0	0	3	**26**	0	0	30
	ROCK	0	0	0	0	0	0	**0**	0	0
	SNOW	1	0	0	0	0	0	0	**1**	2
	% Correct	**57.7**	**38.8**	**100**	**83.3**	**65.3**	**86.7**	**100**	**50.0**	**62.2**

Expected Annual NPP Estimates

Table 3.5 lists the mean annual above and below-ground NPP (ANPP) values for each vegetation class compiled from the literature. Variability in ANPP estimates is low for the barren, sparsely vegetated and dwarf shrub tundra vegetation classes. However, variability increases in the more productive vegetation classes, with the largest variation apparent in the tussock tundra and wet sedge meadow classes (Table 3.5).

Table 3.5. Total above and below ground net primary productivity estimates (g / m^2yr) compiled from literature sources.

Vegetation Class	Mean NPP (±SD)	Max	Min	N	References
Barren	0.95 (±0.07)	1.01	0.87	4	5,10
Sparsely Vegetated	4.45 (±2.45)	8.00	2.13	7	5,8,9,10
Mesic Meadow	155.73 (±25.51)	185.00	138.20	3	6,8
Dwarf Shrub	137.5 (±3.54)	140.00	135.00	2	1,8
Tussock Tundra	524 (±135.76)	620.00	428.00	2	1,4
Wet Sedge Meadow	239.76 (±62.78)	352.00	165.10	8	1,2,6,8,11,12

References
(1) Shaver, and Chapin 1991
(2) Shaver et al. 1997
(4) Shaver and Chapin 1986
(5) Bliss and Matveyeva 1992
(6) Muc 1977
(7) Bliss et al. 1973
(8) Gilmanov and Oechel 1995
(9) Bliss and Gold 1999
(10) Bliss et al. 1984
(11) Haag 1974
(12) Miller et al. 1980

Vegetation Class Proportion Layers

The 1x1km resolution vegetation class proportion images are presented in Figure 3.9. Barren ground vegetation class occurs mainly at high elevations in the central region of the Park (i.e. the Melville Hills) and near the north east coastal region of the Park (Figure 3.9). The sparsely vegetated class occurs mainly on a high elevation plateau west of the Hornaday river, in the western region of the Park, as well as in the north east region of the Park (Figure 3.9). This region is particularly dry, possibly because of a rain shadow effect from the Melville hills. This results in low vegetation

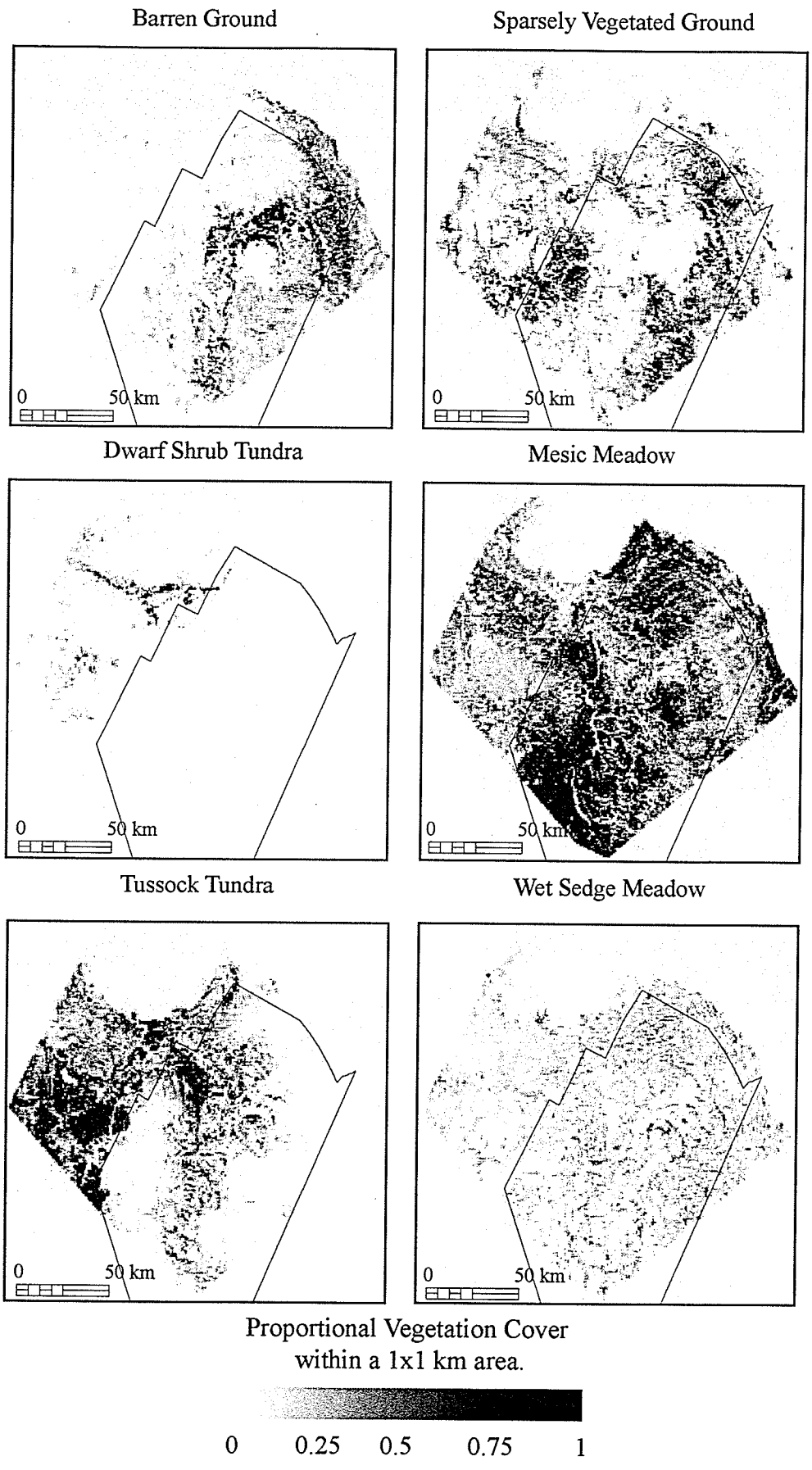

Figure 3.9. Vegetation class proportion images derived from the Landsat vegetation classification. Pixel values represent the proportion of each class within a 1x1 km area.

productivity, as arctic vegetation productivity is highly correlated with water availability (Chapin et al. 1988; Fogg 1998).

Occurrence of the dwarf shrub tundra class is relatively low within the Park, with the exception of the north east region of the Park, within the Hornaday and Brock River deltas. The dwarf shrub tundra class tends to occur in small localized patches on well drained slopes in association with mesic meadow vegetation. Small patch size (i.e. <25x25m) may result in under-classification of dwarf shrub tundra, as the pixel class will be assigned to the dominant vegetation within the pixel. From this classification, mesic meadow class is the dominant vegetation class within the Park, with high occurrence in the southwest corner of the Park to the west of the Hornaday River, and in the west of the Park, near Seven Islands Lake (Figure 3.9). The wet sedge meadow class occurs throughout the Park in a reticulated pattern (Figure 3.9). Wet sedge meadow tends to be associated with water bodies, along rivers and surrounding lakes which results in a reticulated distribution pattern.

Expected ANPP Map

A map of the expected annual NPP is presented in Figure 3.10. Expected ANPP is highest in the northwest region of the Park (ANPP = 200-500 g /m^2yr), and along the east side of the Hornaday river valley. In these areas there is high occurrence of the tussock tundra and mesic meadow classes. It is likely that the high vegetation productivity in this area is supported by run-off from the Melville Hills, which provides a continuous supply of water throughout the growing season. Expected ANPP is low in the northeast region of the Park where ANPP = 10-150 g /m^2yr, and on the southwest side of the Hornaday

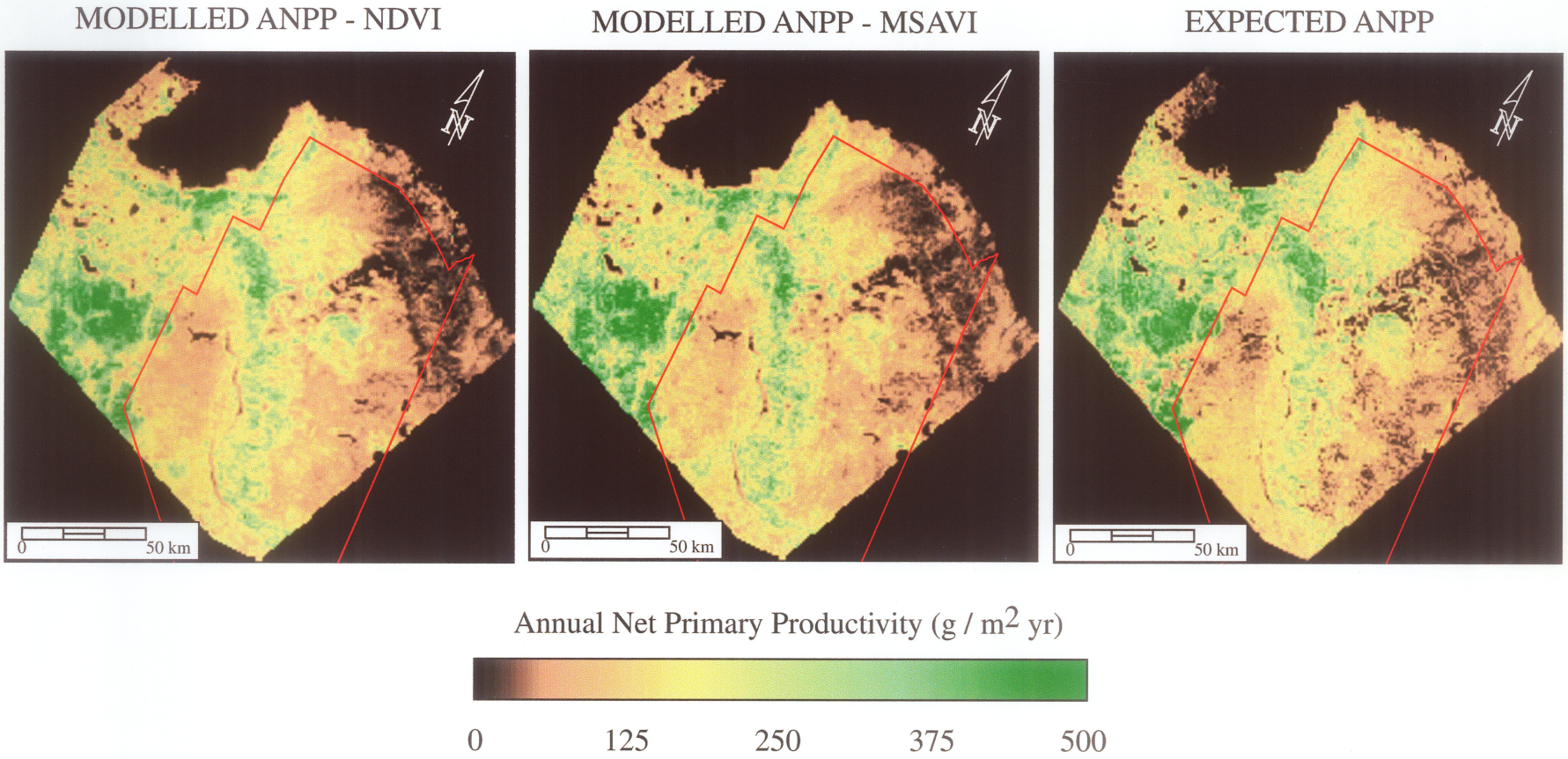

Figure 3.10. A comparison between annual net primary productivity computed from the AVHRR model using either NDVI or MSAVI to compute FPAR, and the expected ANPP map derived from the Landsat vegetation classification and ANPP values taken from the literature.

Valley. These areas correspond to high occurrence of the barren and sparsely vegetated classes. Expected ANPP is lowest at high elevations in the Melville hills where ANPP = 0-50 g $m^{-2}yr^{-1}$, with the exception of a small pocket of high productivity in the center of the Park which corresponds to a concave depression to the southeast of the Melville hills with a high occurrence of the mesic meadow class.

Model Evaluation

Modelled ANPP computed with NDVI

With respect to the relative spatial patterns of ANPP, there is a strong correspondence between modelled ANPP computed using NDVI ($ANPP_{NDVI}$) and expected ANPP ($ANPP_{Exp}$) (Figure 3.10). However, when comparing the absolute values there is less correspondence; in most areas, values for $ANPP_{NDVI}$ were consistently lower than $ANPP_{Exp}$. The normalized percent difference map illustrates the location and magnitude of these differences, and a histogram illustrates the frequency distribution of the differences (Figure 3.11). For $ANPP_{NDVI}$, only 41.76% of the pixels are within 30% of the difference. The mean of the normalized difference of $ANPP_{NDVI}$ and $ANPP_{Exp}$ is 33.55% (±23.96%), indicating $ANPP_{Exp}$ values are 30-35% higher than $ANPP_{NDVI}$ (Figure 3.11). The right tail of the percent difference histogram reveals a high number of pixels with large percent difference (Figure 3.11). These pixels correspond to the northeast portion of the Park along the coastline, where AVHRR NDVI values remain very low throughout the growing season. Despite the presence of vegetation in these areas, persistently low NDVI values throughout the growing season result in negative FPAR values and negative annual NPP values. In a small region in the center of the park (69°11' N, 121° 39' W), modelled ANPP values are 80-90% larger than expected ANPP.

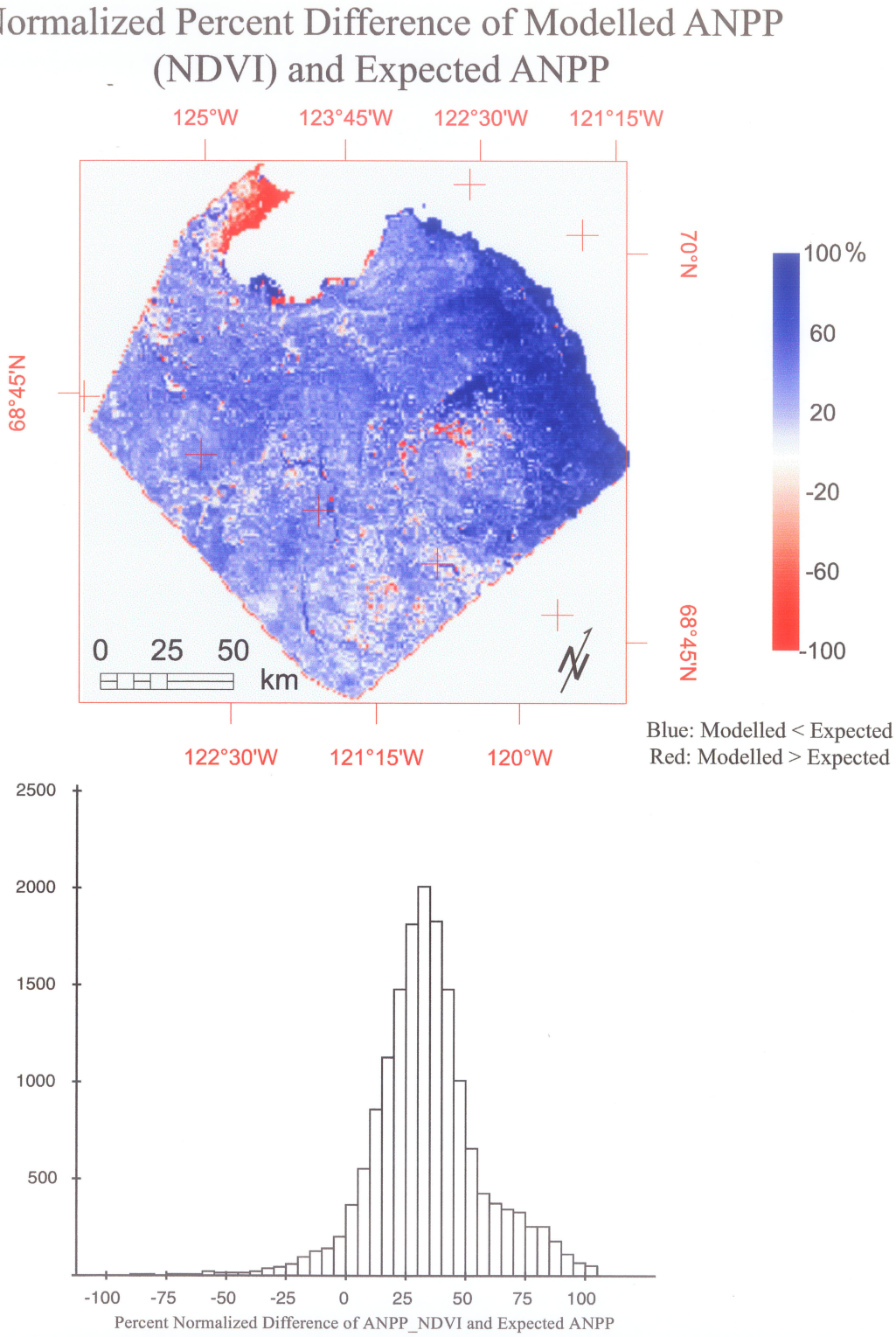

Figure 3.11. Map of the normalized percent difference of annual NPP computed using NDVI to determine FPAR and the expected annual NPP: [(Modelled - Expected / Modelled + Expected) * 100%]. Red indicates modelled ANPP values are higher than expected NPP. Blue indicated modelled ANPP values are less than expected. Overall, 41.76% of the pixels are less than 30% different.

This area corresponds to a high elevation ridge which appears red in a Landsat false colour composite. Although no ground sampling was done in this region, when observed from the air, the ground appeared completely barren. The red appearance of the landscape may be caused by crustose lichens covering the bare rock. High near infrared (NIR) reflectance of stony lichen tundra (biomass < 20 g m^{-2} yr^{-1}) results in NDVI values as high as those obtained for fructicose lichen and dwarf shrub communities, where biomass = 1000 g m^{-2} yr^{-1} (Rees et al. 1998).

Modelled ANPP computed with MSAVI

Correspondence between modelled ANPP computed with MSAVI ($ANPP_{MSAVI}$) and expected ANPP ($ANPP_{Exp}$), is much greater compared to $ANPP_{NDVI}$ both in terms of relative spatial patterns and absolute values (Figure 3.12). Overall, the percent normalized difference values between $ANPP_{MSAVI}$ and $ANPP_{Exp}$ are lower (Figure 3.12). In the histogram, the difference distribution is centered at a mean value of -4.46% (±22.61%), indicating that modelled values are generally 4-5% higher than expected values (Figure 3.12). Larger differences exist in areas where tussock tundra and mesic meadow cover is high. In these areas modelled values are 10-25% lower than expected. For these vegetation classes, expected ANPP may be overestimated. In areas with high barren ground and sparsely vegetated cover, modelled ANPP values tend to be 10-40% higher than $ANPP_{Exp}$. As with $ANPP_{NDVI}$, $ANPP_{MSAVI}$ values are 80-90% higher than $ANPP_{Exp}$ in a small region in the center of the Park, where ground cover is likely crustose lichen covered rock. These discrepancies may also be attributable to inherent inaccuracies in the expected vegetation map.

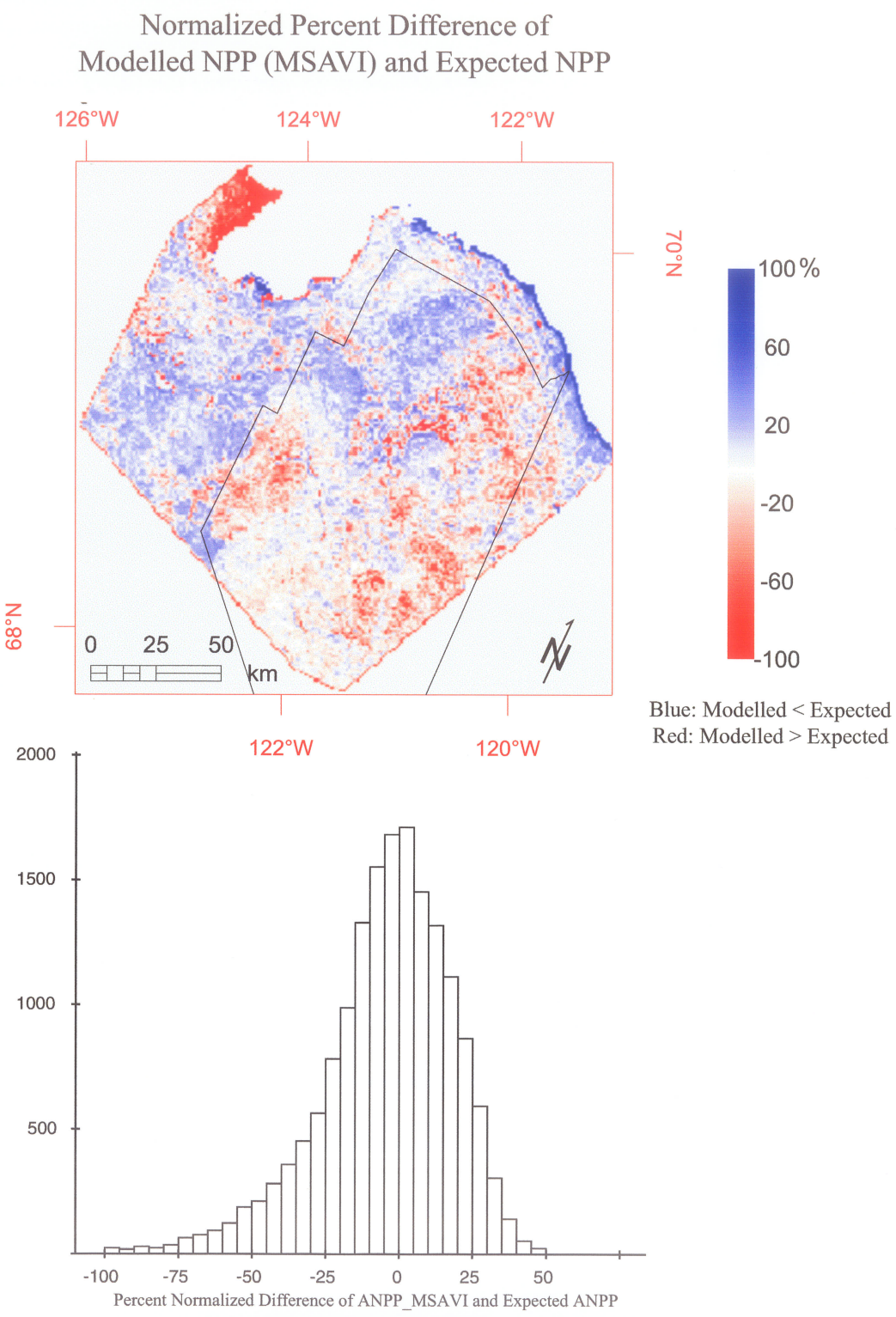

Figure 3.12. Map of the normalized percent difference of annual NPP computed using MSAVI to determine FPAR and the expected annual NPP: [(Modelled - Expected / Modelled + Expected) * 100%]. Red indicates modelled ANPP values are higher than expected NPP. Blue indicated modelled ANPP values are less than expected. Overall, 84.43% of the pixels are less than 30% different.

Regression analysis of modelled and expected ANPP values indicates a significant linear relationship for both $ANPP_{NDVI}$ and $ANPP_{MSAVI}$ (Figure 3.13). Modelled $ANPP_{NDVI}$ and $ANPP_{MSAVI}$ values explain 73.5% and 65.7% of the variation in $ANPP_{Exp}$ values, respectively. Although in both cases a significant linear relation can be fit to the data, the scatter plots of $ANPP_{NDVI}$ and $ANPP_{Exp}$ and $ANPP_{MSAVI}$ and $ANPP_{Exp}$ reveal an non-linear trend; with increasing productivity, the increase in expected ANPP values is greater than for modelled ANPP values (Figure 3.13).

Effects of Sub-Pixel Water Cover and Topography

The effects of water cover and topographic complexity on the relationship between modelled ANPP and expected ANPP were evaluated in a multiple regression (Table 3.6). Water cover had a significant negative effect in the regression with $ANPP_{MSAVI}$, but not with $ANPP_{NDVI}$ (Table 3.6). With increased water cover, modelled values tend to be greater than expected.

For both $ANPP_{NDVI}$ and $ANPP_{MSAVI}$, slope variance has a significant positive effect, whereas slope mean has a significant negative effect (Table 3.6). Elevation variance had no significant effect (Table 3.6). With increasing slope variance modelled values tend to be *lower* than expected values. High slope variance indicates rough terrain. Therefore, in areas with complex topography, the model may underestimate ANPP. With

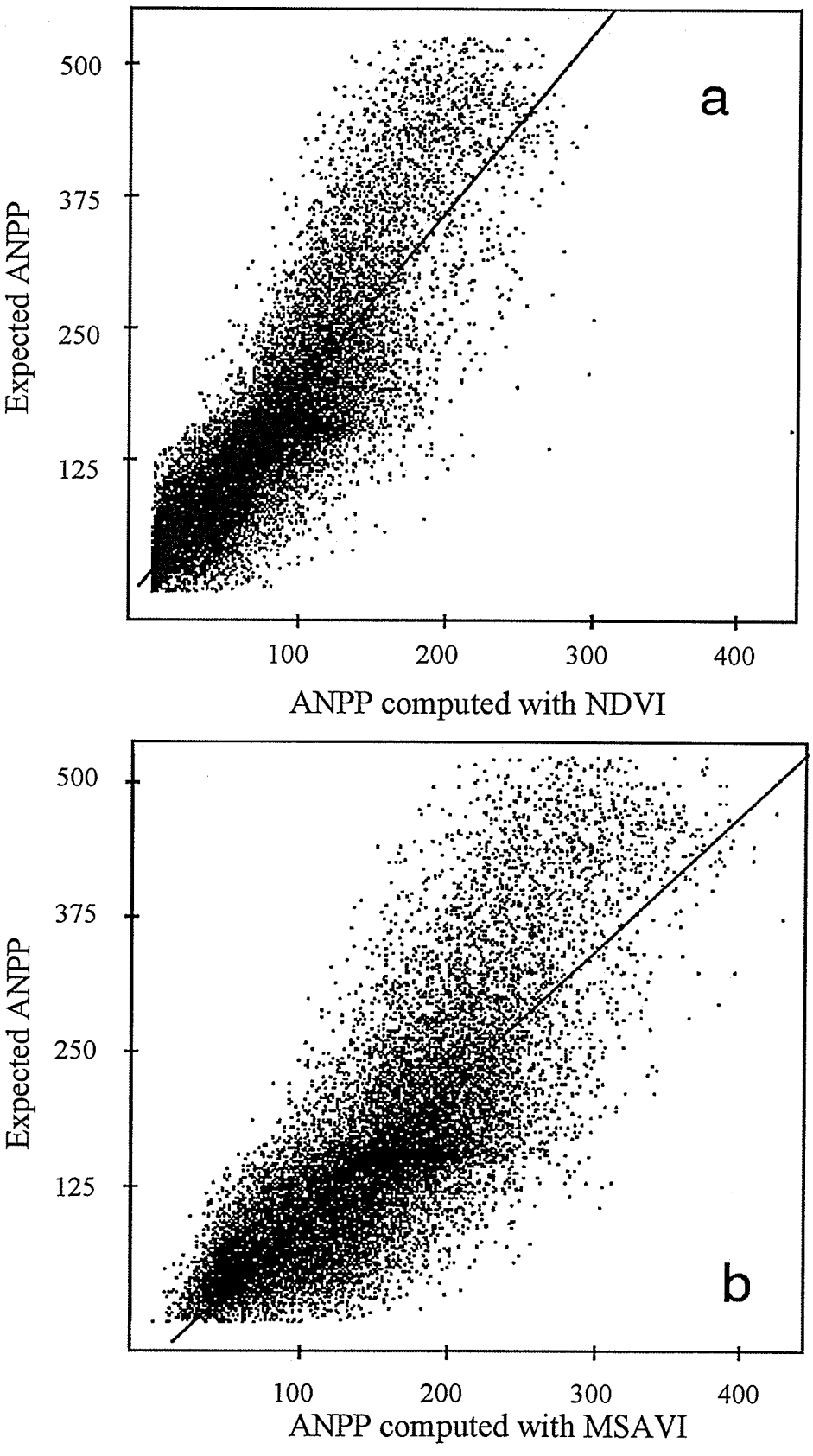

Figure 3.13. Regression of expected ANPP an modelled ANPP computed with (a) NDVI ($ANPP_{exp} = 1.67\ ANPP_{NDVI} + 19.853$; $R^2 = 73.5\%$, $P<0.0001$); and (b) MSAVI ($ANPP_{exp} = 1.263 ANPP_{MSAVI} - 33.485$; $R^2 = 65.7\%$, $P<0.0001$).

increasing mean slope modelled values tend to be *higher* than expected values. High mean slope indicates steep terrain. Thus, in these areas the model may overestimate ANPP.

Table 3.6. Results for multiple regression analysis on the normalized percent difference of modelled ANPP and expected ANPP with the proportion of water and topographic variables.

Dependent variable: NPP-Expected. N= 13975; R^2 = 69.8%			
Variable	Coefficient	T-Ratio	P-Value
Constant	27.28	14.4	<0.0001
NPP-NDVI	1.64	179	<0.0001
%H20	-33.32	-2.38	0.0175
Slope Variance	19.69	7.04	<0.0001
Mean Slope	-6.31	-8.46	<0.0001
Mean Elevation	1.2	0.824	0.4097
Dependent variable: NPP-Expected. n= 13975; R^2 = 60.9%			
Variable	Coefficient	T-Ratio	P-Value
Constant	-13.93	-6.02	<0.0001
NPP-MSAVI	1.2	147	<0.0001
%H20	-58.61	-3.67	<0.0002
Slope Variance	17.46	5.48	<0.0001
Mean Slope	-6.45	-7.59	<0.0001
Mean Elevation	-2	-1.2	0.2293

Effects of Vegetation Type

The results of a multiple regression analysis with the normalized difference of modelled and expected ANPP and the proportion of each vegetation class within each pixel for each of the 6 vegetation classes are presented in Table 3.7. Although significant, only a very small amount of the variation in the normalized difference values for the NDVI model values can be attributable to proportional vegetation cover (R^2 = 6.8%, $p<0.0001$). By contrast, with the MSAVI model 53.0% of the variation in the normalized difference values can be attributed to the proportion of vegetation cover in each vegetation class (Table 3.7). All of the vegetation classes had significant effects, and the

high productivity classes (MM, WSM, and TT) had the greatest effects. This finding supports the interpretation of the difference map (Figure 3.12), where modelled values tend to be lower than expected for high productivity vegetation types, and high for low productivity vegetation types.

Table 3.7. Results for multiple regression analysis on the normalized percent difference of modelled ANPP and expected ANPP with the proportion of vegetation cover for each class.

Dependent variable:Normalized Difference of NPP-MSAVI and Expected NPP. n= 16561; R^2 = 53.0%			
Variable	Coefficient	T-Ratio	P-Value
Constant	-39.56	-42.7	<0.0001
MM	39.49	41	<0.0001
WSM	333.36	51.2	<0.0001
TT	218.34	66.7	0.0001
DST	-31.08	-3.88	0.0008
SPV	-10.72	-3.34	<0.0001
BRN	19.38	5.3	<0.0001
Dependent variable:Normalized Difference of NPP-NDVI and Expected NPP. n= 16561; R^2 = 6.81%			
Variable	Coefficient	T-Ratio	P-Value
Constant	17.66	12.8	<0.0001
MM	8	5.56	<0.0001
WSM	232.15	23.9	<0.0001
TT	63.9	13.1	<0.0001
DST	-158.37	-13.3	<0.0001
SPV	15.14	3.16	0.0016
BRN	91.64	16.8	<0.0001

In summary, when compared to the expected ANPP map, the MSAVI model produced more accurate estimates: with 84.43% of the modelled annual NPP pixel values within 30% of the expected annual NPP pixel values, compared to the NDVI model, where only 41.76% of the pixel values within 30% of the expected annual NPP pixel values.

Inter-Annual Patterns of Mean NPP

A series of NPP images for each composite period throughout the growing season illustrates the spatial patterns of productivity within the Park (Figure 3.14). An annual productivity curve based on the mean of 150 randomly selected points within the Park illustrates the timing of onset, peak and end of the growing season (Figure 3.15). Onset of the growing season occurred directly after snow melt which occurred between June 1 and June 11, 2000. During this period mean values increased from 0 to 18.64 (±16.6) g m^{-2} 10-$days^{-1}$. NPP was highest between July 1 and July 11, 2000 with mean NPP at 22.61(±11.1) g/m^2*10-days. The growing season ended between September 11 and September 21, 2000.

Following the onset of the growing season, NPP values were greatest in the central region of the Park along the Hornaday river valley (Figure 3.14). Tussock tundra and mesic meadow cover are high in this region. During the June 21 composite period, there is a substantial drop in productivity, with mean NPP decreasing from 18.64 (±16.6) to 8.42 (±6.4) g m^{-2} 10-$days^{-1}$ (Figure 3.15 a). Mean total APAR dropped from 94.21 MJ/10-days in the June 11 composite period, to 44.86 MJ/10-days in the June 21 composite period (Figure 3.15 b). In order to examine the cause of this substantial drop in total APAR, mean total APAR values were extracted from raw daily images for the month of June (Figure 3.16). It was evident from this curve that snow melt occurred between June 7 and June 10 (Figure 3.16). After this period there was a steady and large increase in total APAR as the ground dried and vegetation began to green up (Figure 3.16). However, after June 20, daily total APAR values were considerably lower for

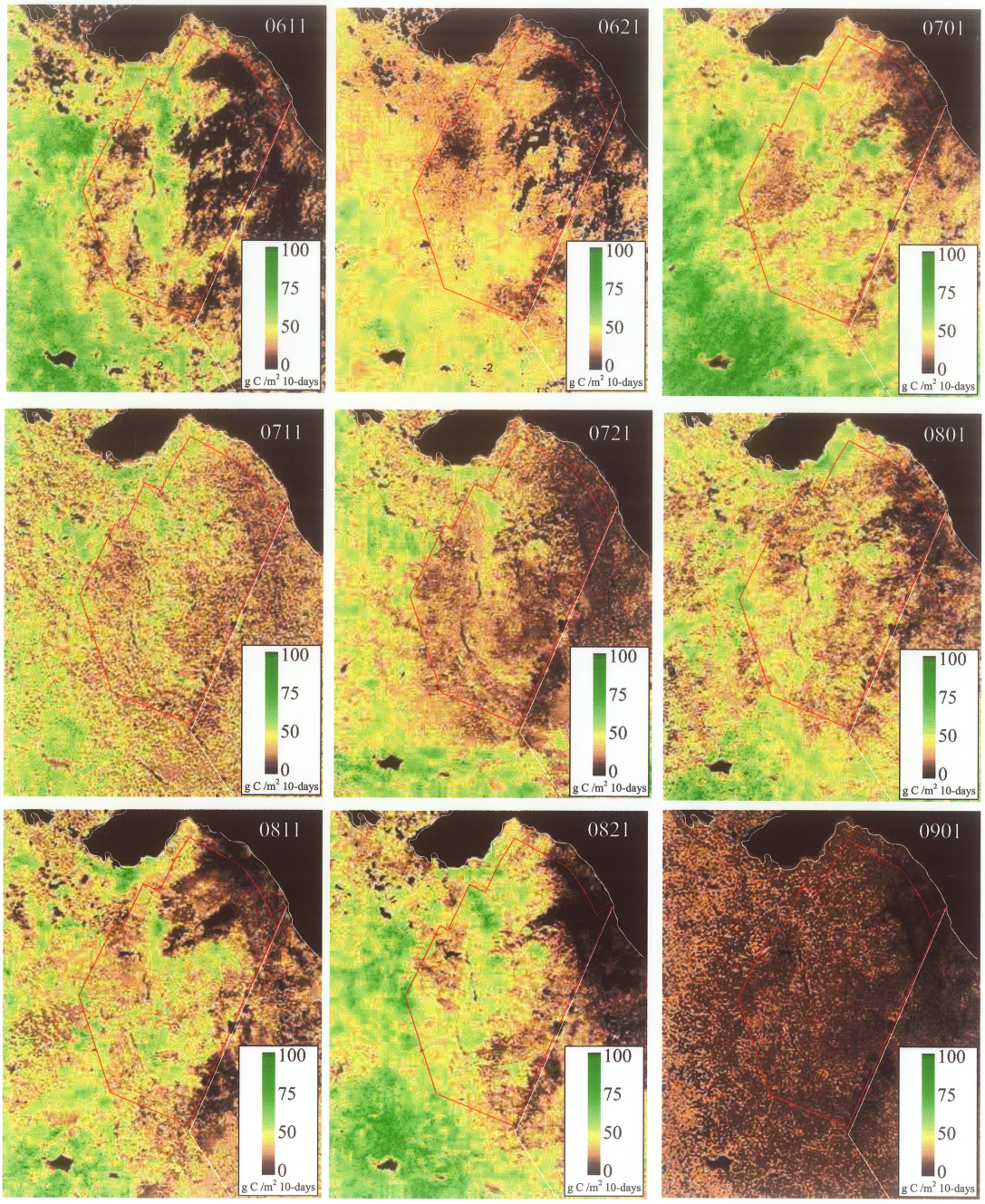

Figure 3.14. Modelled NPP in Tuktut Nogait National Park for each 10-day composite period during the 2000 growing season. FPAR derived from MSAVI. Numbers in upper right indicate date of composite period, (eg. 0611 = June 1 - June 11).

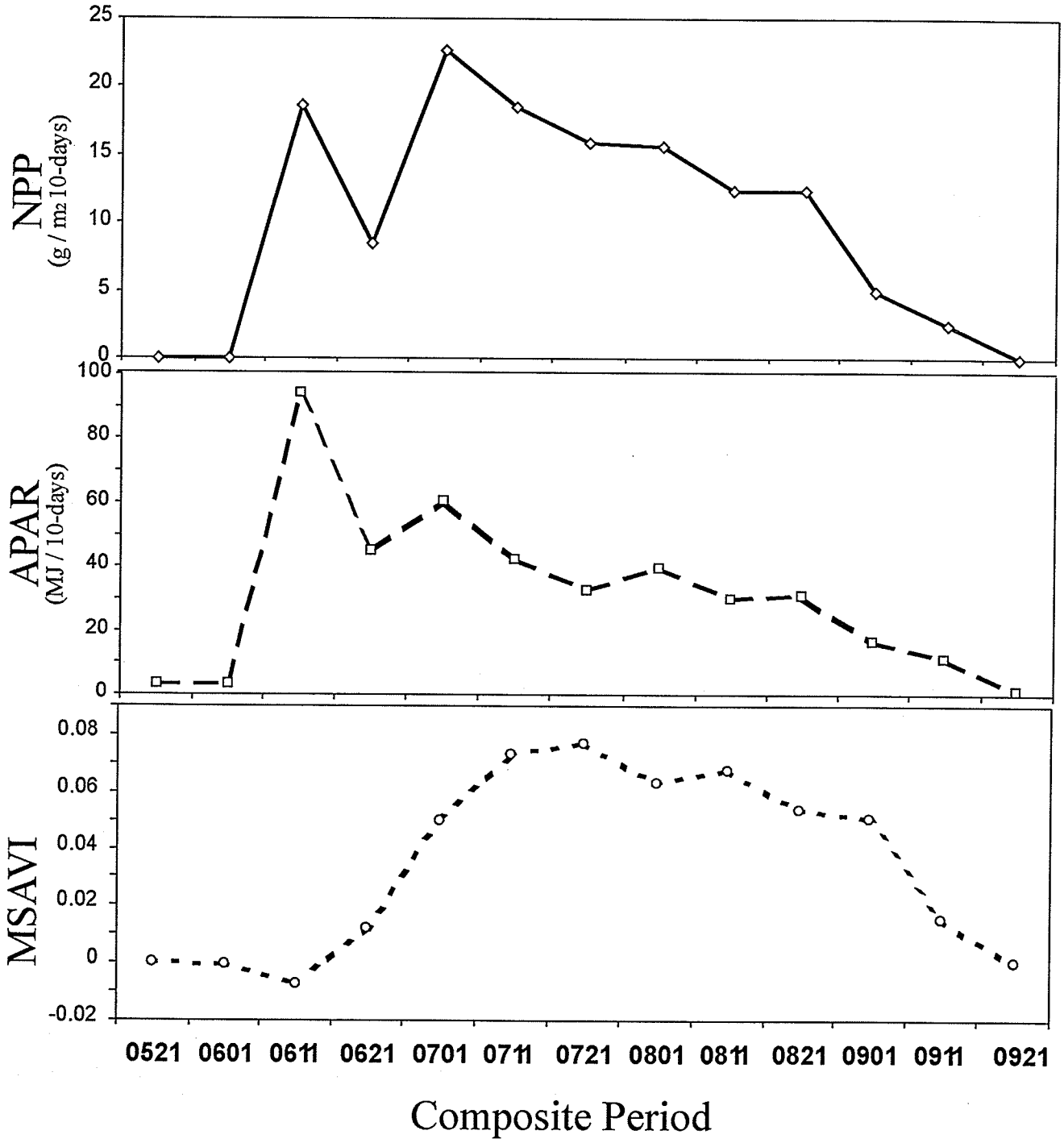

Figure 3.15. Mean values of (a) Net Primary Productivity, (b) Total APAR, and (C) MSAVI from 150 random points located within Tuktut Nogait National Park.

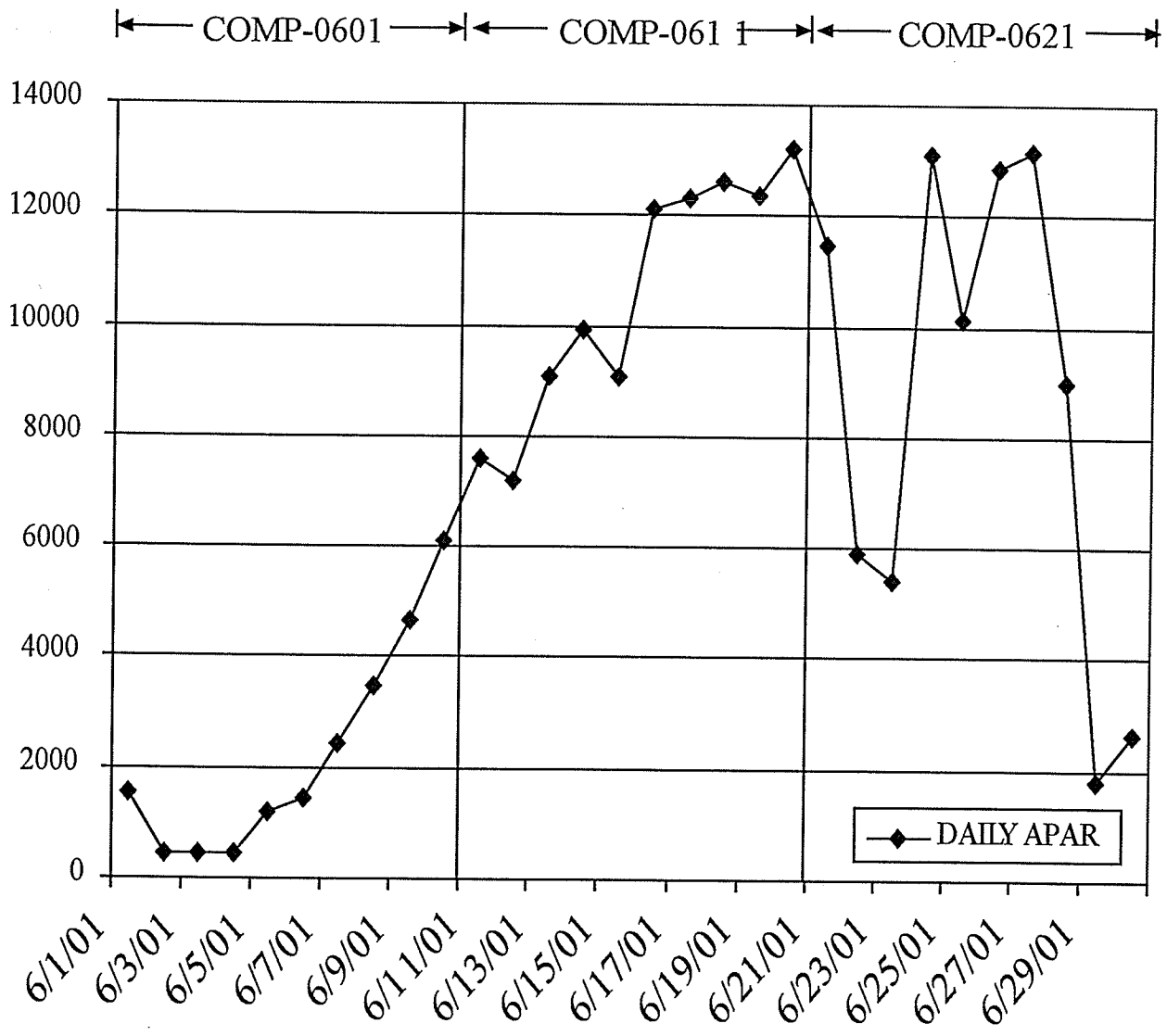

Figure 3.16. Daily Total APAR for the month of June. Values were determind from the mean of 150 random points located within Tuktut Nogait National Park. Snow melt occurred between June 7 and June 10. There was a considerable drop in APAR and subsequently NPP during the June 21 (0621) composite period as a result of extensive cloud cover.

much of the June 21 composite period. Examining the daily APAR and NDVI images, revealed extensive cloud cover during this period which ultimately resulted in low total APAR and NPP values for the composite period. Despite cloud cover during this period, vegetation continued growing and MSAVI values continued to climb (Figure 3.15 c), and despite only a relatively small gain in total APAR for the July 1 composite period, NPP values peaked for the year, with mean NPP values of 22.61(±11.1) $g/m^2$10-days (Figure 3.15 a). During this period, NPP values were relatively large in all areas of the Park, with highest productivity occurring along the east side of the Hornaday River valley. Over the rest of the growing season mean NPP values gradually decreased in all areas of the Park. The growing season ends during the September 11 composite period with mean NPP dropping from 2.4 (±2.7)g m^{-2} to 0 g m^{-2} in the September 21 image (Figure 3.15 a). A map of modelled ANPP computed using MSAVI is presented for in Figure 3.17 that covers the full extent of Tuktut Nogait National Park.

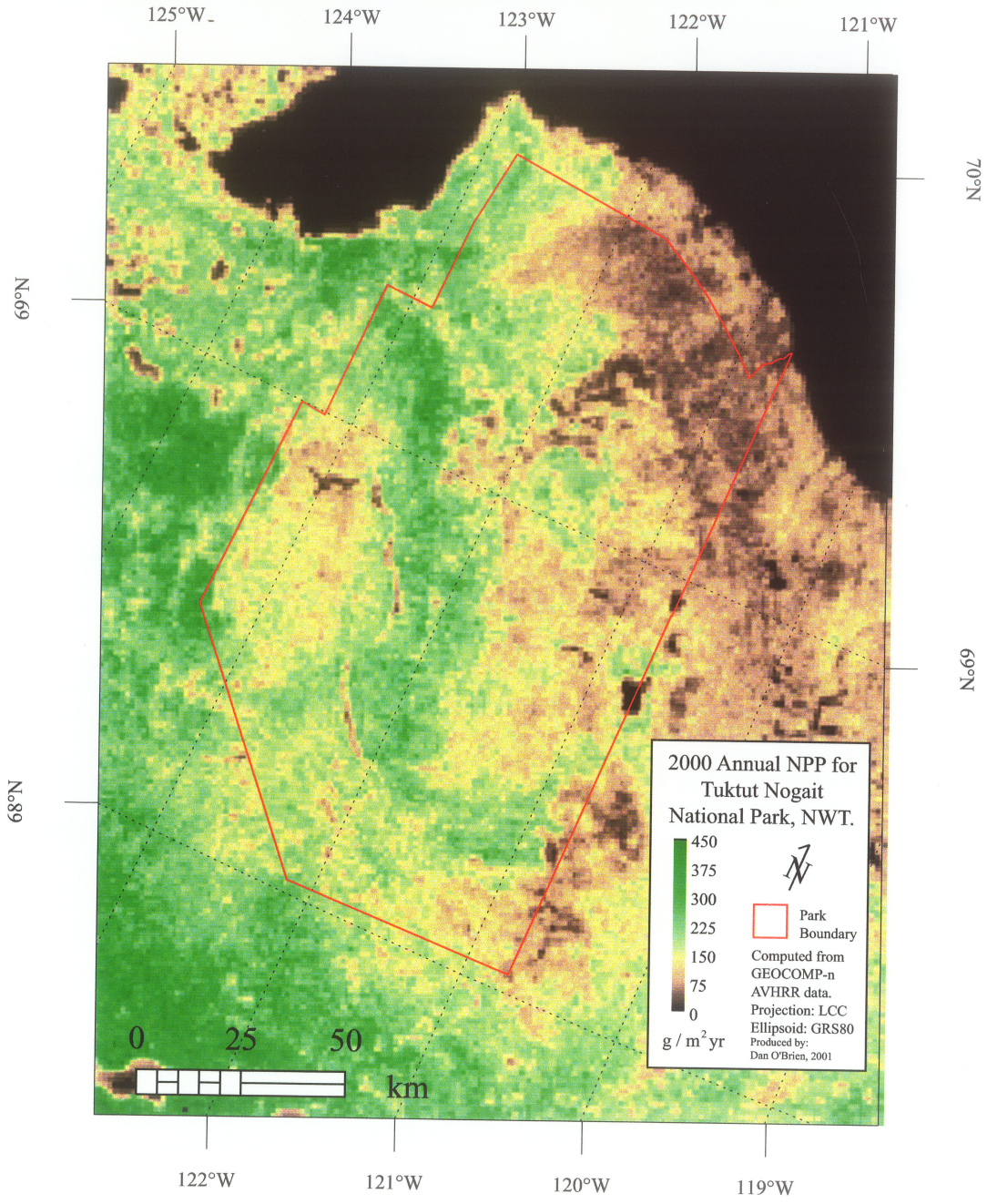

Figure 3.17. Map of modelled annual NPP for Tuktut Nogait National Park computed using GEOCOMP-n AVHRR data with FPAR determined using MSAVI.

3.5. DISCUSSION

Estimates of net primary productivity derived from the AVHRR model provide an excellent relative measure of the distribution of vegetation productivity within Tuktut Nogait National Park. Comparatively, modelled NPP corresponds exceptionally well with expected NPP (Figure 3.10), which is notable considering that the expected NPP map was produced using methodology and data that was completely independent of the model. Furthermore, the model is easily implemented and uses the GEOCOMP-n AVHRR data exclusively. From a park management perspective, the AVHRR NPP estimates will be particularly useful for asking questions; that is, identifying areas of interest that warrant further examination, either with high resolution imagery, or ground surveys.

Model Calibration

The reflectance and structural properties of Arctic landscapes differ fundamentally from more temperate landscapes. As a result, empirical relationships defined between spectral vegetation indices and NPP model parameters for temperate ecosystems will produce inaccurate results when applied to arctic ecosystems (Markon et al. 1995; Rees et al. 1998). The intention of this study was to develop a remote sensing NPP model specific to low-arctic ecosystems by calibrating model parameters using empirical field data. The importance of deriving arctic-specific model parameters is apparent when the results of the FPAR-NDVI relationship are examined. The slope value of the linear relationship between NDVI and FPAR (equation [17]: 0.638) is lower than for linear FPAR-NDVI relationships reported elsewhere in the literature (Table 3.1). Many of the

NDVI-FPAR relations defined in the literature are derived either from empirical FPAR measurements, or from simulation models parameterized for temperate vegetation canopies (e.g. Hatfield et al. 1984; Daugherty 1988; Sellers et al. 1994; Goward and Heummerich 1992). In these studies large ranges of NDVI values are used to define the FPAR relationship and a linear relation is fit, despite the fact that the relationship between FPAR and NDVI is slightly non-linear (Goward and Huemmrich 1992). Defining a linear relationship for an inherently non-linear relation will result in overestimates of FPAR in landscapes with low vegetation cover. A study examining the relationship between NDVI and FPAR for African Sahelian vegetation reported a linear relationship between FPAR and NDVI with a slope of 0.84 (Begue and Myneni 1996); this value is closer to the slope value derived here for Arctic vegetation. Moreover, using a vegetation index that corrected for variable background reflectance (i.e. MSAVI) minimized error in predicting FPAR (Begue and Myneni 1996).

Dry soils with high rock or gravel cover are 'brighter' and have higher reflectance values than wetter, 'darker', clay-loam soils (Richardson and Wiegand 1977). The effects of variable soil background reflectance are apparent in the regression between vegetation cover and $FPAR_{sfc}$ for samples below 30% vegetation cover, from which the FPAR-Vegetation Index relationship was defined (Figure 3.6). Although this regression was significant, the coefficient of determination was low as a result of considerable scatter attributable to variable soil conditions (Figure 3.6). The MSAVI removes some of this variability by including a soil adjustment factor derived from the relationship between red and NIR reflectance for bareground (Qi et al. 1994).

Using the MSAVI, rather than NDVI, to compute FPAR produces modelled NPP results more in line with expected NPP. Although MSAVI is not currently produced by GEOCOMP-n, it is relatively easy to compute with the available data. However, even though MSAVI was demonstrated to reduce variation in the vegetation signal for sparsely vegetated canopies, it is still necessary to use NDVI to derive both the energy conversion coefficient and ecosystem respiration. This is because these parameters are based on published work, from which the data sets used to determine these parameters were defined using only NDVI (Whiting et al. 1992; McMichael et al. 1999).

To evaluate the derived energy to GPP conversion coefficient, GPP was converted to NPP by subtracting R_a, and the energy conversion coefficient for NPP (ε_{NPP}) was determined from the resulting equation between NPP and $APAR_{can}$ ($\varepsilon_{NPP} = 0.851$). This value is comparable to those reported for temperate ecosystems with similar vegetation (reviewed by Gower et al. 1999). Values of ε_{NPP} reported for short grass prairie in Texas range from 0.24 to 0.80 (mean = 0.52 ±0.19), and values for tall grass prairie range from 0.80 to 1.33, (mean = 1.02 ±0.2) (Sims et al. 1978, cited in Gower et al. 1999). A value of 0.48 was reported for subalpine ecosystems in Oregon (Runyon et al. 1994). Although annual productivity in the arctic is low compared to temperate regions, the photosynthetic efficiency of arctic plant species is comparable to, if not higher, than that of temperate species (Dennis et al. 1978). In temperate regions, the photosynthetic efficiency of vegetation is dependent on air temperature, atmospheric humidity and soil moisture (Runyon et al. 1994). However, Arctic vegetation is well adapted to adverse environmental conditions, with optimum growth rates occurring at temperatures well below those of temperate species (Fogg 1998). Low temperature optimization in arctic

plants is related to increased concentrations of RuBP Carboxylase (Chapin and Shaver 1985; Fogg 1998). At higher temperatures, the oxygenase activity of RuBP Carboxylase results in respiration rates that exceed carbon assimilation, prohibiting these plants from surviving in temperate climates. At low temperatures, however, this respiration is not significant and the increased concentrations of the enzyme acts to optimize photosynthetic efficiency.

In the current application of this model, NPP is computed using AVHRR band 1 reflectance corrected for bidirectional and atmospheric effects in place of PAR surface albedo (A_{par}). PAR albedo was not available from GEOCOMP-n as a result of problems with the look-up tables used to define the ground-cover specific coefficients used to convert AVHRR channel 1 to PAR albedo. Although the BRDF corrected channel 1 reflectance are close to true PAR albedo for most vegetated surfaces (Cihlar et al. 1997b), NPP estimates may be improved using actual PAR Albedo measurements.

Model Evaluation

The expected ANPP map provides a extremely useful tool for validating the AVHRR NPP model, providing spatially continuous estimates of annual productivity derived from a data source entirely independent of the model input data. Despite its demonstrated effectiveness, some caution should be used when interpreting the results of the expected NPP map. Results from the error analysis indicated that the classification accuracy of the vegetation map was relatively low, and where no ground data exists (i.e. in the south of the Park) there was no way of evaluating the accuracy of the classification. The mesic meadow class was the most problematic and may have been too broad a class,

including pixels across a large range of vegetation productivity. Incorporating an intermediate class may provide a more accurate catagorization of the range of vegetation productivity within the Park. Error in the classification can also be attributed to the fact that the TM image and the ground samples were acquired at different times. For example, where wet sedge meadow was incorrectly classified as snow in the 1992 image, it is likely that in the 2000 image the snow had melted revealing wet sedge meadow beneath. Although the classification accuracy of this vegetation map could be improved considerably, producing a high quality vegetation map for this Park is beyond the scope of this study.

Error in the expected ANPP map can also be attributed to variability in the ANPP values obtained from literature sources (Table 3.5). This variability was largest in the high productivity vegetation classes (wet sedge meadow (WSM) and tussock tundra (TT)) and is likely attributable to differences in below-ground NPP estimates for these classes. It is very difficult to obtain accurate measures of below-ground biomass, and estimates of below-ground NPP must be determined from ratio estimates of above to below-ground biomass (Shaver and Chapin 1991). Furthermore, in arctic vegetation, rates of below-ground root growth vary throughout the growing season (Shaver and Billings 1977). Therefore, estimates of below-ground NPP obtained from ratios of above to below-ground biomass will vary depending on when the biomass samples were obtained. This has important implications when evaluating the results of the model against the expected ANPP map.

Normalized percent difference values for the MSAVI model were highest where tussock tundra and wet sedge meadow cover was high (Figure 3.12). When proportional

vegetation cover for each class was included in a multiple regression analysis comparing modelled ANPP and Expected ANPP, WSM and TT cover had the greatest influence on the regression (Table 3.7). Moreover, the categorization of vegetation into discrete classes ignores the actual range in vegetation productivity, resulting in overestimates of expected ANPP where actual ANPP is lower than the mean for that class. Thus, in areas of high productivity vegetation, modelled values may be lower than expected because of inaccurate estimates of ANPP for these vegetation classes.

The opposite is true in some areas where modelled estimates of ANPP are higher than expected and cover of the low productivity classes is high (Figure 3.12). Estimates of expected ANPP for the barren and sparsely vegetated classes may be too low. Expected ANPP values for these vegetation types were obtained from data for high arctic polar desert and semi-desert vegetation (Bliss et al. 1984; Bliss and Matveyeva 1992; Bliss and Gold 1999). Although the floristic structure is similar in the barren and sparsely vegetated vegetation classes, it is likely that ANPP is higher at lower latitudes where the growing season is longer, and mean annual temperatures are higher.

Others have examined the effects of subpixel water bodies and variable topography on AVHRR satellite imagery (Burgess et al. 1995; Cihlar et al. 1997a). In this study correspondence between modelled ANPP and expected ANPP was significantly affected by variable topography and sub-pixel water cover. With increasing water cover, modelled ANPP values tended to be greater than expected ANPP (Table 3.6). This is likely caused by the residual effect of resampling large AVHRR pixels at high view zenith angle to 1x1 km during the processing of the imagery (Cihlar et al. 1997a). Where adjacent pixels with high and low reflectance values occur (i.e. over water bodies), higher

reflectance values in the large AVHRR pixels over land will dominate the values in the smaller resampled pixels, effectively reducing the apparent effects of water on the landscape (Cihlar et al 1997). Furthermore, in areas of rough terrain the model may underestimate ANPP, whereas in areas of steep terrain the model may overestimate ANPP. Areas with high steep terrain correspond to mountainous areas in the central region of the Park. Overestimates of ANPP in these areas may be caused by higher than expected vegetation index values as a result of increased NIR reflectance from lichen covered rock (Rees et al. 1998). Although these results may provide insight into the effects of water and topography on modelled ANPP estimates, it should be emphasized that the effect of these variables on the overall regression relationship was relatively small; R^2 increased by only 0.7% for the MSAVI model, and 0.3% for the NDVI model (Tables 3.6 & 3.7). In a similar study, Burgess et al. (1995) found that the influence of variable topography on AVHRR NDVI values was minimal.

Factors Influencing NPP in Tuktut Nogait National Park

The least productive areas of Tuktut Nogait National Park lack wind protection, resulting in minimal snow accumulation during the winter. With little insulation from snow, severely cold temperatures and wind abrasion pose severe limitations on vegetation. With little vegetation to insulate the soil, the ground thaws quickly and the gravelly soils retain little water as melted snow drains off quickly (Fogg 1998). Compounded with low annual precipitation, most arctic plants cannot survive these conditions. This is apparent in the barren Melville Hills in the central region of Tuktut Nogait where vegetation productivity is lowest; and the coastal region to the northeast, where a rain shadow effect results in very dry conditions (Figure 3.16).

The presence of flowing water greatly affects nutrient availability by bringing nutrients to the root surfaces (Chapin et al. 1988). Some of the most productive arctic vegetation communities, with the highest biodiversity, are on slopes of river valleys where water runs freely between the permafrost and the soil surface (Chapin and Shaver 1985; Chapin et al. 1988). This is apparent on the east side of the Hornaday River Valley, where continuous run-off from the Melville Hills and southern exposure results in the highest vegetation productivity in the Park (Figure 3.16). This area experiences a surge in productivity early in the growing season, followed by decreased, but steady productivity throughout the rest of the growing season (Figure 3.14). Along the east slopes of the Hornaday river valley deciduous plant species are common. For deciduous arctic plants above-ground growth occurs most rapidly just following snow melt, when solar radiation, water availability and air temperature are most favourable (Chapin and Shaver 1985). Above-ground growth slows in mid to late summer with below-ground root growth increasing (Shaver and Billings 1977). The concentration of above-ground growth in early spring, followed by increased below-ground production in mid to late summer, enables growth of each plant structure to occur when conditions are most favourable.

Application of the NPP Model.

The productivity model presented in this study enables regional scale patterns of NPP within Tuktut Nogait National Park to be spatially quantified with a relatively high degree of accuracy. The model is easy to implement and uses GEOCOMP-n AVHRR data exclusively. An assessment of the accuracy of the absolute NPP values produced from the model indicates good correspondence. However, this accuracy assessment is limited by the accuracy of the expected annual NPP map and could potentially be higher.

The NPP estimates will provide useful information for ecosystem monitoring in northern regions, enabling the identification of high productivity areas where biodiversity is expected to be highest. Furthermore, model results will provide the necessary empirical data to justify management activities in areas of high biodiversity. The 1x1 km spatial resolution of the AVHRR NPP maps enable patterns of productivity to be evaluated and analyzed at a regional scale. The 10-day temporal resolution of these data will enable Park managers to study interannual patterns of productivity both within and among Parks. This will provide information about the timing of events such as onset and duration of the growing season, when and where peak productivity occurs within the Park, and how environmental factors such as global warming influence productivity patterns. Spatially and temporally continuous estimates of NPP will be extremely useful to wildlife managers. These data could be used to improve the efficiency of aerial surveys. For example, aerial surveys could be stratified by correlating caribou density with spatial and temporal patterns of productivity within a Park. Considering that there is currently no other practical way of assessing regional scale productivity patterns in Canada's northern national Parks, the NPP model will provide a useful tool for ecosystem monitoring and a source of empirical data for justifying management decisions.

4. VALIDATING GEOCOMP-N AVHRR SATELLITE IMAGERY USING SCALED-UP FIELD MEASUREMENTS OF REFLECTANCE

4.1. ABSTRACT

The remoteness and large spatial extent of the arctic makes remote sensing a necessary tool for monitoring the effects of anthropogenic disturbance and the potential effects of climate change on northern ecosystems. Accurate landscape-scale measurements of ecosystem processes derived from satellite imagery require data that has been corrected for atmospheric and bi-directional reflectance effects. The effectiveness of these corrections for AVHRR imagery acquired in a region of low-arctic vegetation was evaluated using scaled-up measurements of surface reflectance obtained in the field with a hand-held radiometer. The influence of landscape heterogeneity on scaling-up fine resolution observations was examined by aggregating Landsat NDVI to AHVRR resolution in both homogeneous and heterogeneous areas. Results indicate that landscape heterogeneity has a large influence on scaling-up fine scale observations because of the influence of numerous small water bodies and differences in sensor bandwidths. Scaled-up field measurements of NDVI trended well with atmospherically corrected AVHRR NDVI, although field measurements of NDVI were consistently higher. This difference is likely attributable to directional reflectance effects as a result of large sun angles. Applying a bi-directional reflectance correction (BRDF) should improve correspondence between AVHRR NDVI and NDVI computed from field measurements of surface reflectance. However, current BRDF corrected imagery should not be used until improvements have been made to the GEOCOMP-n bi-directional reflectance correction procedures.

4.2. INTRODUCTION

Large scale models of terrestrial net primary productivity (NPP) commonly utilize satellite imagery from the NOAA Advanced Very High Resolution Radiometer (AVHRR) as input data to derive biophysical model parameters (Field et al. 1995; Ruimy et al. 1996; Liu et al. 1997; Malmström et al. 1997; Goetz et al. 1999). The AVHRR sensor produces coarse resolution multispectral images (1.1 km at nadir) with very high temporal frequency (twice daily global coverage). Variable spectral response of vegetation in the red and near infrared (NIR) region of the spectrum enable vegetation indices to be computed from linear combinations of the first 2 AHVRR bands (B1=Visible; and B2=NIR). The most common of these indices is the normalized difference vegetation index (NDVI), which is computed from the difference of B2 and B1 divided by the sum of these bands (Rouse et al. 1973). AVHRR NDVI is frequently used to indirectly measure biophysical properties of vegetation canopies such as vegetation biomass (Tucker 1979; Box et al. 1989), leaf area index (Chen 1996), primary production (Box et al. 1989), and fraction of absorbed photosynthetically active radiation (Begue and Myneni 1996; Moreau and Li 1996).

Relationships between NDVI and these biophysical parameters are typically derived from empirical measures of surface reflectance obtained in the field (e.g. Chen 1996). However, atmospheric attenuation of visible and near-infrared reflected radiance, caused by atmospheric aerosols and water vapour, produces considerable variation in normalized difference vegetation index (NDVI) (Tanré et al. 1992; Goetz 1997). NDVI is also strongly influenced by directional surface reflectance effects (Holben et al. 1986). Thus, when applying relationships defined from fine-scale ground measurements to

coarse-resolution satellite imagery, it is imperative that the imagery be corrected for such effects so that the pixel values in the image are a true representation of surface reflectance.

The GEOCOMP-n image processing system at the Manitoba Centre for Remote Sensing uses the simplified method of atmospheric correction (SMAC) to correct AVHRR channels 1 and 2 for atmospheric effects (Cihlar et al. 2000). The SMAC algorithm utilizes sun-sensor angle information, estimates for vertically integrated gaseous constants, aerosol optical depth, atmospheric water vapour and ozone content to compensate for atmospheric absorption and scattering (Rahman and Dedieu 1994). Bidirectional reflectance (BRDF) effects are corrected for using landcover specific coefficients and information on sun-sensor geometry (Cihlar et al. 2000). However, large sun angles and long sensor path lengths present significant challenges when working with AVHRR imagery in northern latitudes (Holben 1986; Rahman and Dedieu 1994). At high solar zenith angles, differences between the actual state of the atmosphere and the state assumed by the SMAC algorithm likely contribute considerable error to the imagery (Cihlar et al. 1997b). Furthermore, georeferencing accuracy is not consistent or reliable in spring, autumn and winter months, as many of the GCP points used to georeference images are located on northern coastlines and cannot be used when covered by snow or ice. The BRDF correction uses landcover-specific correction coefficients, requiring that each AVHRR pixel be assigned to a landcover class. Thus, concerns regarding the reliability of BRDF corrected AVHRR surface reflectance have been raised because of the dependence of spatially collocating AVHRR pixels with a land cover classification of limited detail (G. Fedosejevs pers. comm.).

Rigorous validation of biophysical parameters derived from AVHRR data has been conducted in grassland (Sellers et al. 1992), boreal forests (Sellers et al. 1995), grassland/ savannah (Prince et al. 1995), and coastal, montane and subalpine ecoregions (Goward et al. 1994). However, there is a paucity of empirical ground validation for biophysical parameters derived from AVHRR imagery in terrestrial Arctic ecosystems. Often, when NPP models are applied to arctic ecosystems, it is assumed that model coefficients are equivalent to those defined for rangeland or pasture (eg. Cihlar et al. 1997a). Although arctic vegetation is similar in structure to rangeland of pasture, the reflectance properties of arctic vegetation are unique (Rees et al. 1998).

Validating biophysical parameters derived from satellite imagery involves comparison with independently obtained data sources, such as field data or other independent satellite data sets (Cihlar et al.1997). Alternatively, results can be compared with output from empirical models describing physical and biophysical processes for a specific location (Cihlar et al.1997). When interpreting results of such inter-comparisons, it is important to consider the possibility of error in the comparison data set. Indeed, both the comparison data and the data being evaluated may be subject to similar error or bias (Cihlar et al.1997). Degraded high resolution satellite imagery can be used to evaluate the accuracy of bio-physical parameters computed from coarser resolution imagery (Cihlar et al. 1997 b), however, only ground measurements are representative of actual surface reflectance in the absence of atmospheric effects. The fundamental challenge in comparing reflectance measurements obtained in the field, to reflectance values derived from AVHRR imagery lies in characterizing a continuous surface equivalent to the resolution of the AVHRR pixel, using discrete fine-scale measurements.

The main objective of this paper is to evaluate the accuracy of corrected AVHRR NDVI for arctic landscapes, by comparing AVHRR NDVI pixel values with scaled-up measurements of NDVI obtained in the field using a hand-held radiometer. Comparing AVHRR NDVI pixel values with discrete field measurements of NDVI integrated across a 1x1 km area is potentially subject to error attributable to a number of factors. Raw AVHRR pixels are resampled from 1.1km (or larger) resolution to 1 km resolution, thereby altering the original pixel values. Also, the positional accuracy of the AVHRR image data is relatively low (±500m) and the area of ground from which the field measurements of NDVI are obtained may not match up exactly with that covered by the AVHRR pixel. Furthermore, bandwidth differences between the sensor of a hand-held radiometer and the AVHRR sensor will result in different NDVI values, with the magnitude of this difference increasing with increasing vegetation cover (Figure 4.1). It is hypothesized that these factors will have a larger effect on correspondence in heterogeneous landscapes compared to homogeneous landscapes. If this hypothesis is true, the accuracy of AHVRR NDVI validation may be improved by locating field samples in homogeneous areas. The objectives of this study are:

1. To evaluate the correspondence between aggregated Landsat NDVI and AVHRR NDVI in homogeneous and heterogeneous areas.

2. To evaluate the influence of the above factors on scaling-up 1x1 m field measurements of NDVI to Landsat and AVHRR resolution.

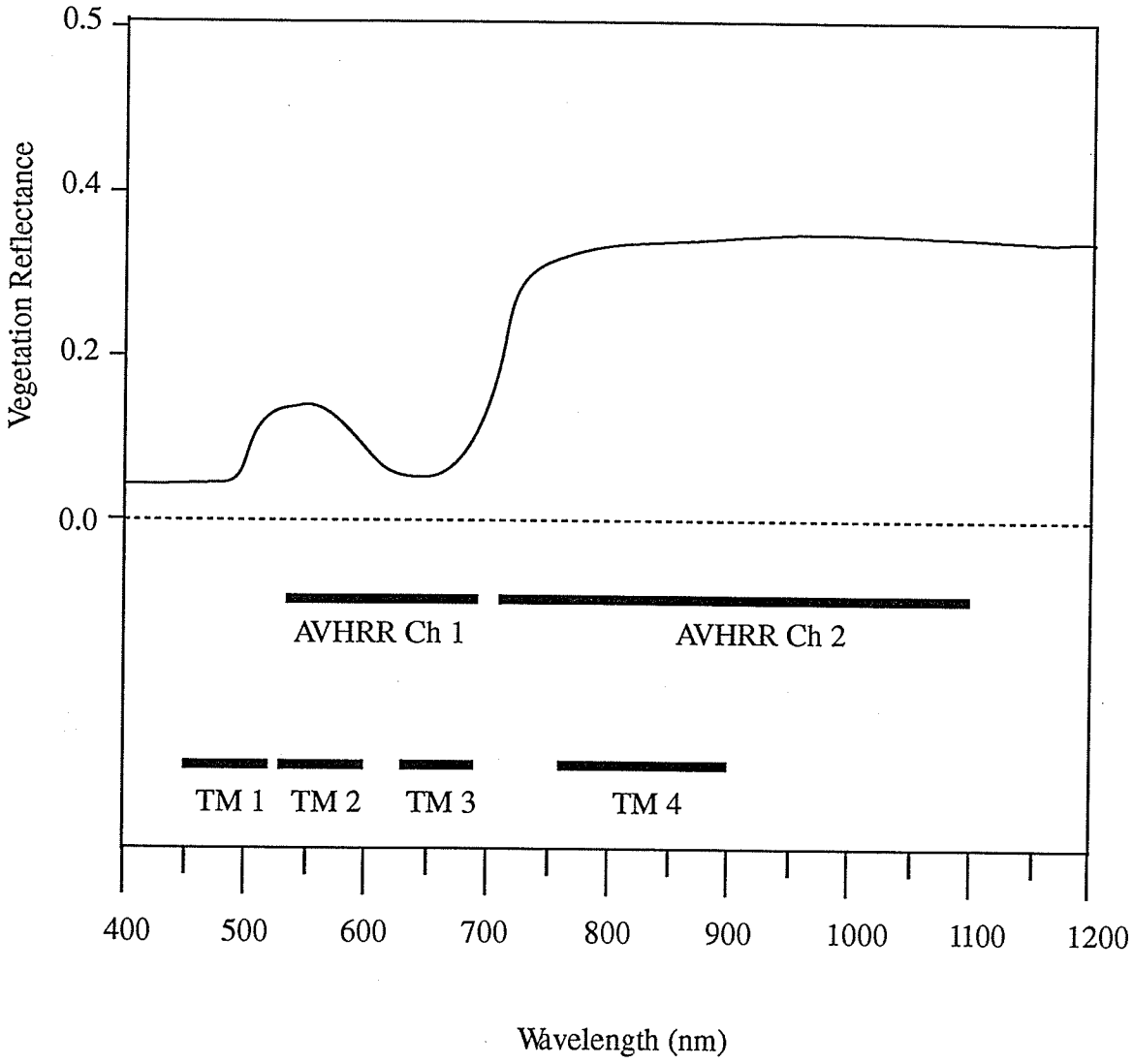

Figure 4.1. Differences is bandwidths between the AVHRR visible (Ch1) and near infrared (Ch2) bands, and the Landsat 7 ETM visible bands (TM1, TM2, TM3) and near infrared (TM4).

4.3. METHODOLOGY

Study Area and Ground Data.

Ground data used for this analysis were collected between July 8th and August 10th, 2000 within a 20 km radius of three areas within Tuktut Nogait National Park, NWT (See Chapter 2: Study Area, Figure 2.1). The vegetation within the Park is characteristic of low arctic tundra, consisting of a mosaic of sparse and barren vegetation cover mixed with mesic dwarf shrub/ sedge meadow, tussock tundra, and wet sedge meadow (See Chapter 2: Study Area). Arctic vegetation productivity is strictly governed by water availability and exposure (Chapin and Shaver 1985; Chapin et al. 1988), and the most productive vegetation communities within the Park exist at low elevations in valleys, along rivers and on hill slopes (personal observation).

A total of 18 (1x1 km) sites were selected to represent the range of vegetation communities within the Park. Sites were located in relatively homogeneous landscapes (i.e. free of small lakes and of a consistent vegetation type within a 1x1 km area). Plot layout was designed to facilitate scaling-up ground measurements to a 1x1km area for comparison with spatially collocated AVHRR pixels (Figure 3.2). Within each site, nine 30x30 m plots were located in a 3x3 grid, located 250m in from the edge of the site boundary (Figure 3.2). The southwest corner of each plot was located on the ground using a hand-held global positioning system with a positional accuracy of ±4m. Within each plot, five 1x1 m sample quadrats were located in a cross pattern using a compass and a line of fixed length (Figure 3.2). For each sample quadrat (n=865), incident and reflected radiance was measured in 5 spectral regions (450-520 nm, 520-600 nm, 630-690

nm, 760-900 nm and 1550-1750 nm) using a Cropscan MSR 5 radiometer (Cropscan Inc., www2.isl.net/cropscan). The radiometer was attached to a boom and held 2 meters above the surface, enabling a 1 meter field of view, and the average of five scans was recorded. Up and down-looking sensor pairs were calibrated to each other and all radiance measurements were corrected for sensor-temperature effects and variable sun-angle, using a post-processing program supplied by the manufacturer. Percent surface reflectance of each sample was calculated from the down- and up-looking radiance measurements. With both up and down-looking sensors it was possible to accurately measure surface reflectance under variable cloud conditions and various sun-angles.

Satellite Image Data

The AVHRR imagery used in this analysis were provided by the Manitoba Centre for Remote Sensing (MCRS). Raw AVHRR imagery were processed using the GEOCOMP-n image processing system developed by the Canadian Centre for Remote Sensing (CCRS). Raw daily images are georeferenced, resampled to 1x1 km resolution and projected in Lambert Conformal Conic projection. Georeferencing accuracy was reported to be ±500m (P. Hurlbert, pers. comm.). The image is then calibrated to reflectance and corrected for atmospheric and bidirectional reflectance effects. Cloud-free 10-day maximum value NDVI composites are then created by selecting the pixel with the largest NDVI value from the daily images within the 10-day composite period. An AVHRR NDVI maximum value composite image covering the study area was obtained consisting images acquired between July 11 and July 21, 2000. This composite period best corresponded to the peak of the growing season, a period when variation in NDVI values are minimal. This period also best coincided with the time period during which

ground samples were obtained. For the following analyses three of the available GEOCOMP-n channels were used: NDVI computed from top of atmosphere reflectance ($NDVI_{retoa}$); NDVI computed from atmospherically corrected visible and NIR reflectance ($NDVI_{smac}$); and NDVI computed from AVHRR b1 and b2 corrected for bi-directional reflectance effects ($NDVI_{brdf}$).

A precision geocorrected and radiometrically calibrated Landsat 7 ETM scene acquired on July 13, 2000 and centered at 69° 08' 43" N 122° 41' 57"W, was obtained from Radarsat International (Richmond, BC). The image provided by Radarsat International was georeferenced using 10 control points (RMS ± 18.34m) and projected in UTM zone 10 North (NAD 83). Image radiance was converted to top of atmosphere reflectance using acquisition date, sun angle and azimuth to convert Landsat ETM radiance to exoatmospheric reflectance. NDVI was then computed as:

$$NDVI = (B4-B3)/(B4+B3) \quad [1]$$

where B3 and B4 is the Landsat visible (red) and NIR reflectance, respectively.

Landscape Heterogeneity

Examining the effects of landscape heterogeneity on integrated reflectance required a number of sample sites located in both homogeneous and heterogeneous areas. Twenty homogeneous and 20 heterogeneous areas, each 1x1 km in size, were visually located within the Landsat NDVI image. These areas were selected to be representative of the range of vegetation types and productivity within the Park. Homogeneous areas were selected from areas with no or very few lakes, simple topography and overall low variation in NDVI. Heterogeneous areas were selected in areas with variable NDVI

values, containing numerous small water bodies, and complex topography. From the AVHRR NDVI image, the position of the upper left corner for each AVHRR pixel was delineated in a vector point file. Using the pixel corner points as a guide, 20 1x1 km image 'chips' were extracted from the heterogeneous areas, and 20 from the homogeneous areas. For each 1x1 km image chip B3, B4 and NDVI pixel values were extracted from the Landsat image. Because the Landsat image had not been corrected for atmospheric effects, pixel values corresponding to each of the 1x1 km Landsat image chips were extracted from the AVHRR NDVI image computed from top of atmosphere reflectance (AVHRR $NDVI_{retoa}$).

Scaling-up Field NDVI

To compare the integrated field measurements of NDVI with Landsat and AVHRR image data, each 1x1 km field site was located within the Landsat and AVHRR images using the GPS coordinates measured in the field. For each of the 18 field sites, 1x1 km image chips were extracted from the Landsat image. For each 30x30 m field plot, the corresponding Landsat NDVI pixel value was also extracted. Pixel values corresponding to the location of the center plot within the 1x1 km field site were extracted from both the atmospherically corrected AVHRR image (AVHRR $NDVI_{smac}$), and the bidirectional reflectance corrected AHVRR NDVI image (AVHRR $NDVI_{brdf}$).

Spatial Degradation of Landsat NDVI

A non-linear interaction between NDVI and the visible and NIR reflectance of a surface will result in different values of aggregated NDVI depending on how the Landsat NDVI values are degraded to AVHRR resolution (Aman et al. 1992). Spatially degraded

NDVI from high resolution image pixels (i.e. Landsat) can be computed in two ways. Integrated NDVI (iNDVI) is obtained by determining the mean of the NDVI pixel values within the aggregate area: iNDVI = $\sum$ NDVI / n, where n is the number of NDVI pixels within the aggregate area. The spatial average of NDVI (mNDVI) is obtained by computing NDVI from the mean of visible and NIR reflectance pixels within the aggregate area: mNDVI = (/x – /y) / (/x + /y), where /x is the mean of near infrared reflectance (NIR) pixels and /y is the mean of visible reflectance (VIS) pixels across the aggregate area. Differences between iNDVI and mNDVI can be as large as 7%, and the slope and intercept of the linear correlation between iNDVI and mNDVI are dependent on the spatially heterogeneity of the surface (Aman et al. 1992). To determine whether the method in which Landsat NDVI was aggregated had any influence on the correspondence with AVHRR NDVI , both iNDVI and mNDVI were computed from the extracted Landsat image chips.

To examine the effects of different sensor bandwidths in comparing NDVI values derived from different sensors, field measurements of NDVI were computed using the mean of radiometer bands 2 and 3 as the visible band in the NDVI calculation. By computing the mean of radiometer bands 2 and 3, the radiometer visible reflectance values should be closer to the AVHRR visible reflectance, as the AVHRR visible band covers a larger portion of the visible spectrum compared to the radiometer band 3 alone.

Quantifying Landscape Heterogeneity

The influence of water cover on the correspondence between aggregated Landsat NDVI and AVHRR NDVI was examined by determining the proportion of water cover

within each 1x1km image chip. A water mask was created by performing an unsupervised k-means classification of the Landsat image. The proportion of water cover within the 1x1km image chip was then computed by determining number of water pixels, then dividing by the total number of pixels within that area.

The coefficient of variation (CV) was used to quantify heterogeneity within the sample areas. The CV is a standardized measure of spatial variability and was determined by dividing the standard deviation of the 1600 Landsat NDVI pixel values within each 1x1 km area by the mean of the pixel values within that area.

Statistical Analyses

Correspondence between both iNDVI and mNDVI computed from aggregated Landsat data and AVHRR NDVI in homogeneous and heterogeneous areas was evaluated using linear regression analysis. The influence of water cover on the correspondence between iNDVI and mNDVI computed from aggregated Landsat data was evaluated by including proportional water cover in a multiple regression analysis. Similarily, the influence of landscape heterogeneity on the correspondence between iNDVI and mNDVI was evaluated by including CV in a multiple regression analysis.

For each 30x30m field plot, the mean of the five individual radiometer measurements of NDVI values was determined. Radiometer data was accidentally not recorded for plots 21 and 69 therefore reducing the number of 30x30m field plots from n=162 to n=160. Correspondence between these values and the individual Landsat NDVI pixel values was evaluated using linear regression analysis. For each of the 18 1x1 km field sites, NDVI was integrated over the 1x1 km area by determining the mean of the 45

1x1 m radiometer measurements of NDVI (or 40 1x1 m measurements, for sample 2 and 6 where data was missing). Correspondence between integrated field NDVI and the aggregated Landsat NDVI, AVHRR $NDVI_{smac}$ and AVHRR $NDVI_{brdf}$ values was evaluated using linear regression analysis. The influence of landscape heterogeneity on the relationship between integrated field NDVI and AVHRR $NDVI_{smac}$ was evaluated by including CV in a multiple regression.

4.4. RESULTS

Influence of Landscape Heterogeneity on the Correspondence Between Aggregated Landsat NDVI and AVHRR NDVI

Mean CV was significantly lower in the homogeneous 1x1 km sample areas compared to the heterogeneous sample areas, indicating that visual interpretation of the Landsat NDVI image was adequate in distinguishing homogenous from heterogeneous areas (Table 4.1).

Table 4.1. Quantifying spatial heterogeneity in 1x1 km sections of a Landsat NDVI image. CV is the coefficient of variation for the NDVI pixel values within each section.

	Mean CV
Heterogeneous (n=20)	45.46%
Homogeneous (n=20)	14.58%
P-Value for one-tailed T-Test	0.0002

Correspondence between aggregated Landsat NDVI and AVHRR NDVI was considerably higher in homogeneous areas compared to heterogeneous areas (Figure 4.2). In homogeneous areas, the linear regressions were highly significant for both iNDVI and mNDVI (iNDVI: $R^2 = 97.5\%$, $p<0.0001$, $n=20$; mNDVI: $R^2= 97.4\%$, $p<0.0001$, $n=20$) and there was very little difference in the R^2 values between iNDVI and mNDVI (Figure 4.2). In heterogeneous samples, the correspondence between aggregated Landsat NDVI pixels and AVHRR NDVI pixel values was considerably lower (Figure 4.2). Furthermore, the proportion of variance explained by the linear regression between AVHRR NDVI and Landsat mNDVI was slightly higher compared to the regression between AVHRR NDVI and iNDVI, with R^2 increasing from 75.7 to 77.9% (Figure 4.2).

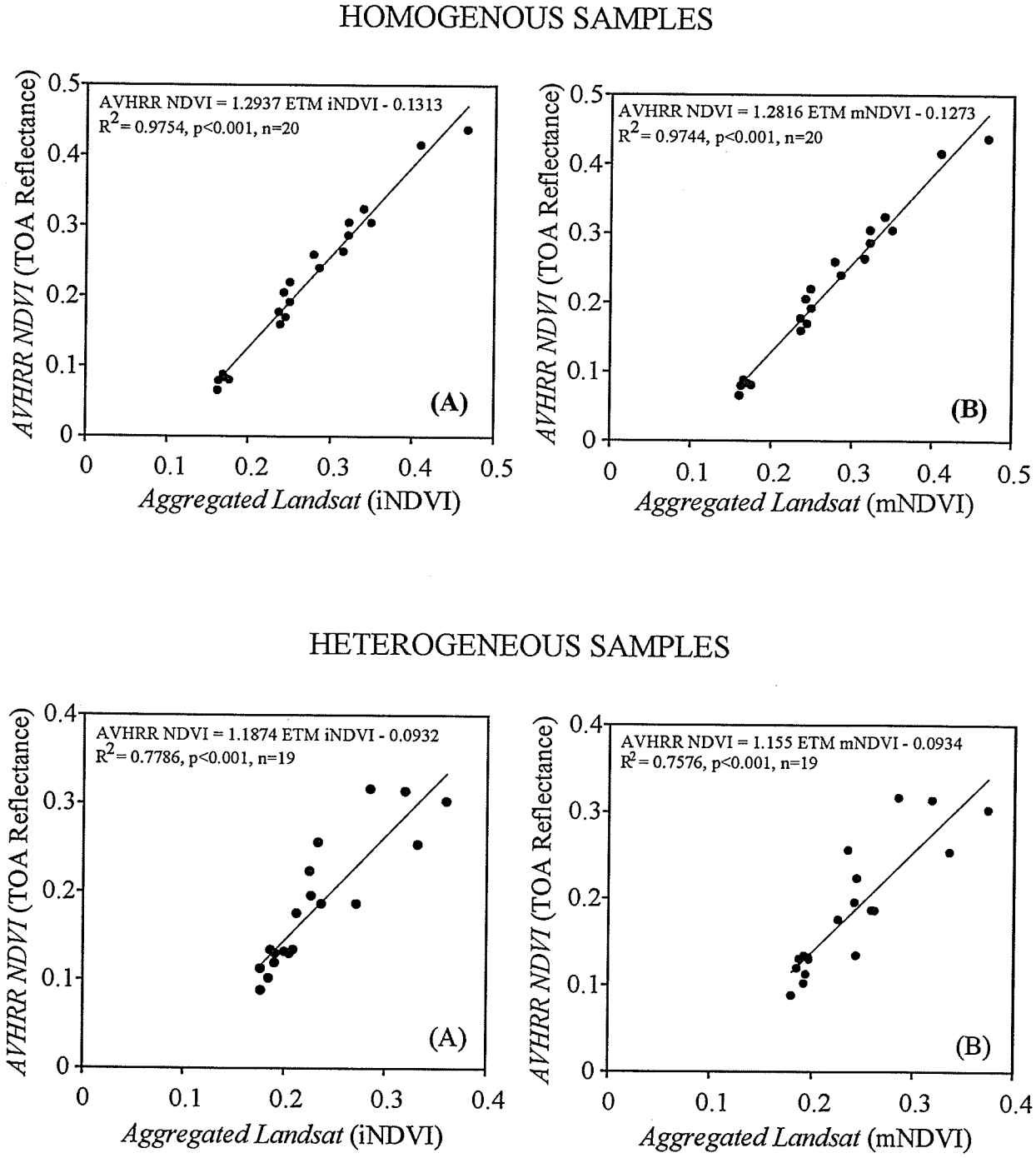

Figure 4.2. Scatterplots of (A) Integrated Landsat NDVI (iNDVI) and AVHRR NDVI computed from top of atmosphere reflectance; and (B) Mean Landsat NDVI (mNDVI) and AVHRR NDVI computed from top of atmosphere reflectance. For heterogenous samples, R^2 is nearly equal, indicating no increase in correspondence with mNDVI. For heterogeneous samples, R^2 is slightly higher for iNDVI, suggesting iNDVI corresponds better with AVHRR NDVI. Overall, correspondence is higher in homogenous samples compared to heterogenous samples.

For all cases, aggregated Landsat NDVI values were higher than AVHRR $NDVI_{retoa}$. This difference was largest where NDVI values were low (Figure 4.2). With increasing NDVI, the difference decreased and at NDVI=0.5, AVHRR NDVI exceed Landsat NDVI. For example, at AVHRR NDVI =0.2, Landsat iNDVI =0.26, and at AVHRR NDVI =0.41, Landsat iNDVI =0.4 (Figure 4.2 a).

The linear regression between iNDVI and mNDVI for homogeneous samples was highly significant (R^2 = 99.9%, $p<0.0001$, n=20) with near 1:1 correspondence (Figure 4.3 a). Correspondence was lower for the linear regression between iNDVI and mNDVI for heterogeneous samples as a result of increased scatter in the scatterplot (R^2 = 95.3%, $p<0.0001$, n=20; Figure 4.3 b) In heterogeneous samples, where NDVI values were low, mNDVI tended to be higher than iNDVI (Figure 4.3 b). Results from a multiple regression indicate the proportion of water within the 1x1 km area had a significant effect on the correspondence between iNDVI and mNDVI when both homogeneous and heterogeneous samples were pooled (Table 4.2 a). The inclusion of water cover in the regression increased the coefficient of determination from 98.5% (mNDVI vs. iNDVI) to 99.6% (mNDVI vs. iNDVI + H_20)(Table 4.2 a). The slope coefficient for water cover was equal to 0.129, indicating that with increasing water cover, iNDVI decreases with respect to mNDVI. Although significant, the CV had no effect on the correspondence between iNDVI and mNDVI (Table 4.2 b).

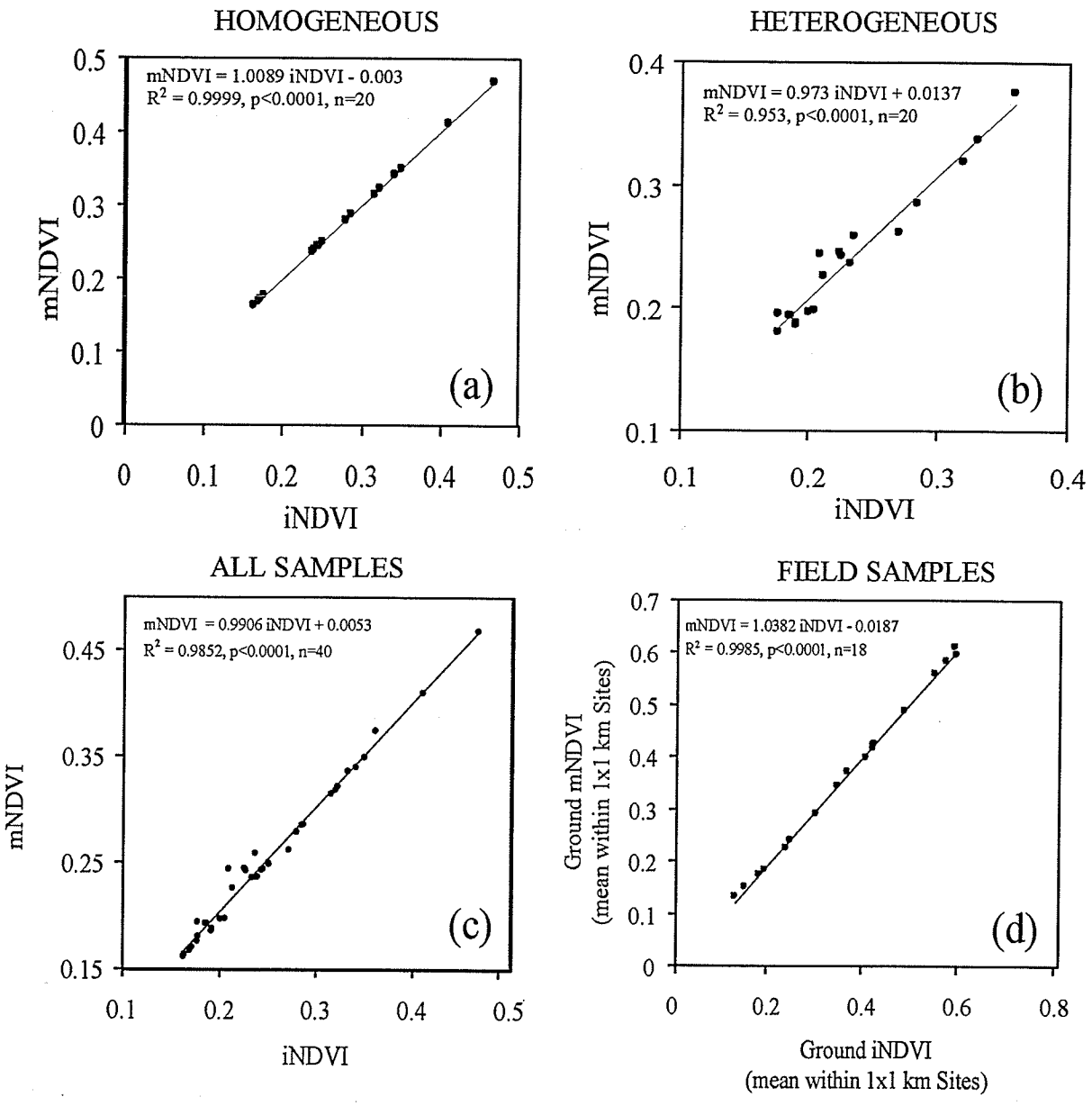

Figure 4.3. Scatterplots of Landsat NDVI aggregated over the 1x1 km pixel area corresponding to the AHVRR NDVI pixel for (A) Homogeneous samples; (B) Heterogeneous samples; (C) All samples; and (D) Field samples. Aggregated Landsat NDVI was computed by either integrated NDVI over the 1x1 km area (iNDVI) or by computing NDVI from integrated B3 and B4 (mNDVI).

Table 4.2. Multiple regression between mNDVI and iNDVI pooled for both homogeneous and heterogreneous areas, with the proportion of water within each sample area, (a) H20; and with the coefficient of variation, (b) CV.

(a) H_20	Dependent Variable		$R^{2=}$ 99.60%
	mNDVI		N= 40
	Independent Variables	Coefficient	P-Value
	Y-Intercept	-0.006	0.0614
	iNDVI	1.019	<0.0001
	$\%H_20$	0.129	<0.0001
(b) CV	Dependent Variable		$R^{2=}$ 98.50%
	mNDVI		N= 40
	Independent Variables	Coefficient	P-Value
	Y-Intercept	0.0031	0.59
	iNDVI	0.988	<0.0001
	CV	112.6 E-6	0.038

Evaluating Correspondence Between Scaled-Up Ground Measurements of NDVI and AVHRR NDVI.

Field NDVI vs. Landsat NDVI

Overall, integrated field measurements of NDVI trended extremely well with the corresponding satellite measurements (Figure 4.4 a-d). The integrated field measurements of NDVI were consistently higher than both Landsat NDVI and AVHRR $NDVI_{smac}$. A highly significant linear relation between the mean of five 1x1m NDVI measurements and the corresponding individual Landsat NDVI pixels (R^2=82.95%, p<0.0001, n=160) demonstrated not only the effectiveness of characterizing surface reflectance across a 30x30 m area with discrete 1 m field measurements, but that locational error is minimal for both the Landsat image and the ground measurements (Figure 4.4 a). High

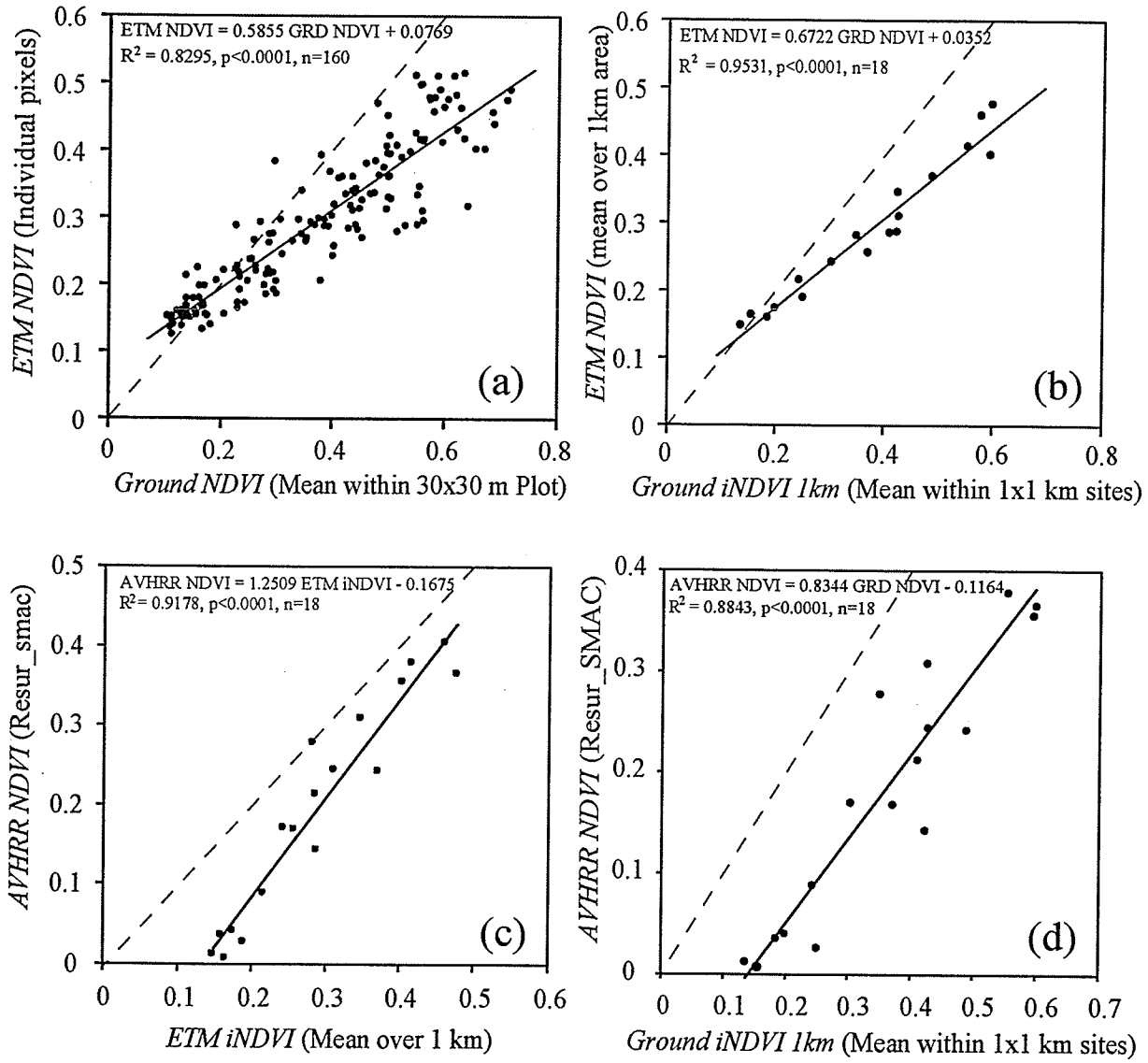

Figure 4.4 Scatterplots of (A) The mean of 5 1x1 m ground measurements of NDVI vs. spatially collocated individual Landsat NDVI pixels; (B) The mean of all 1x1 m ground NDVI measurements within the 1x1 km sample area vs. Landsat NDVI integrated over the sample site; (C) Landsat NDVI integrated over the sample site vs. atmospherically corrected AVHRR NDVI; (D) The mean of all 1x1 m ground NDVI measurements within the 1x1 km sample area vs atmospherically corrected AVHRR NDVI. Dashed lines indicate one to one correspondence.

correspondence between aggregated Landsat iNDVI and the mean of the field measurements of NDVI within each 1x1 km site clearly illustrates the effectiveness of characterizing reflectance across a large area by scaling up 1m ground measurements to 1 km (R^2=95.31%, $p<0.0001$, n=18; Figure 4.4 b).

Low positional error in both the Landsat image (RMS = ±18 m) and the field samples (RMS = ±4 m) resulted in highly accurate spatial collocation between the Landsat image pixels and the field samples. Thus, there was also high accuracy in the spatial correspondence between Landsat NDVI pixels aggregated over 1x1 km, and the 1x1 km integrated field measurements of NDVI. Therefore, it follows that a highly significant linear regression between aggregated Landsat NDVI and AVHRR NDVI within the 1x1 km field sample areas (R^2=91.8%, $p<0.0001$, n=18) indicates error attributable to the spatial collocation of the integrated field measurements of NDVI and the corresponding AVHRR NDVI pixels was minimal (Figure 4.4 c).

Field NDVI vs. AVHRR NDVI

The integrated field measurements of NDVI were consistently higher than both the Landsat NDVI and AVHRR $NDVI_{smac}$ values. Correspondence between integrated field NDVI values to Landsat NDVI values was not 1:1, with integrated field NDVI values increasing relative to Landsat NDVI as NDVI increases (Slope = 0.67; Figure 4.4 b). Although not a perfect 1:1 relationship, the correspondence between the integrated field measurements of NDVI and AVHRR NDVI values was close to 1:1, and integrated field NDVI values were consistently higher than AVHRR NDVI (Figure 4.4 d).

Considering the potential error involved in matching field measurements with coarse resolution image pixels, the integrated field measurements of NDVI correspond very well with the AVHRR $NDVI_{smac}$ (R^2=88.4%, p<0.0001, n =18; Figure 4.4 d). Computing mNDVI for the integrated field measurement did not improve correspondence with AVHRR $NDVI_{smac}$. This can be attributed to the fact that the field samples were selected in homogeneous areas, and from the preceding analysis it is evident that mNDVI is equal to iNDVI in homogeneous areas (Figure 4.3 a).

Correspondence between BRDF corrected AHVRR NDVI (AVHRR $NDVI_{brdf}$) and integrated field measurements of NDVI was considerably lower than with the AVHRR $NDVI_{smac}$ (R^2_{brdf} = 65.72%, p<0.0001) suggesting that the BRDF correction contributed error or noise into the AVHRR NDVI values.

Correspondence between integrated field measured NDVI computed with the average of radiometer bands 2 and 3 and the AVHRR $NDVI_{smac}$ values was slightly lower than with field NDVI computed with band 3 alone (R^2 =87.5%; p<0.0001; n=18). However, the linear equation for the best fit produced a slope value slightly higher than the best fit line for field NDVI computed with band 3 alone (AVHRR NDVI = 0.8789 GRD $NDVI_{b23}$ – 0.1532). The values for Integrated field measured NDVI computed with the mean of bands 2 and 3 are closer in absolute terms to the AVHRR NDVI values.

4.5. DISCUSSION

Parameters in remote sensing driven NPP models are often derived from relationships defined from fine-resolution ground measurements (i.e 1 to 10m), that are scaled-up and applied to coarse resolution (i.e. 1 km) satellite imagery (Field et al. 1995; Ruimy et al. 1996; Liu et al. 1997; Malmström et al. 1997). The accuracy of productivity estimates derived from these models depends on the ability of the AVHRR NDVI data to represent the actual physical conditions at the surface. It is therefore imperative that the AVHRR NDVI computed from surface reflectance data be validated using independent data sets obtained from measurements in the field. However, evaluating AVHRR pixel values with scaled-up field measurements of surface reflectance is subject to error from a number of sources, including: error in positional accuracy of AVHRR image and the comparison data set (Cihlar et al. 1997a); altered AVHRR pixel values, the result of resampling larger off-nadir pixels to a specific resolution (Cihlar et al. 1997b); non-linear scaling interactions between NDVI and surface reflectance (Aman et al. 1992); differences in sensor bandwidths (Teillet et al. 1997); and attempting to characterize a continuous and inherently variable surface using a sample of discrete ground measurements.

One objective of this paper was to assess the degree to which these sources of error influence the correspondence between integrated field measurements of NDVI and AVHRR NDVI. It is apparent from the preceding analyses that selecting sample sites in homogeneous areas had the effect of minimizing spatial collocation error, non-linear scaling interactions in NDVI, as well as improving the ability to characterize a continuous surface with a sample of discrete measurements. The results suggest these

data sets are indeed comparable, and therefore field measurements of NDVI can be used to evaluate the effectiveness of the atmospheric and bi-directional reflectance corrections on AVHRR NDVI data obtained from Arctic landscapes, provided that sample sites are located in homogeneous regions.

Relatively low significance in the regressions between aggregated Landsat NDVI and AVHRR NDVI pixels for heterogeneous areas suggests a large degree of error in the spatial collocation of these data sets. Cihlar et al. (1997) noted a large degree of scatter when comparing aggregated Landsat NDVI with AVHRR NDVI in boreal forest. This scatter was attributed to misregistration between the data sets and high variation in NDVI from one pixel to the next, as well as the influence of neighbouring pixels as a result of the resampling of originally larger AVHRR pixels to 1x1 km resolution (Cihlar et al. 1997b). In heterogeneous areas, the influence of these factors on the discrepancy between aggregated Landsat NDVI and AVHRR NDVI will increase with large spatial collocation errors. However, despite misregistration error, the effects of these factors are less apparent when comparing data extracted from homogeneous areas, and as a result, correspondence was higher between aggregated Landsat NDVI and AVHRR NDVI (Figure 4.2). In homogeneous areas, the Landsat NDVI pixels within each of the 1x1 km image chips exhibited lower variation compared to heterogeneous areas (Table 4.1). This suggests greater persistence in the landscape and high autocorrelation between adjacent pixels. Within the AVHRR NDVI image, high autocorrelation inherent to homogeneous landscapes is further compounded by autocorrelation introduced as a result of resampling large off-nadir AVHRR pixels to 1x1 km resolution. Thus, even though AVHRR pixel values may not correspond to the exact section of land covered by the ground sample site,

in homogeneous areas the data are comparable. The inherently high autocorrelation in such areas infers a high probability that the difference between adjacent AVHRR pixels will be small.

Typical landscape features in arctic ecosystems have spatial resolutions that are less than that of AVHRR image pixels (Stow et al. 1998). Thus, reflectance recorded by the AVHRR pixel will be influenced by a mixture of landscape elements. Examining the influence of this mixture is important as it has implications in extending relationships between NDVI and model parameters defined at a small scale (i.e. 1-10m) to 1km AVHRR data (Stow et al. 1998). The influence of water proportion on AVHRR NDVI will be of particular importance as water does not contribute to terrestrial NPP.

The linear correlation between mNDVI and iNDVI is not affected by the time of acquisition, spatial resolution and landcover type (Aman et al. 1992), and the effects of topography have been shown to be minimal in AVHRR NDVI data (Burgess et al. 1995). However, the effects of non-linear scaling interactions between NDVI and surface reflectance appear to be sensitive to water cover (Table 4.2 a). This is because water is absorptive of both visible and NIR light, whereas vegetation is absorptive of visible light, and reflective of NIR light. The relative difference in visible reflectance over water and land is smaller compared to the relative difference between NIR reflectance for water and land. Therefore, computing the mean of NDVI pixels within an area with partial water cover will produce an aggregate NDVI value considerably lower than if NDVI were computed from the mean of visible and NIR reflectance. However, in homogeneous areas with little or no water cover, the difference between iNDVI and mNDVI is minimal (Figure 4.3 a).

Differences in visible bandwidths will effect NDVI values derived from different sensors with NDVI decreasing as visible bandwidth increases (Teillet et al. 1997). Because the visible channel of the AVHRR sensor covers more of the visible spectrum, with increasing vegetation cover AVHRR NDVI values decrease with respect to Landsat TM NDVI values (Figure 4.1). Both the integrated field measurements of NDVI and aggregated Landsat NDVI values are higher than atmospherically corrected AVHRR NDVI (Figure 4.4 b). Cihlar et al. (1997), found that aggregated Landsat pixels over boreal forest were 10% higher than atmospherically corrected AVHRR NDVI and attributed these discrepancies to differences in sensor bandwidth and differences in view geometry and sunangles. The AVHRR visible band covers a larger portion of the visible spectrum compared to Landsat and the radiometer visible band (Figure 4.1). With increasing vegetation cover, green light reflectance increases, and because the AVHRR B1 covers part of the green spectrum, AVHRR NDVI values are lower than Landsat NDVI. For low NDVI values this is apparent, however, as NDVI increases the difference between Landsat NDVI and AVHRR NDVI decreases, with Landsat NDVI equal to AVHRR NDVI at ~0.5 (Figure 4.4 b).

Scaling-up field measurements of NDVI and comparing these data to coarse resolution satellite imagery depends on the ability to characterize total surface reflectance using discreet fine-scale measurements of NDVI. A highly significant linear regression between individual Landsat NDVI pixels and field NDVI measurements integrated within each 30x30 m plot, demonstrates the effectiveness of characterizing total surface NDVI over a relatively large area (i.e. 30x30m) with a limited sample of fine-scale ground measurements. Moreover, high correspondence between aggregated Landsat NDVI

values and field measurements of NDVI integrated over each 1x1 km sample area demonstrates that a sample of fine-scale ground measurements can effectively characterize reflectance over an even larger surface area (i.e. 1x1 km).

Although correspondence was high, the linear relationship was not 1:1, and the difference between field NDVI values Landsat NDVI values increased with larger NDVI values (Figure 4.4 b). Walker et al. (1995) found field measurements of NDVI values in arctic tundra vegetation were up to 40% greater than NDVI values measured from SPOT images, with the greatest differences in the more productive graminoid/ dwarf shrub tundra and shrubland communities (Walker et al. 1995). Shippert et al. (1995) also found field NDVI values measured from arctic vegetation were higher than SPOT NDVI and attributed the differences to low sun angles and high view angle of the satellite sensor. The satellite sensor receives backscattered light, while the field sensor receives forward scattered light (Shippert et al. 1995). As forward scattered light travels through more vegetation, visible light reflectance is reduced and NDVI increases (Shippert et al. 1995). The structure of the vegetation canopy largely influences the degree of forward and backscatter of light (LeBlanc et al. 1997). At low vegetation cover, directional reflectance effects are minimal. With simulated AVHRR data, at nadir viewing angles NDVI in the forward and backscatter directions decreases with solar zenith angle, and this decrease is greater with higher biomass (Holben 1986; Vierling et al. 1997). Furthermore, with increasing view angle, in both forward and backscatter directions, NDVI in tussock tundra decreased (Vierling et al. 1997). Because field reflectance measurements were taken at nadir and were cosine corrected for bi-directional reflectance effects caused by large solar zenith angles, bi-directional reflectance effects in the field NDVI data should

be minimal. Therefore, the lack of a 1:1 correspondence between field NDVI and Landsat NDVI can be attributed to directional reflectance effects in Landsat reflectance values caused by large solar zenith angles, and large view zenith angles (Shippert et al. 1995). Because these effects are greater with increasing biomass (Holben 1986; Vierling et al. 1997), Landsat NDVI values decrease with respect to field NDVI with increasing NDVI.

When integrated ground measurements were compared to the BRDF corrected AVHRR NDVI, correspondence was considerably lower. It has been suggested that at high latitudes, with large solar zenith angles the GEOCOMP-n BRDF correction may actually increase noise in the image data (Cihlar et al. 1997b). GEOCOMP-n BRDF correction is based on landcover specific coefficients and BRDF correction requires spatial collocation of each AVHRR pixel with a landcover class defined in a vegetation map. Error in the BRDF correction can be attributed to problems with spatial collocation between AVHRR pixels and vegetation map pixels, especially at borders between vegetation classes. Furthermore, problems with the GEOCOMP-n system implementation when processing the 2000 data involving use of the wrong vegetation map to assign the BRDF correction coefficients will have further contributed error to the BRDF corrected imagery (G. Fedosejevs pers. comm.). Indeed, large difference between atmospherically corrected AVHRR NDVI values and the integrated field measured NDVI is likely caused by directional reflectance effects. Large sun-angles at high latitudes create strong directional scattering effects which will have a considerable influence on NDVI (Holben et al. 1986). Therefore, for the AVHRR NDVI to be a true representation of surface reflectance, BRDF correction is absolutely necessary.

Strong correspondence between the rescaled ground NDVI measurements and the AVHRR NDVI measurements demonstrates the effectiveness of using hand-held radiometer measurements to validate coarse resolution satellite imagery. It also illustrates the existence of considerable differences between surface and satellite measurements of NDVI. Correcting NDVI is important because derived surface parameters are sensitive to small changes in NDVI. Chen and Cihlar (1996) found differences in NDVI of 5% can cause leaf area index (LAI) to change by 20%. With a highly significance regression relationship defined between integrated field measurements of NDVI and the AVHRR $NDVI_{smac}$, it is possible to rescale the AHVRR NDVI data to true ground reflectance using the linear best-fit relationship derived from the sample data. However, this relationship can only be assumed accurate for the time and location for which the sample data was obtained, as atmospheric conditions and reflectance properties of the vegetation will vary throughout the growing season.

Selecting ground sample sites in homogeneous areas produces a more tractable model than in heterogeneous areas. From the analysis comparing correspondence between aggregated Landsat pixels with AVHRR pixels in homogeneous and heterogeneous areas it is apparent that locating ground samples in heterogeneous areas will reduces correspondence resulting in lower R^2 values. Selecting samples in homogeneous areas has the important effect of removing noise or covariation from the model which is analogous to a carefully designed experimental in which one attempts to minimize and control for confounding factors. Careful selection of field sample sites in homogeneous areas on the landscape has enabled the scaling-up of discrete fine-scale field measurements to 1x1km resolution. This study has important implications for

validating AVHRR image products in the arctic, as it demonstrates the effectiveness of using a relatively inexpensive and easy to obtain source of data (i.e. hand-held radiometer measurements) for validating coarse resolution satellite imagery in arctic vegetation.

5. CONCLUSION

5.1. VEGETATION PRODUCTIVITY IN TUKTUT NOGAIT NATIONAL PARK

In arctic tundra vegetation distribution of biomass and net production are most closely influenced by variation in soil moisture, wind protection and nutrient availability (Webber 1978; Chapin and Shaver 1985). Plant production is closely tied to gradients in soil moisture conditions which depend on the depth of the thawed active layer of soil. Active layer depth increases in areas that lack an insulating layer of soil and vegetation (Courtin and Labine 1977; Chapin and Shaver 1985). Areas where snow accumulates offer more protection for vegetation as well as providing a source of water throughout the growing season. Thaw depth is limited where vegetation cover is high as the frozen ground is insulated and organic soils have a high thermal inertia. In wet tundra, limited thaw depth results in poor drainage as water pools over the permafrost, and up to 70% of net incident radiation is absorbed by evaporating water (Barry et al. 1981). Low soil temperature, acidic conditions and poor soil aeration prevents microbial activity, limiting decomposition rates resulting in low nutrient availability. Ammonium and phosphate are limiting nutrients in the arctic as is apparent by an increase in plant productivity around decaying animal bones (Fogg 1998). Disturbance also greatly increases local productivity by increasing nutrient availability and vegetation proliferates on frost heaves which bring nutrient rich soil buried in the permafrost closer to the surface (Fogg 1998). Lack of nutrients results in high below to aboveground biomass ratios, and roots in many species grow right down to the margin of the permafrost. The downward growth of roots, despite cold temperatures, slow rate of thaw, and poor aeration, may be in response to a depletion

of available soil nutrients near the surface, and a gradual release during thawing of nutrients held in still frozen portions of the active layer (Dennis et al. 1978).

5.2. POTENTIAL EFFECTS OF CLIMATE CHANGE/ GLOBAL WARMING

Arctic vegetation is well adapted to arctic environments, producing photosynthetically efficient tissues with high levels of metabolic activity. Optimum growth rates occur at 15°C, compared to 25°C for temperate species, with photosynthetic rates relatively insensitive to changes in temperature down to –4°C (Billings et al. 1971; Johnson and Tieszen 1976; Mayo et al. 1977; Tieszen et al. 1980). High photosynthetic rates at low temperatures are related to increased concentrations of RuBP Carboxylase (Berry and Bjorkman 1980). At higher temperatures, the oxygenase activity of RuBP Carboxylase results in light respiration that exceeds assimilation prohibiting survival of these plants in warmer environments. At low temperatures, however, this respiration is not significant and the increased concentrations of the enzyme acts to optimize carbon assimilation. Arctic plants also have high respiration rates at low temperatures (Billings et al. 1971; Mayo et al. 1977; Tieszen 1973). This is necessary to allow rapid growth in a short growing season. The high respiratory capacity of arctic plants leads to exhaustion of carbohydrate reserves and increased mortality when grown at warm temperatures (Chapin and Chapin 1981).

NPP of arctic biomes will likely decrease under global warming, although total NPP will eventually increase due the northward shift of the boreal biome (Plochl and Cramer 1995). Warmer temperatures will create less than optimum conditions for arctic plants, and with increased autotrophic respiration and decreased photosynthetic

efficiency, the net productivity of arctic ecosystems will decrease. Furthermore, with increasing temperatures arctic ecosystems could switch from a CO_2 sink to a CO_2 source as previously inaccessible carbon is released from increased soil microbial activity (Plochl and Cramer 1995). Boreal species will move north, out competing arctic species as they thrive in the warmer, dryer conditions and newly fertile soils.

The arctic productivity model presented in this thesis produces an excellent representation of regional scale patterns of NPP within Tuktut Nogait National Park. The model is relatively easy to implement and uses GEOCOMP-n AVHRR data exclusively. An assessment of the accuracy of the absolute NPP values produced from the model indicates relatively good correspondence. However, it is important to recognize that this accuracy assessment is dependent on the accuracy of the expected annual NPP map. Considering there is currently no way of assessing regional scale productivity patterns in Canada's northern national Parks, the NPP model will provide a useful tool for ecosystem monitoring and a source of empirical data for justifying management decisions.

6. REFERENCES

Aman, A. H.P. Randriamanatena, A. Podaire, and R. Frouin. 1992. Upscale integration of normalized difference vegetation index: The problem of spatial heterogeneity. IEEE Transactions on Geoscience and Remote Sensing, 30(2): 326-337.

Asrar, G., M. Fuchs, E.T. Kanemasu, and J.L. Hatfield. 1984. Estimating absorbed photosynthetic radiation and leaf area index from spectral reflectance in wheat. Agronomy Journal, 76:300-306.

Asrar, G.M., E.T. Kanemasu, R.D. Jackson, and P.J. Pinter. 1985. Estimation of total above-ground phytomass production using remotely sensed data. Remote Sensing of Environment, 17:211-220.

Baret, F., G. Guyot, and D. Major. 1989. TSAVI: A vegetation index which minimizes soil brightness effects on LAI or APAR estimation. Proceedings of the 1989 International Geoscience and Remote Sensing Symposium (IGARSS '89) and the Twelfth Canadian Symposium on Remote Sensing, Vancouver, Canada. pp. 1355-1358.

Barry, R. G., G. M. Courtin and C. Labine. 1981. Tundra climates. *In*: L.C. Bliss, J. B. Cragg, D W. Heal and J. J. Moore, *Eds.*, *Tundra Ecosystems: A Comparative Analysis*. Cambridge University Press, Pp. 81-114.

Begue, A. and R. Myneni. 1996. Operational relationships between NOAA-advanced very high resolution radiometer vegetation indices and daily fraction of absorbed photosynthetically active radiation, established for Sahelian vegetation canopies. Journal of Geophysical Research, 101: 21,275-21,289.

Berry, JA and O. Bjorkman. 1980. Photosynthetic response and adaptation to temperature in higher plants. Annual Review of Plant Physiology, 31: 491-543.

Bliss, LC, and NV Matveyeva. 1992. Circumpolar arctic vegetation. *In* Arctic ecosystems in a changing climate: an ecophysiological perspective. San Diego, Academic Press. Pp.59-90.

Billings, W.D., P.J. Godfrey, B.F. Chabot and D.P. Bourque. 1971. Metabolic acclimation to temperature in arctic and alpine ecotypes of *Oxyria digyna*. Arctic and Alpine Research, 3: 277-289.

Billings, W.D., K.M. Peterson, G.R. Shaver. 1978. Growth, turnover rates, and respiration rates of roots and tillers in tundra graminoids. *In* Vegetation and Production Ecology of an Alaskan Arctic Tundra, ed L.L. Tiezen. Springer-Verlag, New York. Pp. 113-138.

Box, E.O., B.N. Holben, and V. Kalb. 1989. Accuracy of the AVHRR vegetation index as a predictor of biomass, primary production, and net CO_2 flux. Vegetatio, 80:71-89.

Burgess, D.W., P. Lewis, J.P.A.L. Muller. 1995. Topographic effects in AVHRR NDVI data. Remote Sensing of Environment, 54: 223-232.

Braswell, B.H., D.S. Schimel, J.L. Privette, B. Moore, W.J. Emery, E.W. Sulzman and A.T. Hudak. 1996. Extracting ecological and biophysical information from AVHRR optical data: An integrated algorithm based on inverse modelling. Journal of Geophysical Research, 101: 23,335-23,348.

Chapin, F.S. III and M.C. Chapin. 1981. Ecotypic differentiation of growth processes in *Carex aquatilis* along latitudinal and local gradients. Ecology, 62:1000-1009

Chapin, S. F. and G.R. Shaver. 1985. Arctic. *In* Physiological Ecology of North American Plant Communities, *eds* B.F. Chabot and H.A. Mooney. Chapman and Hall, New York.

Chapin, F. S., N. Fletcher, K. Kielland, K.R. Everett, and A.E. Linkins. 1988. Productivity and nutrient cycling of Alaskan tundra: enhancement by flowing soil water. Ecology, 69:693-702.

Chen, J.M. 1996. Evaluation of vegetation indices and a modified simple ratio for boreal applications. Canadian Journal of Remote Sensing, 22:229-242.

Chen, J.M. and J. Cihlar. 1996. Retrieving leaf area index of boreal conifer forests using Landsat TM images. Remote Sensing of Environment, 55: 153-162.

Cihlar, J. J. Chen., and Z. Li. 1997a. On the validation of satellite-derived products for land applications. Canadian Journal of Remote Sensing, 23(4): 381-389.

Cihlar, J., J. Chen, and Z. Li. 1997b. Seasonal AVHRR multichannel data sets and products for studies of surface-atmosphere interactions. Journal of Geophysical Research, 102 (D24): 29,625-29,640.

Cihlar, J., J. Chen, Z. Li, R. Latifovic, G. Fedosejevs, M. Adair, W. Park, R. Fraser, A. Trishenko, B. Guindon, D. Stanley. 2000. GeoComp-n, an advanced system for the processing of coarse and medium resolution satellite data. Part 2: biophysical products for northern ecosystems. *In Press.*

Colpaert, A., J. Kumpula, M. Nierminen. 1995. Remote sensing, a tool for reindeer range land management. Polar Record 31: 235-244.

Cohen, W.B., T.A. Spies, G.A. Bradshaw. 1990. Semivariograms of digital imagery for analysis of conifer canopy structure. Remote Sensing of Environment, 34:167-178.

Colwell, J.E. 1971. Vegetation canopy reflectance. Remote Sensing of Environment, 3:175-183.

Courtin, G.M. and C.L. Labine. 1977. Microclimatology studies on Truelove Lowland, *in*: L.C. Bliss *Ed.* Truelove Lowland, Devon Island, Canada: A High Arctic Ecosystem. University of Alberta Press, Edmonton, pp. 73-106

Cracknell, A.P. 1998. Synergy in remote sensing—what's in a pixel? International Journal of Remote Sensing, 19(11): 2025-2047.

Dearden, P. and R. Rollins. 1993. Parks and Protected Areas in Canada: Planning and Management. Oxford University Press, Toronto.

Dennis, J.G., L.L. Tiezen, and M.A. Vetter. 1978. Seasonal dynamics of above- and belowground production of vascular plants at Barrow, Alaska. *In* Vegetation and Production Ecology of an Alaskan Arctic Tundra, ed L.L. Tiezen. Springer-Verlag, New York. Pp. 113-138.

Eastman, J.R., M. Fulk. 1993. Long sequence time series evaluation using standardized principal components. Photogrammetric Engineering and Remote Sensing, 59:1307-1312.

Eck, T.F. and D.G. Dye. 1991. Satellite estimation of incident photosynthetically active radiation using ultraviolet reflectance. Remote Sensing of Environment 38:135-146.

Field, C.B., J.T. Randerson, and C.M. Malmstrom. 1995. Global net primary production: combining ecology and remote sensing. Remote Sensing of Environment 51:74-88.

Fogg, G. E. 1988. The biology of polar habitats. Oxford University Press, Oxford.

Friedl, Mark A. 1997. Examining the Effects of Sensor Resolution and Sub-Pixel Hetreogeneity on Spectral Vegetation Indices: Implications for Biophysical Modeling. *Scale in Remote Sensing and GIS.* Dale A. Quattrochi and Michael F. Goodchild, Eds. Boca Raton, FL: CRC Lewis. pp:113-139.

Gilmanov, T.G. and W. Oechel. 1995. New estimates of organic matter reserves and net primary productivity of the North American tundra ecosystems. Journal of Biogeography, 22: 723-741.

Goetz, S.J. 1997. Multi-sensor analysis of NDVI, surface temperature and biophysical variables at a mixed grassland site. International Journal of Remote Sensing, 18(1): 71-94.

Goetz, S.J., S..D. Prince, S.N. Goward, M.M. Thawley, and J. Small. 1999. Satellite remote sensing of primary production: an improved production efficiency modelling approach. Ecological Modelling, 122: 239-255.

Goward, S.N, C.J. Tucker, and D.G. Dye. 1985. North American vegetation patterns observed with NOAA-7 AVHRR. Vegetatio 64: 3-14.

Goward, S.N. and Huemmrich, K.F. 1992. Vegetation canopy PAR absorptance and the normalized vegetation index: an assessment using the sail model. Remote Sensing of Environment, 39: 119-140.

Goward, S. N., R. H. Waring, D. G. Dye and J. Yang. 1994. Ecological remote sensing at OTTER: Macroscale satellite observations. Ecological Applications, 4 (2): 322-343.

Gower, S.T., C.J. Kucharik, and J.M. Norman. 1999. Direct and indirect estimation of leaf area index, fAPAR and net primary production of terrestrial ecosystems. Remote Sensing of the Environment, 70(1): 29-51.

Hansen, B.U. 1991. Monitoring natural vegetation in southern greenland using NOAA AVHRR and field measurements. Arctic, 44: 94-101.

Hatfield, J.L., G. Asrar, and E.T. Kanemasu. 1984. Intercepted photosynthetically active radiation estimated by spectral reflectance. Remote Sensing of Environment 14:65-75.

Hawley, V., A. Hawley, D. Poll, and R. Brown. 1979. The Bluenose caribou herd, 1974-1976. Technical Report Series - Canadian Wildlife Service, no. 113. Edmonton, Alberta.

Holben, B., C.J. Tucker, and C.J. Fan. 1980. Spectral assessment of soybean leaf area and biomass. Photogrammetric Engineering and Remote Sensing 46:651-656.

Holben, B.N., D.S. Kimes, and R.S. Fraser. 1986. Directional reflectance in AVHRR red and near-IR bands for three cover types and varying atmospheric conditions. Remote Sensing of Environment, 46:651-656.

Hope, A. S., J. B. Fleming, G. Vourlitis, D. A. Stow, W. C. Oechel and T. Hack. 1995. Relating CO_2 fluxes to spectral vegetation indices in tundra landscapes: Importance of footprint definition. Polar Record 31:245-250.

Hunt, E.R. 1994. Relationship between woody biomass and PAR conversion efficiency for estimating net primary production from NDVI. International Journal of Remote Sensing 15:1725-1730.

Jarvis, P.G. and J.W. Leverenz. 1983. Productivity of temperate, deciduous and evergreen forests. *In* Physiological Plant Ecology IV, Ecosystem Processes: Mineral cycling, productivity and Man's influence, Eds. O.L. Lange, P.S. Nobel, C.B. Osmond, and H. Ziegler. Springer-Verlag, New York. Pp. 234-272.

Johnson, D.A., and L.L. Tieszen. 1976. Aboveground biomass allocation, leaf growth, and photosynthesis patterns in tundra plant forms in arctic Alaska. Oecologia (Berlin), 24: 159-173.

Jordan, C.F. 1969. Derivation of leaf area index from quality of light on the forest floor. Ecology 50:663-666.

Law, B.E. and R.H. Waring. 1994. Combining remote sensing and climatic data to estimate net primary production across Oregon. Ecological Applications 4:717-728.

Leblanc, S.G., J.M. Chen, J. Cihlar. 1997. NDVI directionality in boreal forests: A model interpretation of measurements. Canadian Journal of Remote Sensing, 23(4):369-380

Li, Z.Q. and L. Moreau. 1996. A new approach for remote sensing of canopy absorbed photosynthetically active radiation. 1. Total surface absorption. Remote Sensing of Environment 55(3) 175-191.

Lieth, H. 1975. Modeling the primary productivity of the world. *In* Primary Productivity of the Biosphere, eds. H. Leith and R.H. Whittaker. Springer-Verlag, New York.

Liu, J., J. M. Chen, J. Chilar, and W.M Park. 1997. A process-based boreal ecosystem productivity simulator using remote sensing inputs. Remote Sensing of Environment, 62: 158-175.

Los, S.O., C.O. Justice, and C.J. Tucker. 1994. A global 1° x 1° NDVI data set for climate studies derived from the GIMMS continental NDVI data. International Journal of Remote Sensing, 15: 3493-3518.

Malmström, C.M., M.V. Thompson, G.P. Juday, S.O. Los, J.T. Randerson, and C. Field. 1997. Interannual variations in global-scale net primary production: Testing model estimates. Global Biogeochemical Cycles, 11(3): 367-392.

Markon, C.J., M.D. Fleming, and E.F. Binnian. Characteristics of vegetation phenology over the Alaskan landscape using AVHRR time-series data. Polar Record, 31: 179-190.

Mayo, J. M., A.P. Hartgerink, D.G. Despain, R.G. Thompson, E.M. van den Zinderen Bakker, S.D. Nelson. 1977. Gas exchange studies of Carex and Dryas, Truelove Lowland, Devon Island. In Bliss, L. C. Truelove Lowland, Devon Island, Canada: a High Arctic Ecosystem. Edmonton, Alberta, Canada: University of Alberta Press; p265-280.

McCanny, S. 1998. Accounting for nature: The northern national parks ecological monitoring program. Parks Canada Research Links, 6(3): 8,11.

McMichael, C.E., A.S. Hope, D.A. Stow, J.B. Flemming, G. Vourlitis, W. Oechel. 1999. Estimating CO_2 exchange at two sites in Arctic tundra ecosystems during the growing season using a spectral vegetation index. International Journal of Remote Sensing, 20(4): 683-698,

Mellilo, J.M., A.D McGuire, D.W. Kicklighter, B. Moore III, C.J. Vorosmarty, and A.L. Schloss. 1993. Global climate change and terrestrial net primary production. Nature, 363: 234-240.

Miller, P.C., W.A. Stoner, L.L. Tieszen. 1976. A model of stand photosynthesis for the wet meadow tundra at Barrow, Alaska. Ecology. 57:411-430.

Monteith, J.L. 1972. Solar radiation and productivity in tropical ecosystems. Journal of Applied Ecology 9: 747-766.

Moreau, L., and Z.Q. Li. 1996. A new approach for remote sensing of canopy absorbed photosynthetically active radiation. 2. Proportion of canopy absorption. Remote Sensing of Environment 55(3): 192-204.

Muc, M. 1977. Ecology and primary production of Sedge-moss meadow communities, Truelove Lowland. *In* Truelove Lowland, Devon Island, Canada: A high arctic ecosystem, ed. L.C. Bliss. Edmonton, University of Alberta Press. Pp. 155-182.

Myneni, R. B., G. Asrar, D. Tanré, & B.J. Choudhury. 1992. Remote sensing of solar radiation absorbed and reflected by vegetated land surfaces. IEEE Transactions on Geoscience and Remote Sensing, 30(2): 302-314.

Paruelo, J.M., H.E. Epstein, W.K. Lauenroth, and I.C. Burke. 1997. ANPP estimates from NDVI for the central grassland region of the United States. Ecology 78:956-928.

Peterson, D.L., M.A. Spanner, S.W. Running, and K.B. Teuber. 1987. Relationships of thematic mapper simulator data to leaf area index of temperate coniferous forests. Remote Sensing of Environment. 22: 323-341.

Peterson, D.L. and S.W. Running. 1989. Applications in forest science and management. *In.* Theory and applications of optical remote sensing. Ed. G. Asrar. *Wiley.* New York pp.429-473.

Plochl, M. and W. Cramer. 1995. Possible impacts of global warming on tundra and boreal forest ecosystems: comparisons of some geochemical models. Journal of Biogeography, 22: 775-783.

Prihodko, L. and S.N. Goward. 1997. Estimation of air temperature from remotely sensed surface observations. Remote Sensing of Environment, 60: 335-346.

Prince, S.D. 1991. A model of regional primary production for use with coarse resolution satellite data. International Journal of Remote Sensing 12:1313-1330.

Prince, S.D. and S.N. Goward. 1995. Global primary productivity: A remote sensing approach. Journal of Biogeography 22:815-835.

Prince, D.S., Y.H. Kerr, J.P. Goutorbe, T. Lebel, A. Tinga, et al. 1995. Geographic, biological and remote sensing aspects of the hydrologic atmospheric pilot experiment in the Sahel (HAPEX-Sahel). Remote Sensing of Environment, 51:215-234.

Qi, J. A. Chehbouni, A.R. Huete, Y.H. Kerr, and S. Sorooshian. 1994. A modified soil adjusted vegetation index. Remote Sensing of Environment, 48: 119-126.

Rahman, H. and G. Dedieu. SMAC: A simplified method for the atmospheric correction of satellite measurements in the solar spectrum. International Journal of Remote Sensing, 15: 123-143.

Ranson, K.J. and D.L. Williams. 1992. Remote sensing technology for forest ecosystem analysis. In H.H. Shugart, R. Leemans, and G.B. Bonan (eds.), *A Systems*

Analysis of the Global Boreal Forest. Cambridge U. Press, Cambridge. Pp. 267-290.

Rees, W.G., E.I. Golubeva, and M. Williams. 1998. Are vegetation indices useful in the Arctic? Polar Record. 34:333-336.

Richards, J.A. 1994. *Remote Sensing Digital Image Analysis.* Springer-Verlag, Berlin. p.340.

Richardson, A.J. and Weigand, C.L. 1977. Distinguishing vegetation from soil background information. Photogrammetric Engineering and Remote Sensing 43:1541-1552.

Rouse, J.W., R.H. Haas, J.A. Schell, and D.W. Deering. 1973. Monitoring vegetation systems in the great plains with ERTS. 3rd ERTS Symposium, NASA SP-351 I:309-317.

Ruimy, A., B. Saugier, and G. Dedieu. 1994. Methodology for the estimation of terrestrial net primary productivity from remotely sensed data. Journal of Geophysical Research, 99:5263-5283.

Ruimy, A. G. Dedieu, and B. Saugier. 1996. TURC: A diagnostic model of continental gross primary productivity and net primary productivity. Global Biogeochemical Cycles, 10(2): 269-285.

Runyon, J., R.H. Waring, S.N. Goward, and J.M. Welles. 1994. Environmental limits on net primary production and light-use efficiency across the Oregon transect. Ecological Applications, 4: 226-237.

Sellers, P., F.G. Hall, G. Asrar, D.E. Strebel, and R.E. Murphy. 1992. An overview of the first international satellite land surface climatology project (SILSCP) field experiment (FIFE). Journal of Geophysical Research, 97(D17):18345-18371.

Sellers, P.J., C.J. Tucker, G.J. Collatz, S.O. Los, C.O. Justice, D.A. Dazlich, and D.A. Randall. 1994. A global 1 by 1 NDVI data set for climate studies. Part 2: The generation of global fields of terrestrial biophysical parameters from the NDVI. International Journal of Remote Sensing 15:3519-3545.

Sellers, P., F. Hall, H. Margolis, B. Kelly, D. Baldocchi, G. den Hartog, J. Cihlar, M.G. Ryan, B. Goodison, P. Crill, K.J. Ranson, D. Lettenmaier, and D.E. Wickland. 1995. The boreal ecosystem-atmosphere study (BOREAS): an overview and early results from the 1994 field year. Bulletin of the American Meteorological Society, 76(9):1549-1577.

Shaver, G. R., and W. D. Billings. 1977. Effects of daylength and temperature on root elongation in tundra graminoids. Oecologia, 28:57-65.

Shaver, G. R., N. Fetcher and F. S. Chapin, III. 1986. Growth and flowering in *Eriophorum vaginatum*: Annual and latitudinal variation. Ecology, 67:1524-1525.

Shaver, G.R. and F.S. Chapin III. 1991. Production: Biomass relationships and element cycling in contrasting arctic vegetation types. Ecological Monographs, 61:1-31

Shaver, G.R., A.E. Giblin, K.J. Nadelhoffer and E.B. Rastetter. 1997. Plant functional types and ecosystem change in arctic tundras. *In* Plant Functional Types. *Eds.* T.M Smith, H.H. Shubart, F.I. Woodward. Cambridge University Press, pp.157

Shippert, M.M., D.A. Walker, N.A. Auerbach, and B.E. Lewis. 1995. Biomass and leaf-area index maps derived from SPOT images for Toolik Lake and Imnavait Creek areas, Alaska. Polar Record. 31:147-154.

Smith, J.A. and R.E. Oliver. 1974. Effects of changing canopy directional reflectance on feature selection. Journal of Applied Optics 13:1599-1604.

Stow, D., A. Hope, W. Boynton, S. Phinn, D. Walker, N. Auerbach. 1998. Satellite derived vegetation index and cover type maps for estimating carbon dioxide flux for arctic tundra regions. Geomorphology, 21: 313-327.

Tieszen, L.L. 1973. Photosynthesis and respiration in arctic tundra grasses: field light intensity and temperature responses. Arctic and Alpine Research, 5:239-251.

Tieszen, L.L., P.C. Miller, and W.C. Oechel. 1980. Photosynthesis. *In,* J. Brown, P.C. Miller, L.L. Tieszen, and F. L. Bunnell *Eds.* An Arctic Ecosystem: The Coastal Tundra at Barrow, Alaska. Dowden, Hutchinson & Ross, Inc., Stroudsburg, Penn. pp. 102-139.

Townsend, J.R.G., and C.J. Tucker. 1984. Objective assessment of Advanced Very High Resolution Radiometer data for land cover mapping. International Journal of Remote Sensing, 23: 491-494.

Tucker, C.J. 1979. Red and photographic infrared linear combinations for monitoring vegetation. Remote Sensing of Environment 8:127-150.

Vierling, L.A., D.W. Deering, and T.F. Eck. 1997. Differences in arctic tundra vegetation type and phenology as seen using bi-directional radiometry in the early growing season. Remote Sensing of Environment, 60:71-82.

Vourlitis, G.L. , W.C. Oechel, A. Hope, D. Stow, B. Boynton, J. Verfaillie, Jr., R. Zulueta, and S.J. Hastings. 2000. Physiological models for scaling plot measurements of CO_2 flux across an arctic tundra landscape. Ecological Applications, 10(1): 60-72.

Walker, D.A., N.A. Auerbach, and M.M. Shippert. 1995. NDVI, biomass and landscape evolution of glaciated terrain in northern Alaska. Polar Record. 31:169-178.

Walker, D.A. 1999. An integrated mapping approach for northern Alaska (1:4M Scale). International Journal of Remote Sensing, 20(15): 2895-2920.

Walker, D. and N. Kenkel. 2000. Adaptive geometery of boreal conifers. Community Ecology, 1(1): 13-23

Webber, P. J. 1978. Spatial and temporal variation of the vegetation and its productivity, Barrow, Alaska. *In* Vegetation and Production Ecology of an Alaskan Arctic Tundra., *ed.* Tieszen, L. L. New York: Springer-Verlag, pp. 37-112.

Whiting, G.J., D.S. Bartlett, S. Fan, S. Bawkin, and S.C. Wofsy. 1992. Biosphere/ Atmosphere CO_2 exchange in tundra ecosystems: community characteristics and relationships with multispectral reflectance. Journal of Geophysical Research, 97(D15): 16671-16680.

Zoltai, S.C., J. Sirois, and G.W. Scotter. 1992. A natural resource inventory of the Melville Hills region, Northwest Territories. Technical Report Series - Canadian Wildlife Service, no. 135. Edmonton, Alberta.

7. APPENDICES

7.1. APPENDIX I. PREDICTING PHOTOSYNTHETIC BIOMASS WITH SPECTRAL VEGETATION INDICES.

Above ground photosynthetic biomass samples were collected in 2-3 of the quadrats within each 1x1 km plot (See Chapter 3: Methods). Some of the biomass samples were sorted, dried and weighed in the field (n=11), but most were flown back to Winnipeg and frozen until they could be processed (n=29). Wet biomass was determined for the entire sample. A subsampling method was adopted to estimate total dry green biomass because of the extremely long time required to sort a whole sample. Three 10% subsamples were taken with equal proportions of each vegetation type (i.e. graminoid, dwarf shrub, moss and lichen). Each subsample was sorted into green (photosynthetic) biomass and dead biomass. The green fraction was dried at 80°C for 24 hours, and massed. The averaged mass for the three subsamples was multiplied by 10 to determine an estimate of the total biomass. To evaluate the effectiveness of the subsampling method, an entire sample was divided in half. One half the total samples was sorted completely, dried and weighed. For the other half, mass was estimated from 3 subsamples. The two methods produced similar results.

There was a strong positive relationship between NDVI and dry green biomass (DGB), with 62.8% of the variation in DGB explained by NDVI ($R^2 = 62.8$, $p < 0.001$; Figure 7.1 a). The relationship between DGB and MSAVI is stronger compared to NDVI ($R^2 = 70.8$, $p < 0.001$ Figure 7.1 b). The point distribution between DGB and MSAVI appears to be more linear than with NDVI (Figure 7.1 b), MSAVI corrects for soil

background effects and samples with low DGB result in higher MSAVI values than with NDVI. These relationships should be viewed with caution, however, as the quality of the biomass samples is questionable. Some samples had decayed by the time they were processed, so that it was difficult to distinguish live, green biomass for dead biomass. Furthermore, using sub-samples to determine total biomass increased variability in the biomass sample estimates.

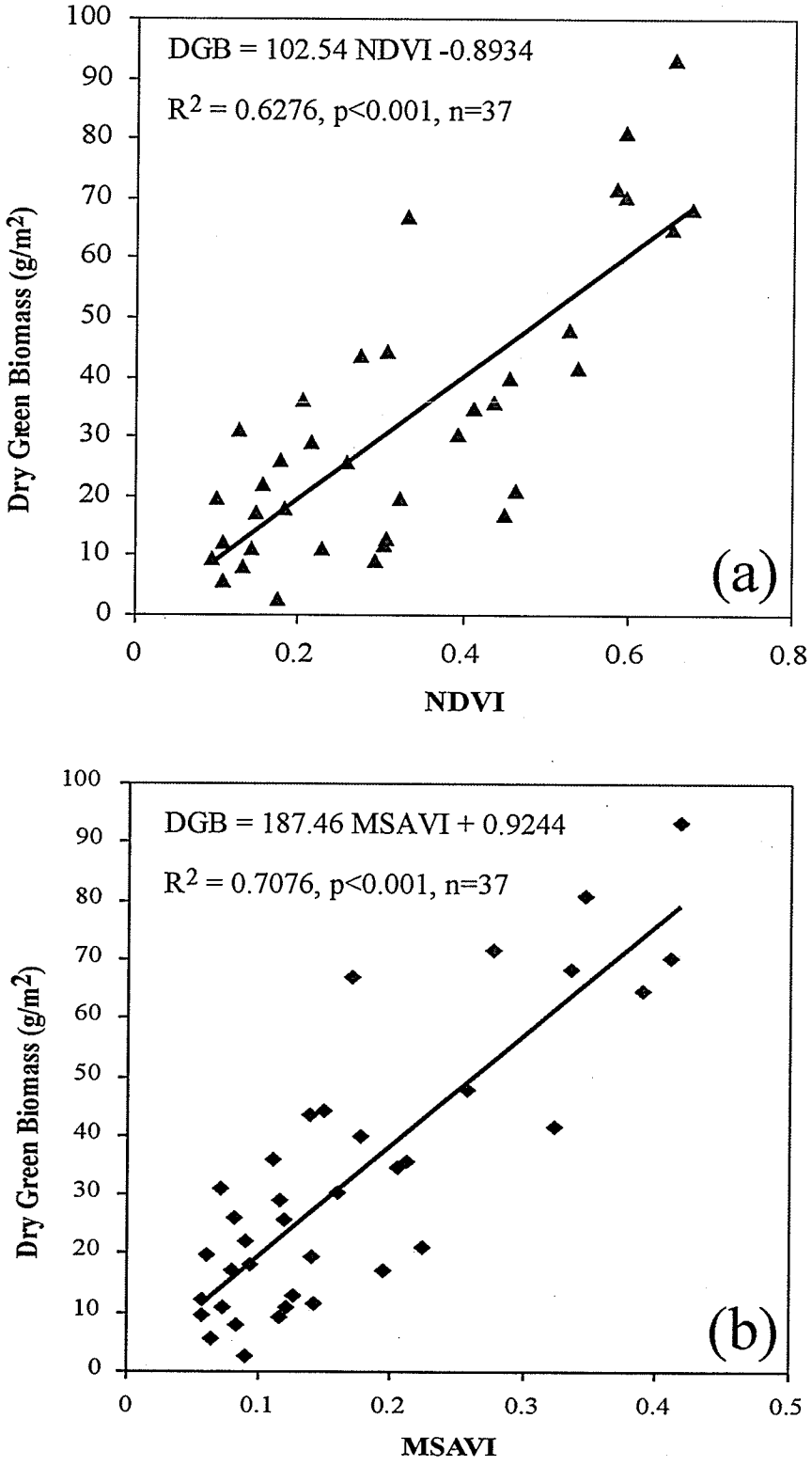

Figure 7.1. Regression between a) NDVI and dry green biomass, and b) MSAVI and dry green biomass, measured from ground samples for all vegetation types.

7.2. APPENDIX II: INTER-ANNUAL PATTERNS OF NDVI AND MSAVI.

Mean values for NDVI and MSAVI computed from 150 random points extracted within the Park for each composite image over the growing season are presented in Figure 7.2. The values of NDVI and MSAVI are unitless and therefore are incomparable in absolute terms. However, the relative shape of the curves for both NDVI and MSAVI reveals a similar pattern, with the exception of the onset of the growing season (Figure 7.2). During the June 11 composite period, mean MSAVI values drop below zero to – 0.008 (±0.045), whereas mean NDVI values increase considerably to 0.0994 (±0.0467) (Figure 7.2). During the following composite period, mean MSAVI increases and mean NDVI decreases, to relatively similar values. For the remainder of the growing season the patterns are very similar. The discrepancy during the onset of the growing season may be a factor of high variability in ground moisture after snow melt, resulting in highly variable soil background reflectance . Therefore, it is likely that the MSAVI values are more accurate, because MSAVI is designed to reduce the effects of variable soil reflectance.

7.3. APPENDIX III: ANNUAL PATTERNS OF AIR TEMPERATURE.

Mean daily air temperature measured from a weather station located in the central region of the Park corresponds with mean NPP measurements (Figure 7.3). The onset of the growing season coincides with mean air temperature rising above 0 °C. Mean NPP increases with mean air temperature during June, where NPP peaks during the July 1st – July 11th composite period. At this point, the rise in air temperature continues at a lower rate to the beginning of August. After this period, mean air temperature begins to

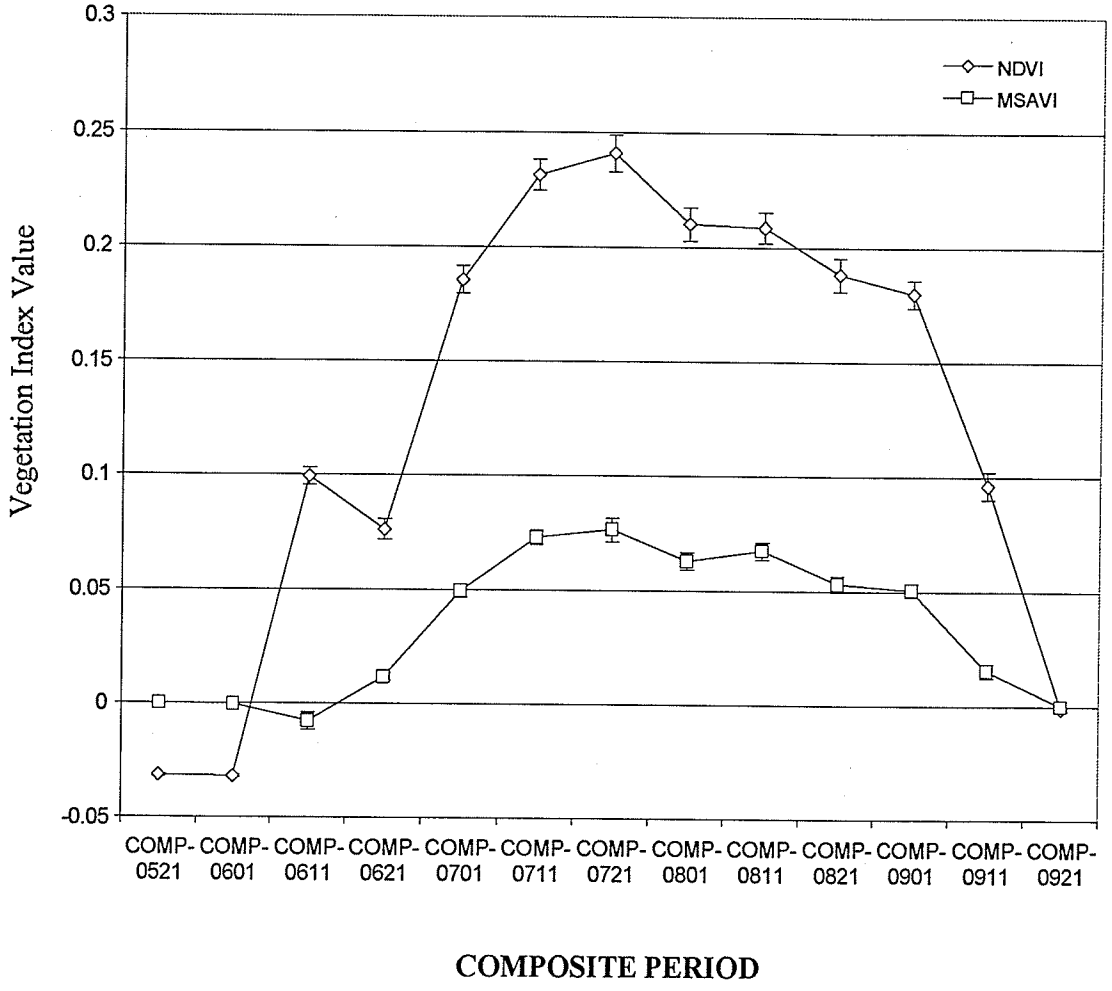

Figure 7.2. Mean values for MSAVI (boxes) and NDVI (diamonds) for each composite period during the growing season. Mean values were determined from 150 random points located within the Park. Error bars represent standard error.

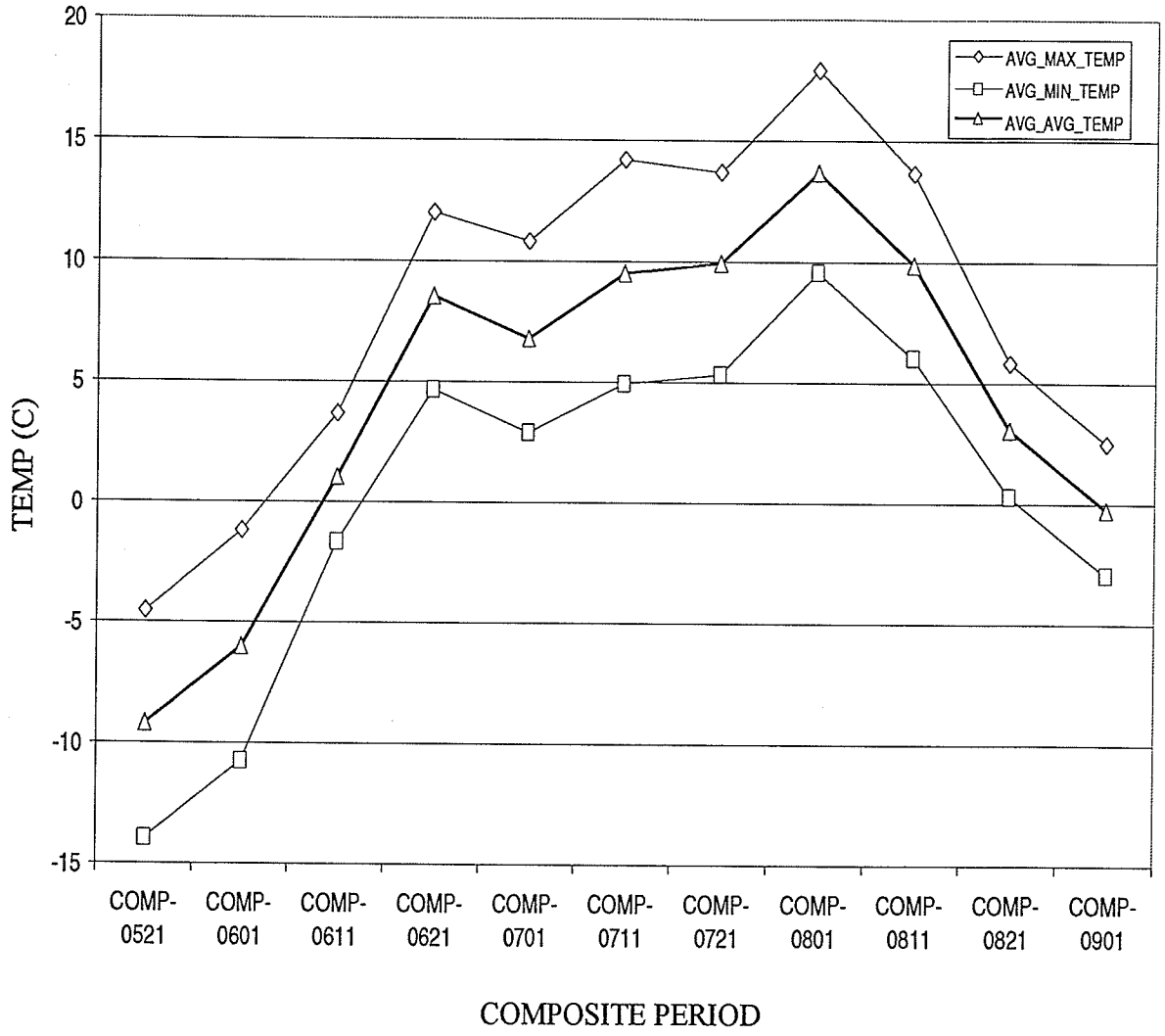

Figure 7.3. Average of daily mean air temperature over each composite period, measured from a weather station located in the central region of the Park.

decrease, until it drops below 0 °C during the Sept. 1- Sept. 11 composite period. Peak NPP coincides with the initial rapid increase in mean air temperature. However, over the remainder of the growing season, NPP actually decreases as mean air temperature increases. Arctic vegetation undergoes a rapid growth spurt at the onset of the growing season as new leaves are produced. However, during the remainder of the growing season, net production decreases as large amounts of photosynthetic product is devoted to developing reproductive structures.